JPL PUBLICATION 80-52

A Parametric Analysis of Performance Characteristics of Satellite-Borne Multiple-Beam Antennas

A.B. Salmasi

March 15, 1980

National Aeronautics and Space Administration

Jet Propulsion Laboratory
California Institute of Technology
Pasadena, California

JPL PUBLICATION 80-52

A Parametric Analysis of Performance Characteristics of Satellite-Borne Multiple-Beam Antennas

A.B. Salmasi

March 15, 1980

National Aeronautics and
Space Administration

Jet Propulsion Laboratory
California Institute of Technology
Pasadena, California

The research described in this publication was carried out by the Jet Propulsion Laboratory, California Institute of Technology, under NASA Contract No. NAS7-100.

ACKNOWLEDGEMENT

The author wishes to thank Dr. W. E. Ackerknecht, formerly at JPL, for the impetus provided by him to the original development of this study. Many of the underlying concepts had been developed by him and his important contributions are reflected throughout the report. I am grateful to Mr. N. F. deGroot for his supervision and numerous helpful suggestions throughout the duration of this work. I would also like to thank Dr. Y. Rahmat-Samii for the many useful technical discussions from which I benefited immensely and Mrs. M. Y. Easterling for her contributions in computer programming work.

ABSTRACT

This report describes a simple analytical and empirical model for parametric study of multiple-beam antenna frequency reuse capacity and interbeam isolation. Two types of reflector antennas, the axisymmetric parabolic and the offset-parabolic reflectors, are utilized to present the use of the model. The parameters of the model are introduced and their limitations are discussed in the context of parabolic reflector antennas. However, the use of this model is not restricted to analysis of reflector antenna performance.

This report is divided into six sections. Section 1 presents an overall summary of the report followed by the results of the analyses covered in two tables. The model parameters, objectives, and descriptions are given in the next three sections. Multiple-beam antenna frequency reuse capacity and interbeam isolation analysis for the two types of reflectors are discussed subsequently. Section 6 discusses future developments of the program model. Multiple-beam antenna is emerging as one of the most important components of communication satellites; and an efficient model for parametric evaluation of their performance could prove most beneficial.

TABLE OF CONTENTS

SECTION 1

SUMMARY

Multiple-beam antennas are becoming a more important part of satellite communication systems as the necessity of electromagnetic spectrum conservation becomes more evident. This is due to the fact that multiple-beam antennas (MBA's) have the potential to conserve the electromagnetic spectrum through frequency band reuse.

This report presents a discussion of performance characteristics of MBA's when two types of antennas, the full-paraboloidal axisymmetric and the offset-parabolic reflectors, are used. A major factor in the design and application of multiple-beam antennas is the presence of interbeam cochannel interference which reduces MBA's frequency reuse capacity. Therefore, the analysis of performance characteristics is based on the interbeam isolation and frequency band reuse performances of the MBA as functions of antenna characteristics.

An analytical/empirical model, consisting of a computer program, was used to obtain the performance analyses. The main parameters of the model are the number of beams, number of frequencies, beam patterns, beam spacing, and footprint level of the hypothetical boundaries between the coverage zones. In this report, the analyses done for parabolic-axisymmetric and parabolic-offset reflector MBA's assume that feed elements in the multi-element feed system possess identical radiation patterns.

In the axisymmetric reflector case, modified versions of the reference pattern for satellite transmitting antenna recommended at WARC-77 and CCIR(78)[1] were used as the beam radiation pattern model. These patterns are modeled using an envelope function to approximate the upper bound of the

sidelobe peaks. However, in this case the effects of the off-axis location of the primary-feeds upon the beam radiation patterns were not considered. For the offset-reflector case, the same type of beam patterns were used; but extensive considerations were given to the pattern deteriorations caused by the off-axis location of the primary feeds (scanning of the beams).

An optimum layout of the beams, a layout which minimizes the interference power from cochannel beams, was used to perform the analyses in all cases. The result of an optimum layout is that only a specific, optimum, number of frequencies needs to be used and any other larger non-optimum number of frequencies can be reduced to the optimum number without increasing the cochannel interference power.

In all analyses done in this report, an approximate "worst case" estimate of MBA performance was obtained by

a) assuming an envelope function to approximate the upperbound of the sidelobe peaks for model patterns;

b) use of worst case sidelobes, for the offset-reflector beam patterns, which corresponds to the case of the beam scanned in a counterclockwise manner with respect to the reflector axis. Also, for the above scanned beam, the sidelobes closer to the reflector axis, which are higher than the sidelobes away from the reflector axis, are used;

c) considering the desired beam with highest interference power, because of its position in the beam layout, and placing the maximum possible number of cochannel interfering beams in that layout (uniform layouts).

Some preliminary results have been obtained, for two types of reflector antennas, by the use of the model.

In the case of offset-parabolic reflector, a 100 wavelength diameter reflector is used while the focal length over parent paraboloid diameter ratios ($F/_{D_p}$) and illumination tapers are varied. It is known that as long as the reflector dimensions ($D/_{\lambda}$ and $F/_{D_p}$) and the antenna characteristics (i.e., illumination tapers) are kept constant, the relative characteristics of the beam patterns, as a function of number of beamwidths scanned, stays the same. Therefore, the analyses done for the 100 wavelength diameter offset-parabolic reflector are valid at all the microwave frequencies. In general, the results are frequency independent as long as the antenna dimensions, relative to the signal wavelength, are preserved the same. However, since the uplink and downlink frequencies of the satellite are not the same (but close), there could be slight variations in the interbeam isolation and frequency reuse performance of the two links. The results of analyses have been summarized in the following tables. Care should be taken in applying the results shown here since these results can greatly vary for different reflector dimensions.

TABLE 1.

Results of Analysis Done for Axisymmetric Reflector MBA with Uniform Beams and Uniform Layout

Parameter	Axisymmetric Reflector MBA with Uniform Beams
Number of Beams	C/I decreases as number of beams is increased (C/I is the carrier-to-interference power ratio, or the interbeam isolation; where the desired carrier power, C, is calculated at an angle θ off the desired beam boresight and the interference power, I, is calculated at the same point).
Number of Frequencies	As the number of frequencies is increased, the C/I performance improves. C/I is more sensitive to number of frequencies when beam patterns contain sidelobe levels of -30 dB or lower. A change in number of frequencies from 3 to 4 produces the largest impact on C/I performance for the lower sidelobes.
Sidelobe Level	A reduction in the level of sidelobes causes considerable improvement in C/I performance. Sidelobe level has a more noticeable effect when larger number of beams and frequencies are used.
Crossover Levels	C/I values are relatively insensitive to the crossover levels of between -2 to -7 dB for very large number of beams and -5 to -7 dB for smaller number of beams with higher number of frequencies. So, the optimum crossover level is dependent on the number of beams and frequencies.
Footprint Level	For a fixed beam spacing, the C/I value is almost a linearly decreasing function of increasing footprint area (or decreasing footprint level). Sidelobe level variation has no effects on the slope of the function.
Beam Spacing	For a fixed footprint level, the C/I performance improves as larger separations between beams are produced. For different number of beams and frequencies, the rate of improvement becomes uniform after 1.65 (HPBW) beam separation for -25 dB sidelobes and 1.25 (HPBW) beam separation for -30 dB sidelobes.
F/D_p	No analysis
Illumination Taper	No analysis
Conclusion	In evaluation of C/I performance of MBA's, number of beams and frequencies are the determining factors. However, C/I performance can be improved by better sidelobe design and, if possible, larger beam spacing.

TABLE 2.

Results of Analysis Done for Offset-Reflector MBA (100 Wavelength Diameter with Non-Uniform Beams and Uniform Layout)

Parameter	Offset-Reflector MBA (100 Wavelength Diameter) With Non-Uniform Beams (Beam Degradations are due to Scanning of the Beams)
Number of Beams	C/I decreases as number of beams are increased. (same as axisymmetric reflector).
Number of Frequencies	As the number of frequencies is increased, the C/I performance improves. When larger frequency reuse factors are used, a small change in number of frequencies causes a considerable improvement in C/I performance. A change in number of frequencies from 3 to 4 produces the largest impact on C/I values. As sidelobe levels are lowered this effect becomes more noticeable.
Sidelobe Level	A reduction in the level of sidelobes causes considerable improvement in C/I performance. Sidelobe level has a more noticeable effect when larger number of beams and frequencies are used (same as axisymmetric reflector).
Crossover Level	The optimum crossover level is independent of the number of beams and frequencies. For the case of a 100 wavelength diameter offset-reflector with F/D_p = 1.0, -10 dB taper, and -25 dB sidelobes, the optimum crossover level is found to be between -5 to -7 dB.
Footprint Level	For a fixed beam spacing, the C/I value is almost a linearly decreasing function of increasing footprint area (or decreasing footprint level). Sidelobe level variation has no effects on the slope of the function (same as axisymmetric reflector).
Beam Spacing	Same as axisymmetric reflector, but the rate of C/I improvement is the same for all number of beams, frequencies, and sidelobe levels.
F/D_p	Comparison made for two different F/D_p ratios of 0.5 and 1.0, with -10 dB taper and -25 dB sidelobes, shows a maximum C/I improvement of 2 dB. This result was obtained for the desired beam at the focal point of the reflector and is immune from large scan losses produced by smaller F/D_p's at large scan angles.

TABLE 2. (Continued)

Results of Analysis Done for Offset-Reflector MBA (100 Wavelength Diameter with Non-Uniform Beams and Uniform Layout)

Parameter	Offset-Reflector MBA (100 Wavelength Diameter) With Non-Uniform Beams (Beam Degradations are due to Scanning of the Beams)
Illumination Taper	Comparison made for two different illumination tapers of -10 and -15 dB, with F/D_p of 1.0, shows an improvement of about 1-4 dB in C/I performance.
Conclusion	Same as axisymmetric reflector. Higher values of F/D_p's and lower values of illumination taper can give C/I improvements of up to 4 dB in some cases.

SECTION 2

INTRODUCTION

It is possible to increase the bandwidth capacity of a band-limited satellite by the use of multiple-beam antennas. This is done by transmitting separate messages to different ground stations by means of many separate narrow beams, instead of a broad beam which illuminates an entire coverage area with all the message signals. An example of multiple-zone coverage beams from a satellite antenna is shown in Figure 1. In this paper only the class of multiple-beam antennas suitable for satellite-borne applications is considered.

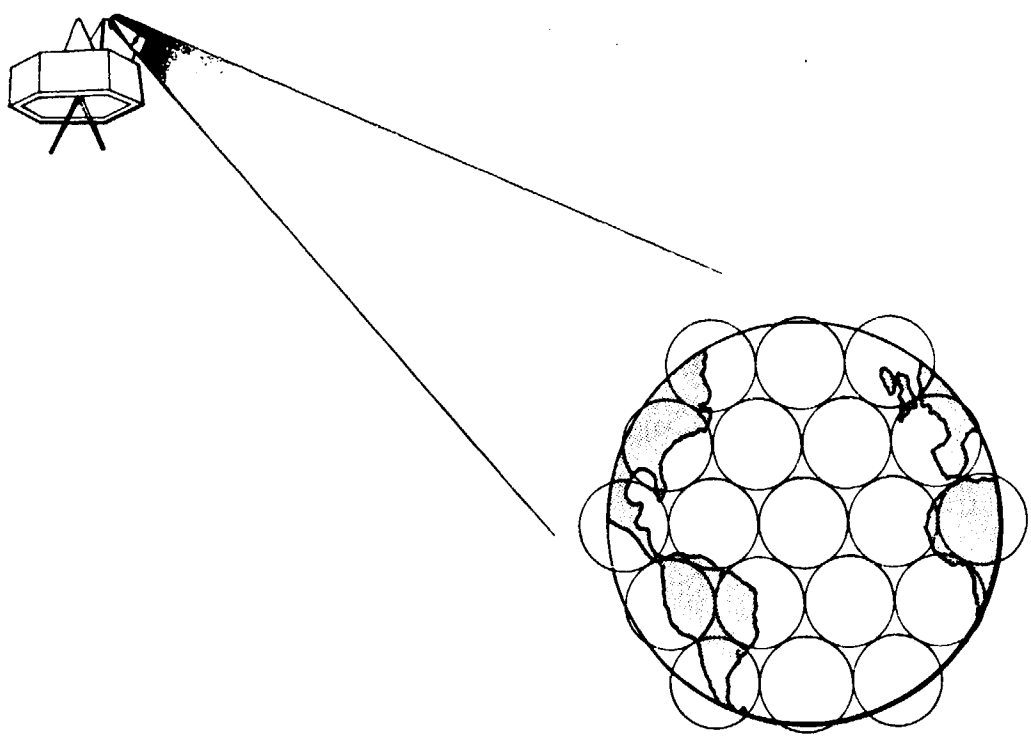

Figure 1. Multiple-Zone Coverage Beams from a Satellite Antenna

A major factor in the design and application of multiple-beam antennas is the presence of the interbeam cochannel interference which reduces frequency reuse capacity. The cochannel interference determines the interbeam isolation or carrier-to-interference power ratio (C/I). Interbeam isolation is defined as the ratio of the power density of the desired beam, at any spot within the coverage area of this beam, to the incoherent summation of the co-polarized components of the power densities of all other cochannel beams at the same spot. The objectives of this paper are:

1) To describe an analytical/empirical model for parametric study of the frequency reuse capacity of multiple-beam antennas, and

2) present some preliminary results obtained by use of the model.

The model consists of a computer program which takes the radiation pattern information of each beam and the geometrical layout of all the beams in the coverage area as its input, and calculates the interbeam isolation of the cochannel beams at any spot within that coverage area. For the purpose of this study, this is done for a cellular-coverage system in which the multiple beams are equally spaced in a triangular matrix with a hexagonal boundary. Figure 2 shows this cellular-coverage beam layout, where in an optimum cellular-coverage beam layout, two adjacent beams cannot operate on the same frequency band. The knowledge of carrier-to-interference power ratio as a function of number of beams, number of frequencies, beam separations and the radiation patterns of the individual beams would provide us with the frequency reuse capacity of the multiple-beam antenna system. In this report, it is assumed that all beams have equal frequency bandwidths and are of equal capacity. Also, the only type of interference considered is the cochannel

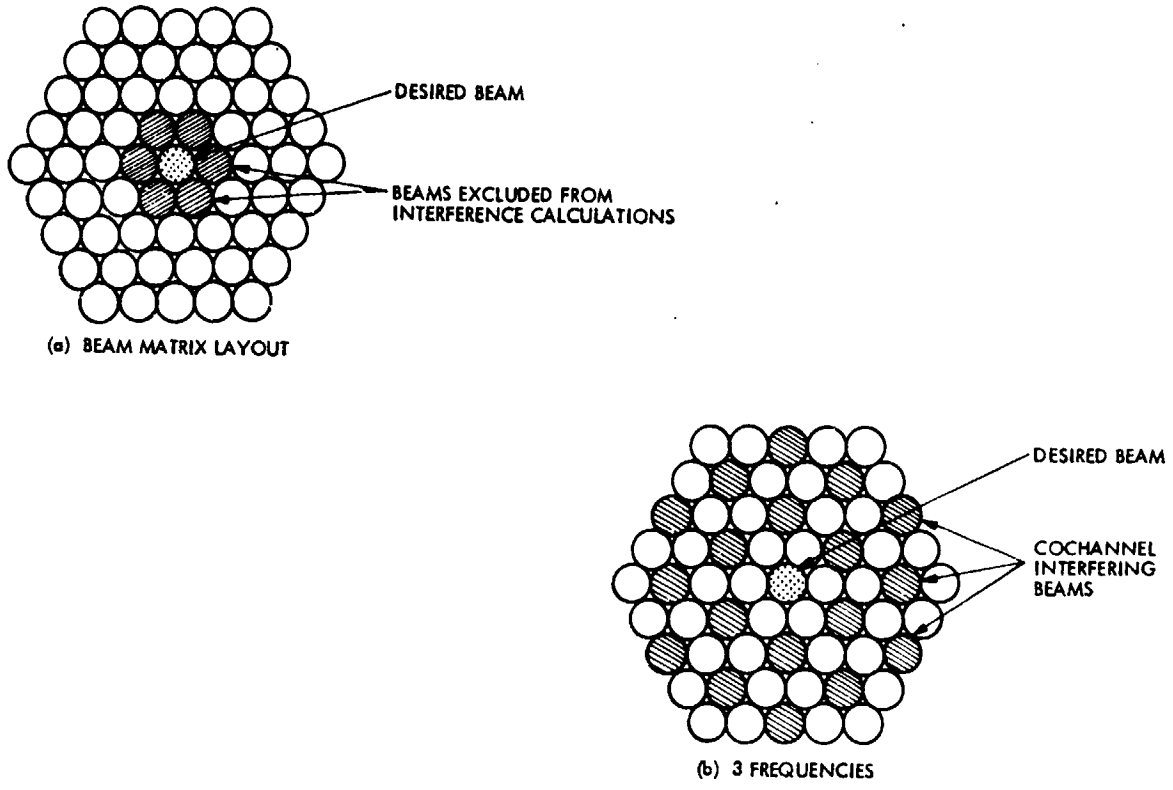

Figure 2. Cellular Coverage Beam Layout with Hexagonal Boundary

interference from the cochannel beams of the multiple-beam antenna system under study.

Because of general interest in offset-reflectors as the antenna type for multiple-beam antennas, only two types of antenna, namely a full-paraboloidal axisymmetric reflector and an offset-parabolic reflector are considered in this report. These antennas consist of a set of linear array feeds located in the focal plane of a parabolic, axisymmetric or offset, reflector. Also, each one of the feed elements in the multi-element feed system is assumed to possess identical radiation patterns. However, the model is not restricted to analysis of reflector antennas or identical feed patterns, since the antenna

beam pattern is just an input to the model. Therefore, other antenna types like lens antennas, phased array antennas, complex feed antennas, and other reflector antennas can be used as well. A major goal in the model development has been to obtain an efficient engineering tool for parametric evaluation of MBA performance.

SECTION 3

PARAMETERS OF THE MODEL

The parameters of interest in this model are as follows:

a) Number of Beams: This determines the number of possible zone coverages.

b) Number of Frequencies: The frequency reuse capacity is determined by this parameter. Frequency reuse factor is defined as the number of beams divided by the number of frequency bands.

c) Beam Spacing: Since the feed separations on the optimal focal plane are determined by the separation of beams within the coverage area, the separation between the beams determines the size of the focal plane. The minimum separation between the feeds is limited by the mutual coupling between the elements [2] and by the physical size of the feeds. On the optimal focal plane, feeds should be placed as close as possible to the reflector focal point; so the beam degradations due to the off-axis location of the primary-feeds are minimized.

d) Beam Patterns: Individual beam patterns are dependent on the feed patterns, the location of the corresponding feeds on the optimal focal plane, and on the antenna characteristics (size, F/D, illumination taper, aperture efficiency, and etc.). Beam patterns of the

MBA system specify many of the model parameters including beamwidths, sidelobe patterns, beam positions and more.

e) Footprint Level: The footprint level is defined as the power density of the beam, relative to the main beam-maximum, at an angle θ off the beam boresight. The footprint level, or calculation point, determines the hypothetical boundaries within the coverage zones where the carrier-to-interference ratios (C/I's) are calculated and specified.

These parameters are discussed in more detail in the context of two reflector antenna systems. The performance of MBA's in terms of its interbeam isolation is solely dependent upon these parameters. In determination of an acceptable or required carrier-to-interference ratio and frequency reuse capacity of MBA systems, the trade-off between these parameters is of utmost concern.

SECTION 4

DESCRIPTION OF THE MODEL FOR DETERMINATION OF THE FREQUENCY REUSE CAPACITY OF MULTIPLE-BEAM ANTENNAS

In this section the objectives of this model and the theoretical basis for its development are explained.

4.1 MODEL OBJECTIVES AND DESCRIPTIONS

The main output of the model is the MBA frequency reuse capacity in terms of carrier-to-interference power ratio (C/I). Figure 3 shows the case of one beam interfering with the desired beam. The desired carrier power, C, is calculated at an angle θ off the desired beam boresight and the interference power, I, is calculated at the same point, which is at an angle $(\theta_c - \theta)$ off the boresight of the cochannel interfering beam. This represents the calculation of C/I or interbeam isolation at any spot within the coverage area. The angle θ specifies the footprint level of the calculation point and angle θ_c specifies the beam separation between the desired beam and cochannel interfering beam under consideration.

The cochannel interference in a frequency reuse system has been found to behave like additive thermal noise as long as it is not correlated with the desired signal. For multiple cochannel interfering beams, which are not coherent to each other, the total interference power is assumed to be the incoherent summation of the signal power from each interfering beam [3]. So the total carrier-to-interference power ratio, up-link or down-link, could be found in the following manner

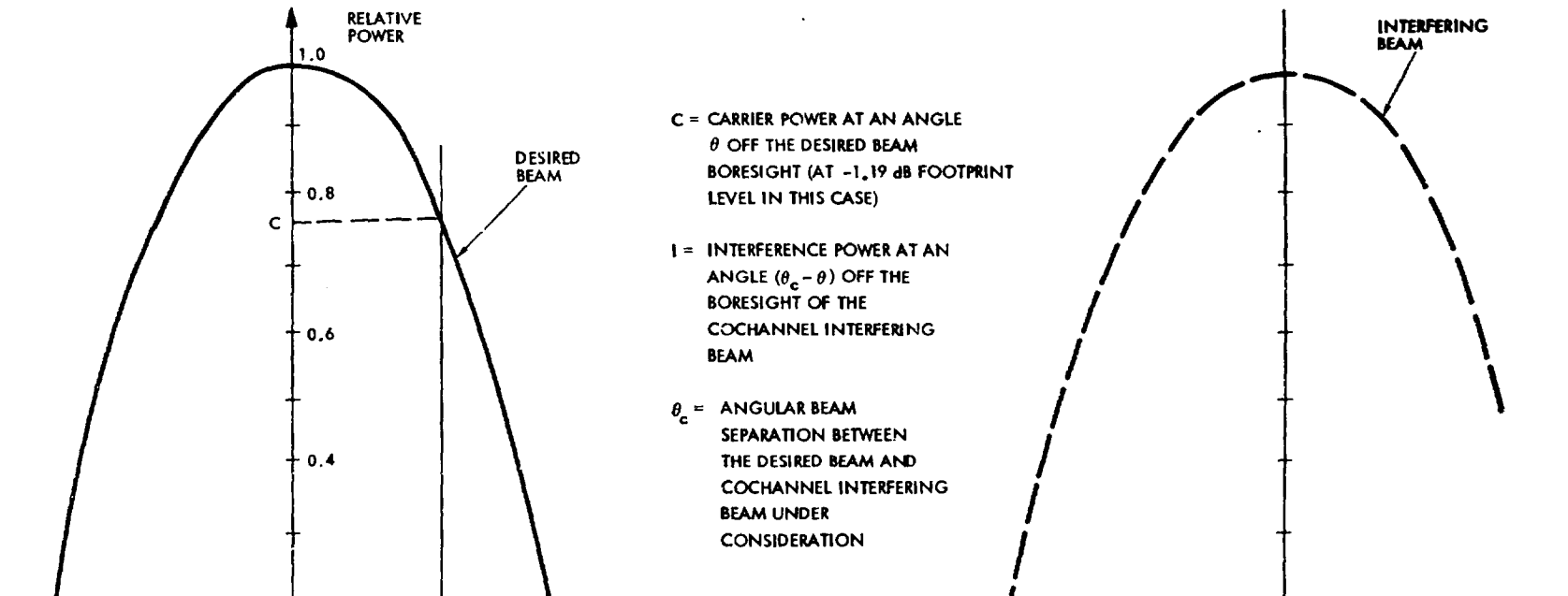

Figure 3. Geometry for Calculating C/I at Angle θ with Single Interfering Beam at Angle θ_c from Desired Beam Boresight. For this case, C ≈ 0.76, I ≈ 0.15, so C/I ≈ 0.76/0.15 = 5.07 = 7.05 dB.

$$(C/I)_{TOTAL} = C \Big/ \sum_{i=1}^{N} I_i$$

where

C = desired carrier power,

I_i = interference power from ith cochannel beam, and

N = total number of interfering beams.

Sometimes, it is possible for cochannel beams to be coherent to each other and, possibly, to the desired beam. For the purpose of this report, we define two cochannel beams as coherent to each other if they carry the same signal and the signals are in phase. In such cases, the total desired power received by a receiver, at some point within the coverage area, is the coherent summation of the desired beam carrier power and the coherent cochannel beams carrier powers. At the same point within the coverage area, the total interference power received by the receiver is found by,

a) the coherent summation of the carrier power from all the interfering beams that are coherent to each other,

b) the incoherent summation of all the sets of cochannel interfering carrier powers found in part (a).

Then at any spot within the coverage area, the total carrier-to-interference power ratio, up-link or down-link, could be found by:

$$(C/I)_{TOTAL} = \frac{\left(DCV + \sum_{i=1}^{Q} CCV_i\right)^2}{\left(\sum_{i=1}^{K} I_i\right)^2 + \left(\sum_{i=1}^{L} I_i\right)^2 + \ldots\ldots + \left(\sum_{i=1}^{N} I_i\right)^2}$$

where

DCV = the desired beam carrier voltage,

CCV_i = the ith coherent cochannel beam carrier voltage (coherent to the desired beam),

I_i = the interference carrier voltage from ith cochannel beam which is coherent to the other interfering cochannel beams within each one of the summations shown above,

Q = total number of cochannel beams that are coherent to the desired beam, and

K, L, ..., N = total number of cochannel interfering beams that are coherent to each other in each summation.

In practice, the cochannel interference could be present in both up-link and down-link. In this case either one or both links may determine the overall C/I performance. Since it is assumed that the cochannel interference is not correlated with the desired signal and behave like additive thermal noise, then it could be shown that [4]

$$(C/I)^{-1}_{TOTAL} = (C/I)^{-1}_{UP\text{-}LINK} + (C/I)^{-1}_{DOWN\text{-}LINK} \quad ;$$

and if $(C/I)_{UP\text{-}LINK} \approx (C/I)_{DOWN\text{-}LINK}$, then

$$(C/I)_{TOTAL} \approx (C/I)_{\substack{DOWN\text{-}LINK \\ OR\ UP\text{-}LINK}}(dB) - 3 \quad (dB).$$

In this report, it is assumed that all the cochannel beams are incoherent to each other and the cochannel interference is only present in the down-link at all times. (It is possible to reduce cochannel interference in voice

channels through the use of voice activated carrier (VOX) in all transmitters. In this case, the C/I performance of the system depends on the percent of the time that any occupied voice channel will have a carrier actually present).

The model program simulates the multiple-beam antenna pattern by the superposition of a two-dimensional array of individual beam patterns. In the case of reflector antennas the beam radiation pattern depends on the antenna characteristics, feed characteristics, and the location of the feeds on the optimal focal plane of the reflector. Considering the effects of the antenna characteristics upon the beam characteristics (scan loss, beam broadening, sidelobe levels, and beam deviation), the relative position of the feeds on the optimal focal plane determines the relative location of the beams within the coverage area.

4.2 COVERAGE BEAM-LAYOUT

Multiple-beam antennas can cover large geographical areas by two-dimensional networks of small coverage beams. Figure 4 shows the case of U.S. coverage with 69 contiguous beams. Covering a geographical region with equal regular polygons (i.e., in order to totally cover the area and closest to a circle) which do not overlap is known as tessellation. In particular, a hexagonal coverage-layout has been considered, since the hexagon has the distinction of being the highest ordered (most sides) regular polygon which tessellates a plane [5]. The circles inscribed in these hexagons would illustrate the actual beam cross sections for some arbitrary footprint level as shown in Figure 4. Because of the high level of interference between adjacent beams which are cochannel, in an optimum beam-layout if a given

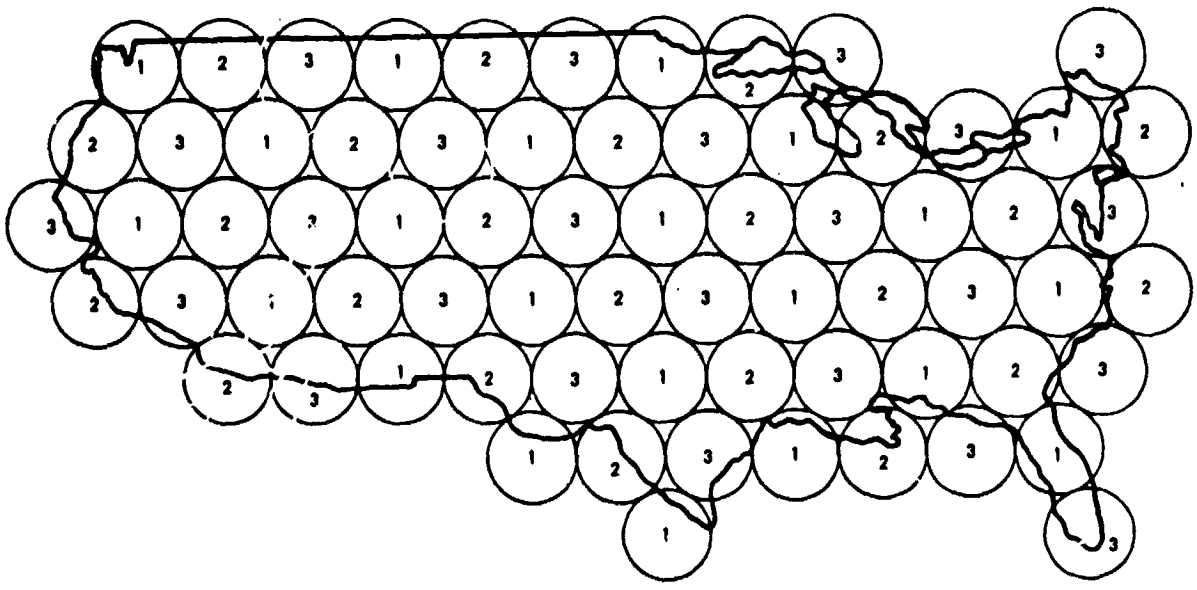

Figure 4. The Case of U.S. Coverage with 59 Contiguous Beams and 3 Frequencies

carrier frequency is used in one beam, then it cannot be repeated in the adjacent beam. The necessary separation between cochannel beams is determined by the requirements on interbeam isolation.

The optimum layout of the beams is an important factor in frequency reuse with multiple-beam antennas when there is a requirement on the interbeam isolation (C/I) of the system. An optimum layout of the beams is achieved by dividing the total number of beams into groups of beams such that each beam in a group utilizes a different frequency-band (or channel). A single frequency-band can be used only by one beam in each group and the number of cochannel beams can be as large as the number of groups. Figure 5(a) depicts the case of seven beams in one group. Of course, the actual beam cross sections are circular, but for convenience they are shown as hexagons. Now, if more beams are needed to cover an area, a new group of beams could be added

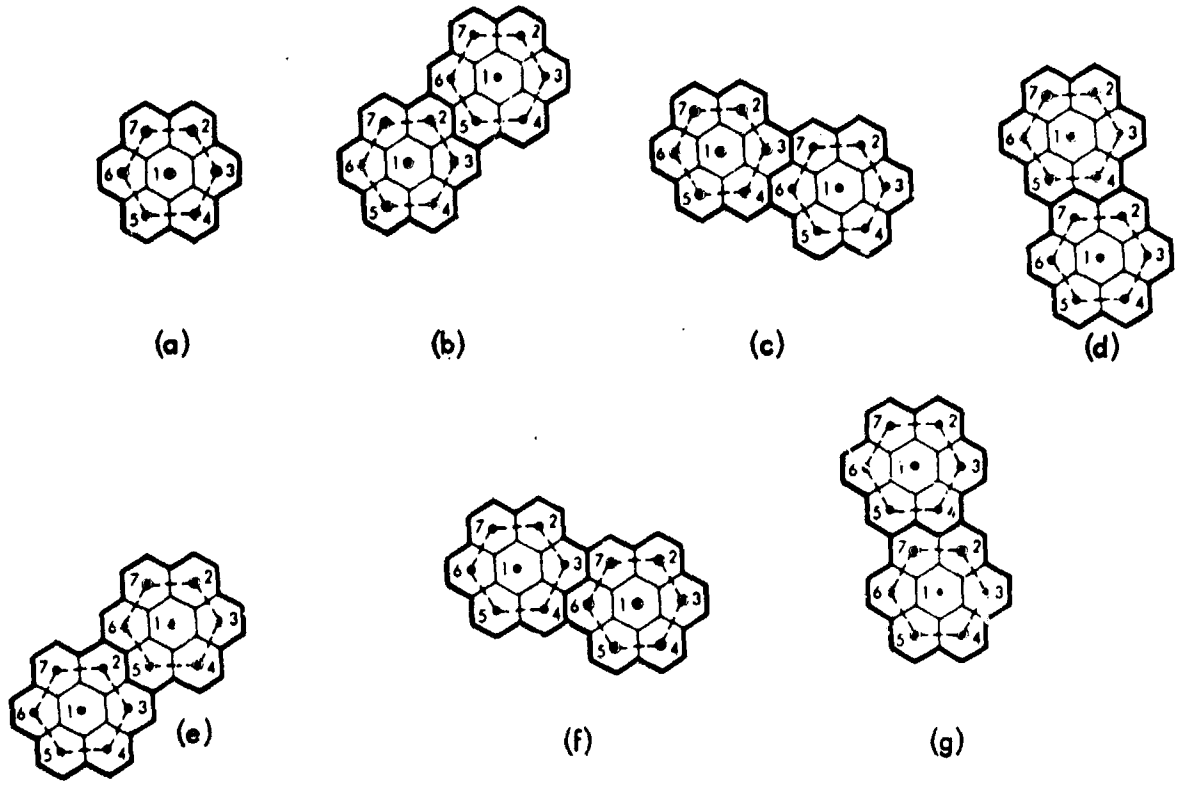

Figure 5. (a) Case of Seven Beams in One Group. The Dots Inside the Hexagons Show the Boresight of the Beams and the Numbers Next to the Dots are the Beam Numbers. (b), (c), (d), (e), (f) and (g) An Added Group of Beams is Rotated Around the First Group. The Distances Between the Cochannel Beams, with the Same Number, are Preserved.

to the first group as shown in Figures 5(b), (c), (d), (e), (f), and (g). It can be seen that in all six cases the distance between the desired beam in the first group, Figure 5(a), and the cochannel interfering beam in the new add group is the same. For instance, the distance between the desired beam number 7 and the cochannel interfering beam number 7 in the added group of beams is the same in all 6 cases. Therefore, as long as the beam layout is generated in a systematic fashion by

a) grouping of the beams in groups with equal number of beams, and

b) starting with one group and building the new groups around it until the required number of total beams is obtained,

the total interference power at any spot within the coverage area of the desired beam would be the minimum obtainable. Figure 6 shows the case of 49 beams with 7 beams per group. As shown in this figure, each group of beams generates a polygonal boundary and centers of the beams 2-7 are located on the vertices of a hexagon. In general, for different number of beams in each group, the centers of beams generate many different polygonal configurations with these centers on the vertices of the generated polygon. In practical applications, each group is not required to contain the same number of beams.

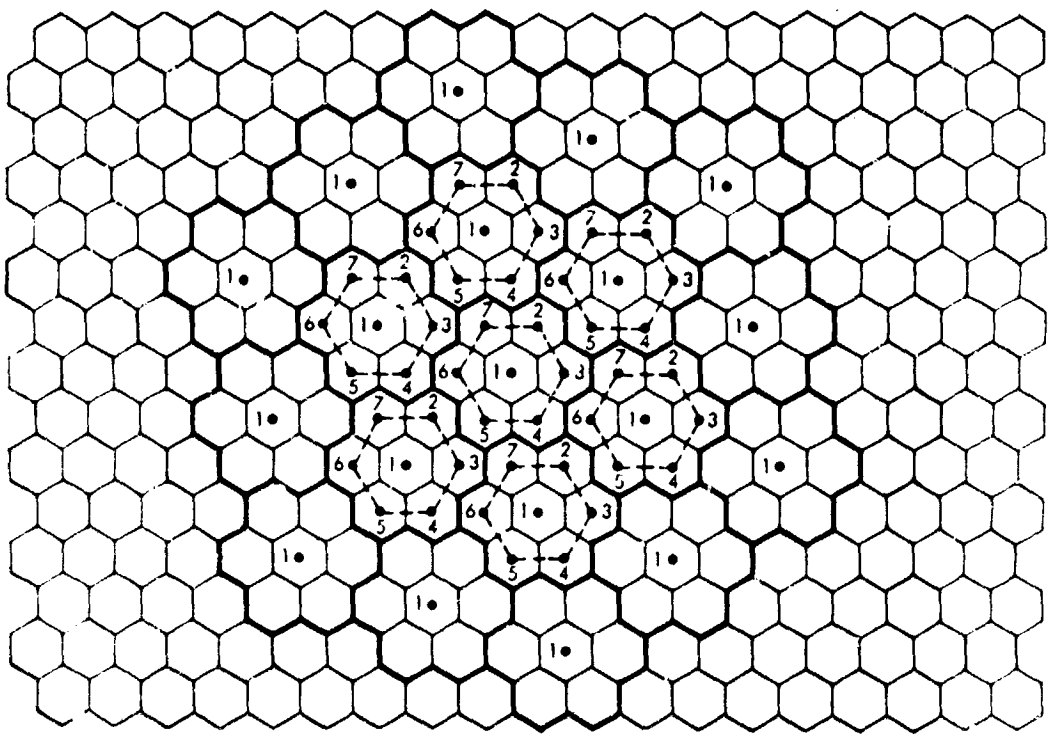

Figure 6. Example of the Seven Beams per Group. Notice that each group of beams generates a polygonal boundary and centers of the beams 2-7 are located on the vertices of a hexagon.

However, for the purposes of our analysis this restriction has been imposed, and thus the total number of beams will be equal to the number of beams per group times the number of groups. This assumption would yield the maximum number of cochannel interfering beams in the beam layout and also the worst case interbeam isolation in coverage of a geographical area.

In comparison of various two-dimensional layouts of the beams, there are three parameters that should be considered. The parameter D is the distance between centers of the closest cochannel beam boresights, R is the maximum distance from the center of a cell to the cell boundary, and NF is the minimum number of channel sets (frequency bands) required to fully cover any planar area. It has been shown [6] that is is possible to identify all possible configurations generated by the center of the beams given the minimum permissible D/R. Also, the minimum number of channel sets is found in [5], which for hexagonal grouping of the beams is given by

$$NF = \frac{1}{3}\left(\frac{D}{R}\right)^2,$$

and NF can take on only the selected values

$$NF = 3, 4, 7, 9, 12, 13, 16, 19, 21, \ldots$$

determined from $NF = (k + \ell)^2 - k\ell$, where k and ℓ range over the positive integers. The relationship between the integers k, ℓ and the optimum number of frequencies (NF) is determined by the spacing between beams on the same frequency [6]. Table 3 lists the possible optimum configurations and the corresponding values of k and ℓ.

Table 3. Number of Frequencies as a Function of k and ℓ for Optimum Cellular Coverage

Number of Frequencies (NF)	k	ℓ
1	0	1
3	1	1
4	0	2
7	1	2
9	0	3
12	2	2
13	1	3
16	0	4
19	2	3
21	1	4

Figures 7-15 show some more layouts as examples of 3, 4, 7, 9, 12, 13, 16, 19, and 21 beams per group. Other numbers of frequencies in between the indicated numbers are, of course, possible, but the case of eight beams per group, for instance, can be reduced to seven without increasing interference. In general, an increase in number of frequencies would improve the C/I performance. The above result means that, for example, an optimum layout which uses seven frequency bands would yield a higher C/I than any layout with eight frequencies, any nonoptimum layout with seven frequencies, and all the layouts with smaller number of frequencies. This important conclusion is a result of an optimum layout of the beams for the purpose of

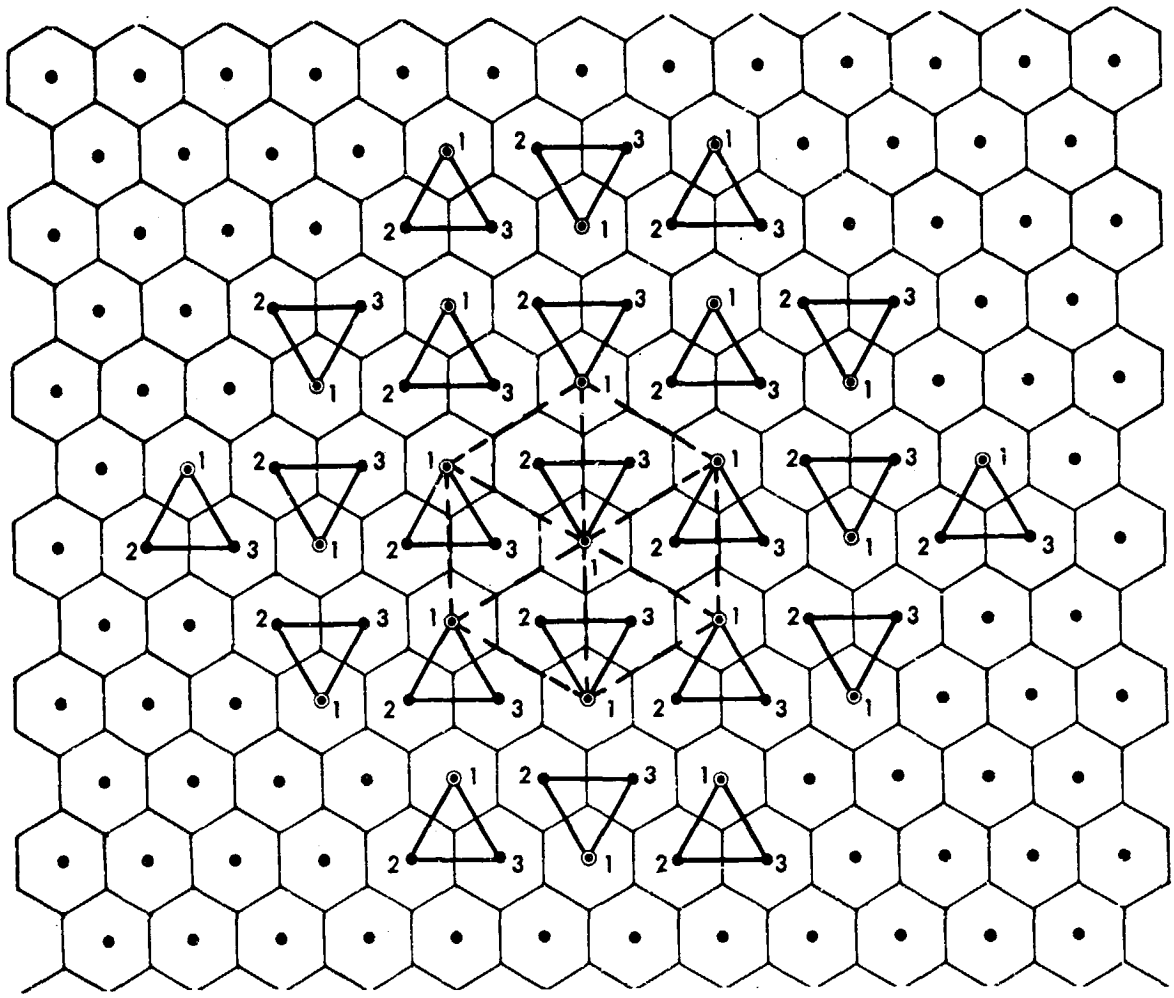

Figure 7. Layout for an Example of 3 Beams per Group. The Broken Lines Show the Distances Between Cochannel Interfering Beams Number 1 and the Desired Beam Number 1 for the Case of 21 Beams. All the Groups of Beams, Shown in this Figure, Make Up the Case of 69 Beams and 3 Frequencies.

cellular coverage of geographical areas. To summarize, there are three rules to be followed in order to achieve an optimum layout:

1. No two adjacent beams should use the same frequency band;
2. Uniform grouping of the beams should be used while no two beams in a group would use the same frequency band;
3. The optimum number of frequencies, which equals the number of beams per group, should be used.

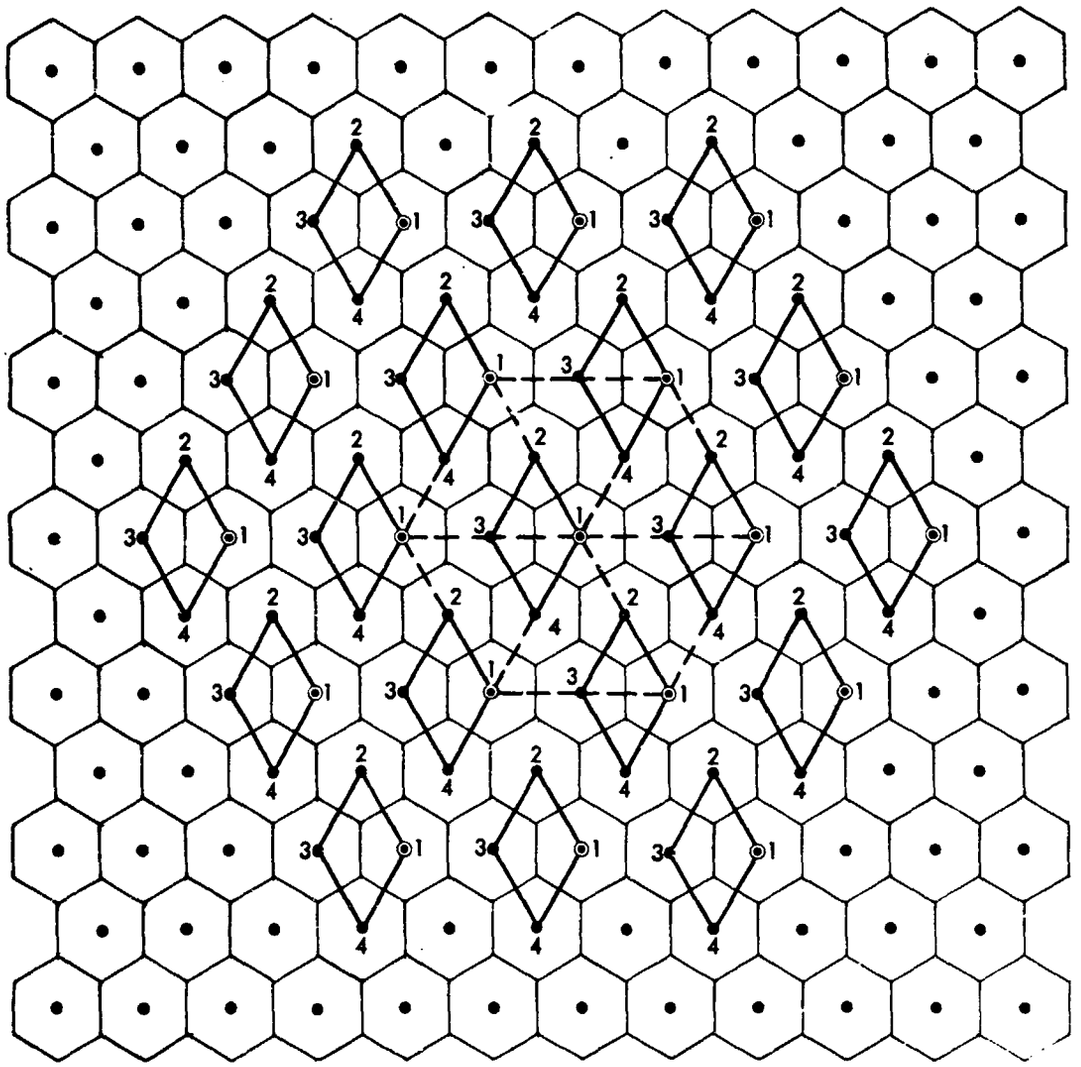

Figure 8. Layout for an Example of 4 Beams per Group. The Broken Lines Show the Distances Between Cochannel Interfering Beams Number 1 and the Desired Beam Number 1 for the Case of 28 Beams. All the Groups of Beams, Shown in this Figure, Make Up the Case of 76 Beams and 4 Frequencies.

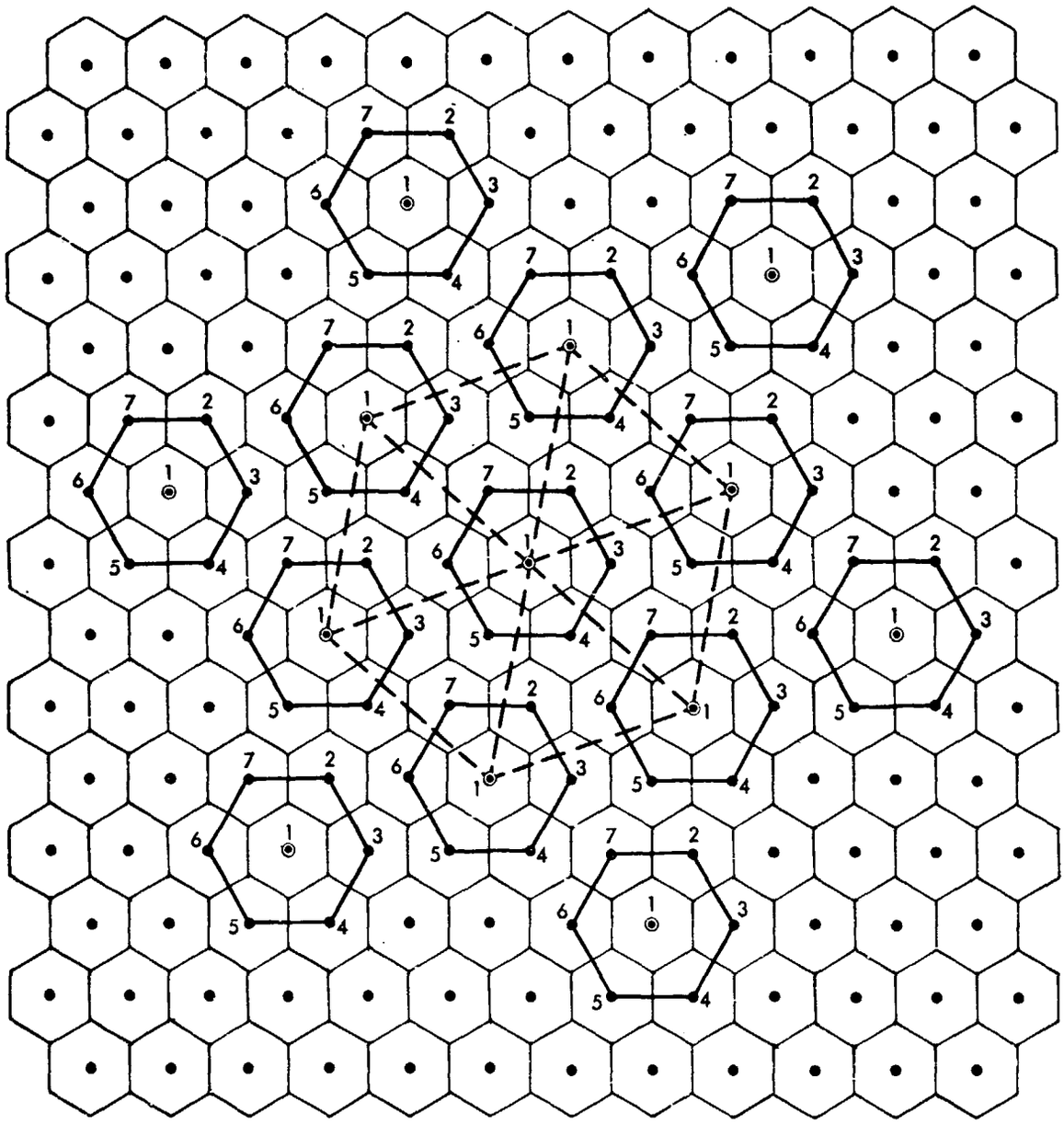

Figure 9. Layout for an Example of 7 Beams per Group. The Broken Lines Show the Distances Between Cochannel Interfering Beams Number 1 and the Desired Beam Number 1 for the Case of 49 Beams. All the Groups of Beams, Shown in this Figure, Make Up the Case of 91 Beams and 7 Frequencies.

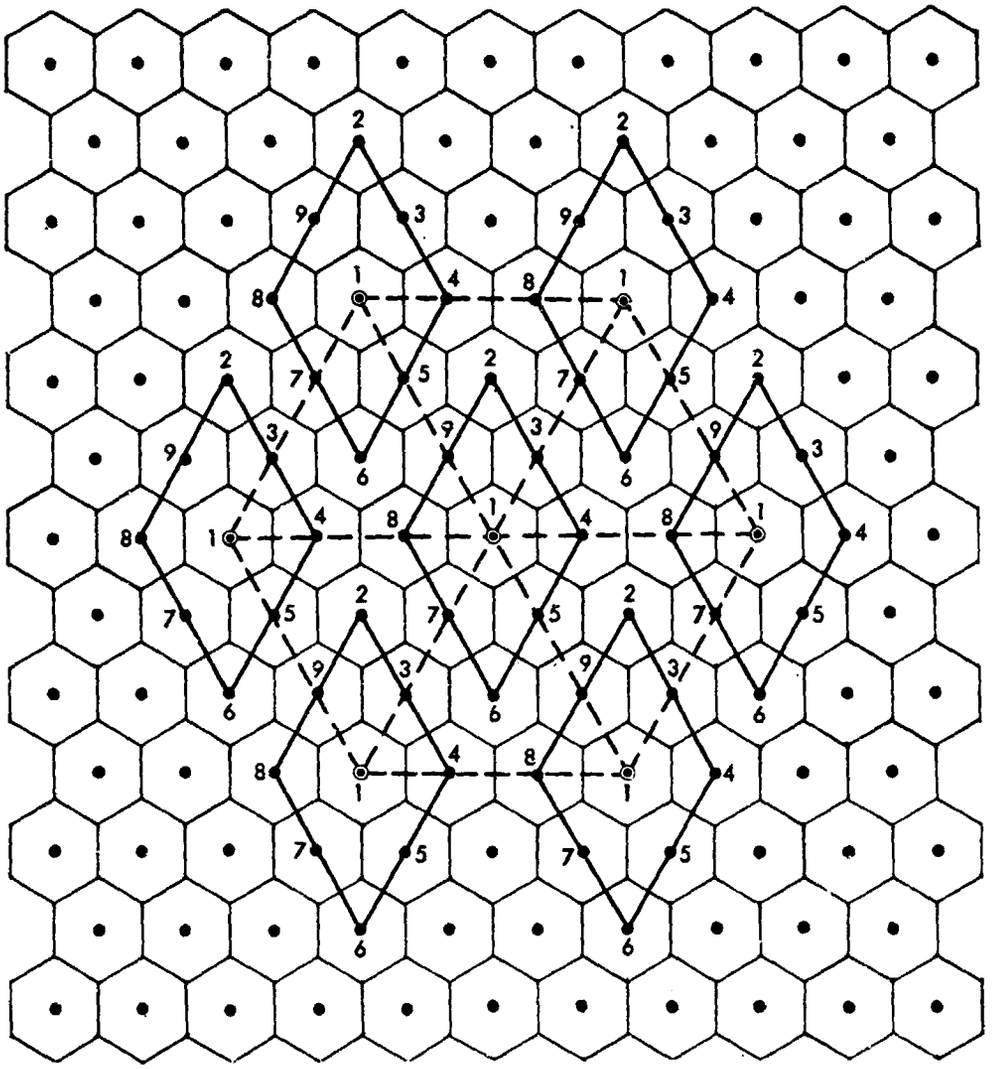

Figure 10. Layout for an Example of 9 Beams per Group. The Broken Lines Show the Distances Between Cochannel Interfering Beams Number 1 and the Desired Beam Number 1 for the Case of 63 Beams and 9 Frequencies.

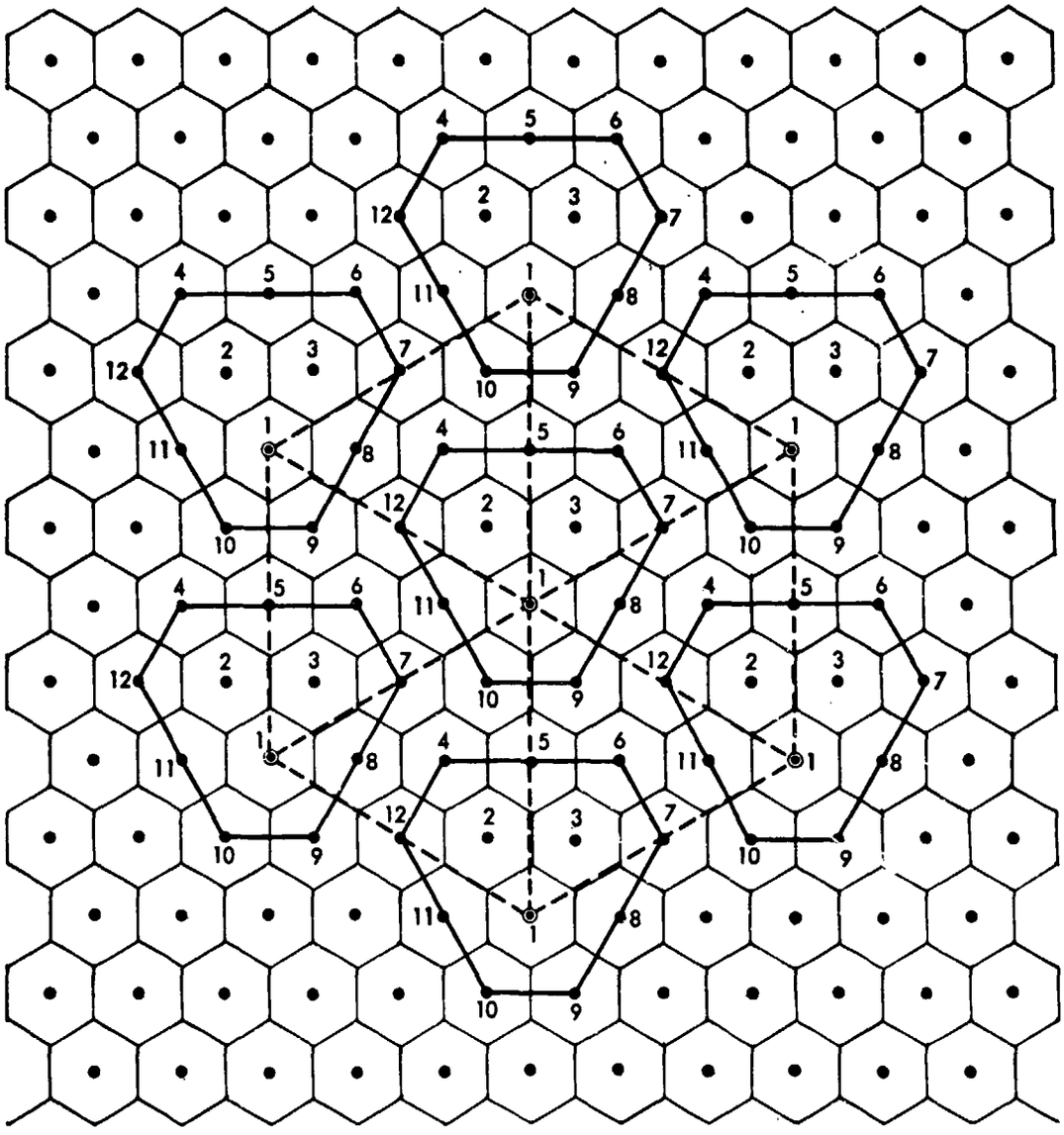

Figure 11. Layout for an Example of 12 Beams per Group. The Broken Lines Show the Distance Between Cochannel Interfering Beams Number 1 and the Desired Beam Number 1 for the Case of 84 Beams and 12 Frequencies.

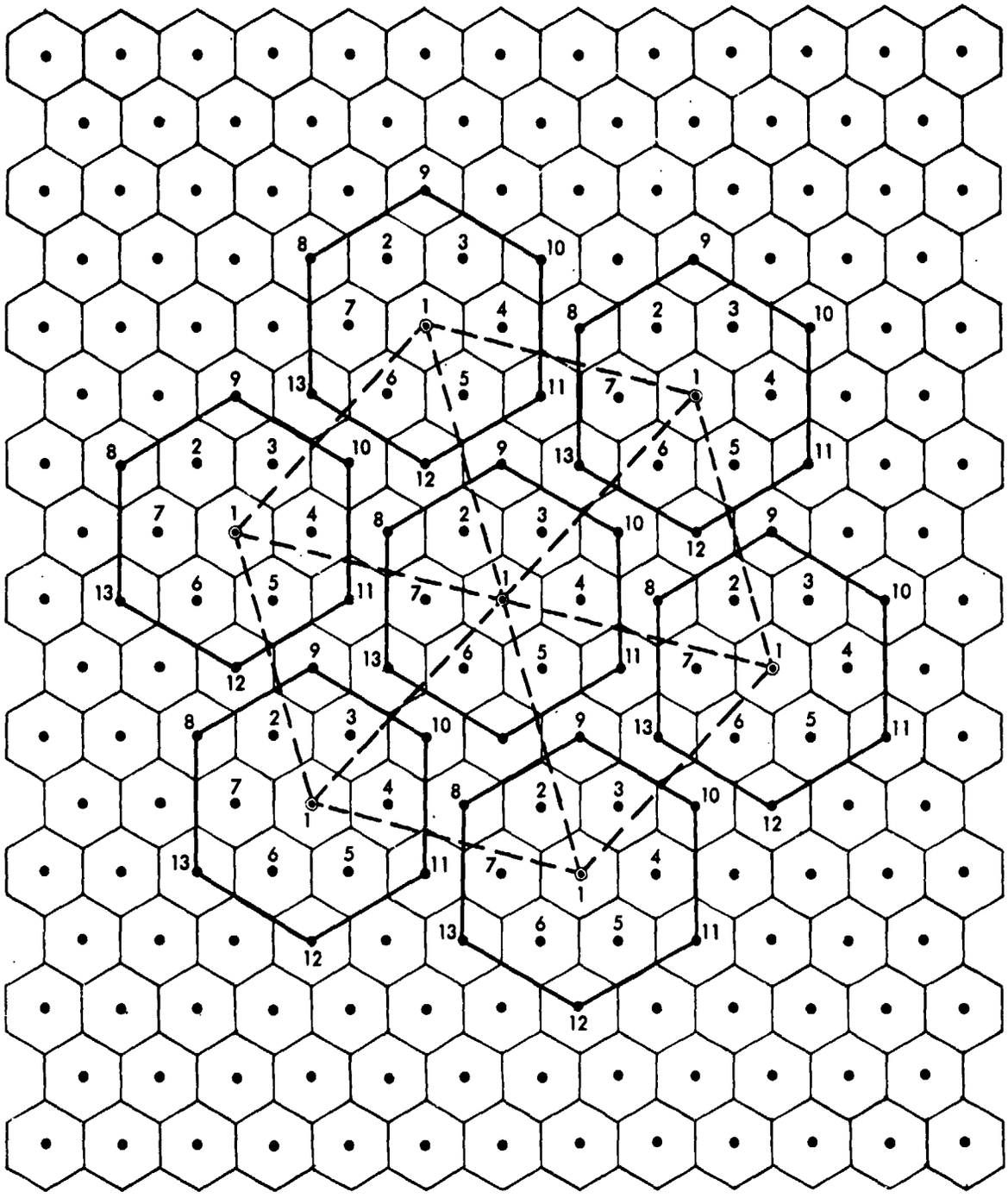

Figure 12. Layout for an Example of 13 Beams per Group. The Broken Lines Show the Distances Between Cochannel Interfering Beams Number 1 and the Desired Beam Number 1 for the Case of 91 Beams and 13 Frequencies.

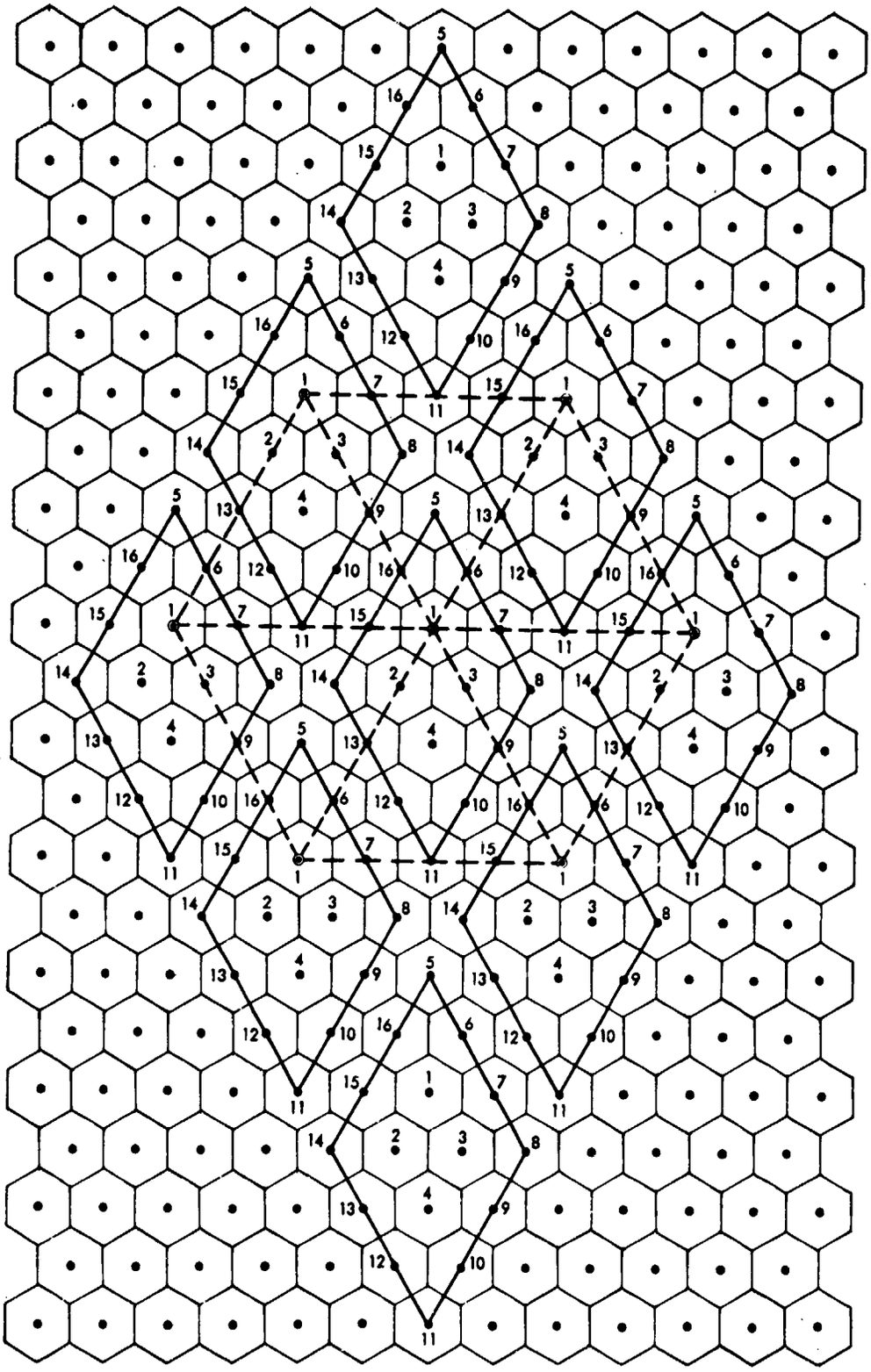

Figure 13. Layout for an Example of 16 Beams per Group. The Broken Lines Show the Distances Between Cochannel Interfering Beams Number 1 and the Desired Beam Number 1 for the Case of 112 Beams. All the Groups of Beams, Shown in this Figure, Make Up the Case of 144 Beams and 16 Frequencies.

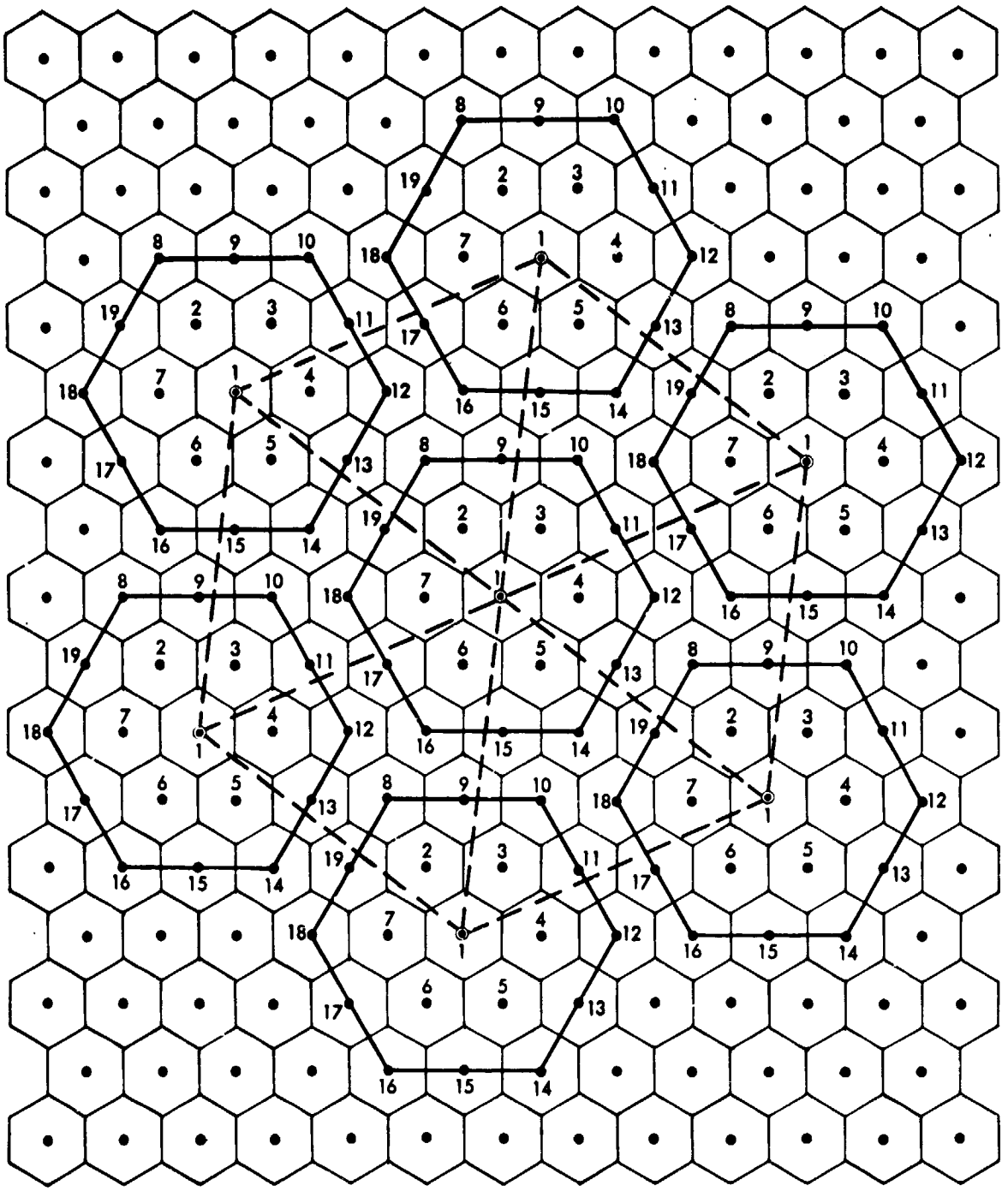

Figure 14. Layout for an Example of 19 Beams per Group. The Broken Lines Show the Distances Between Cochannel Interfering Beams Number 1 and the desired Beam Number 1 for the Case of 133 Beams and 19 Frequencies.

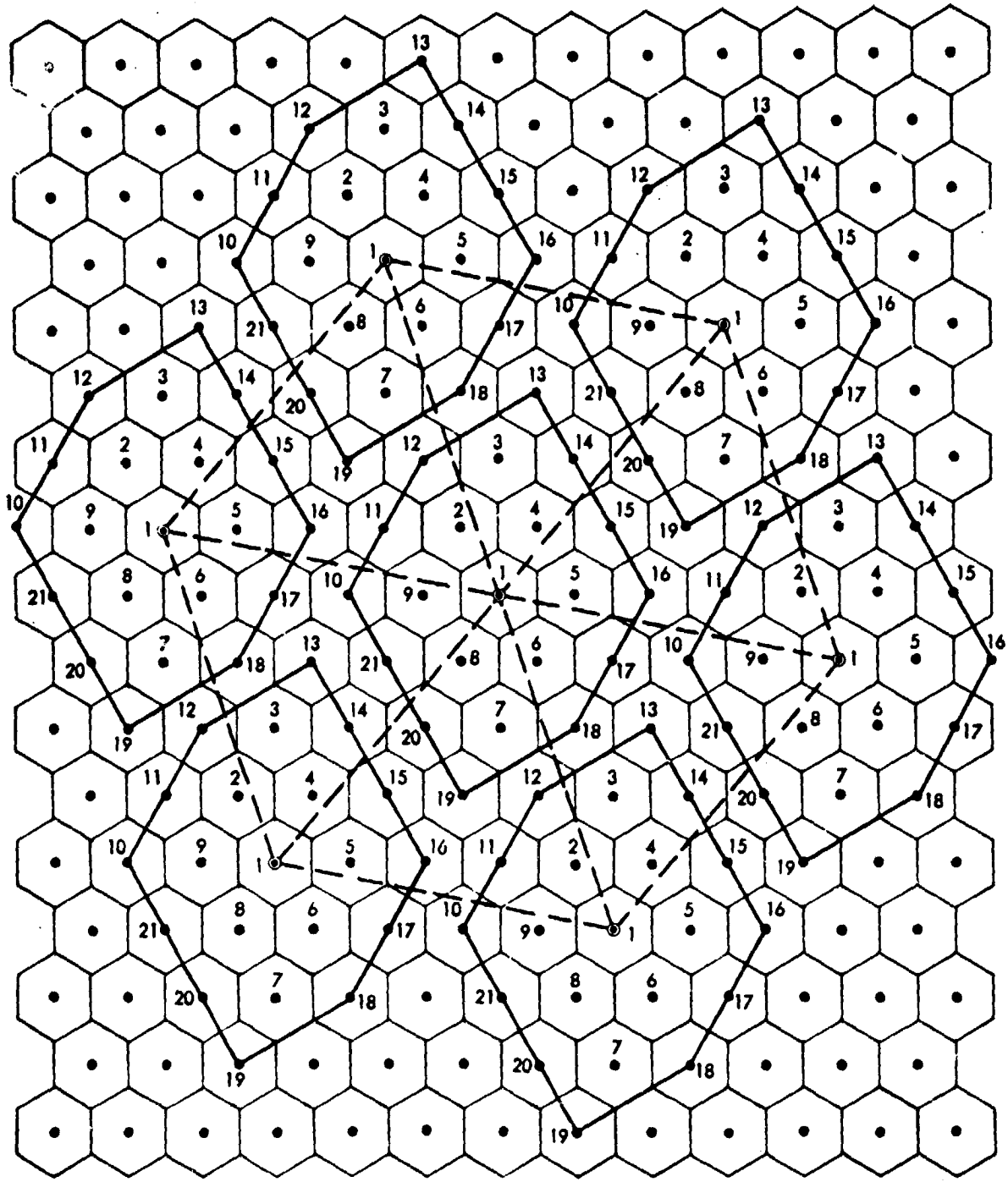

Figure 15. Layout for an Example of 21 Beams per Group. The Broken Lines Show the Distances Between Cochannel Interfering Beams Number 1 and the Desired Beam Number 1 for the Case of 147 Beams and 21 Frequencies.

SECTION 5

MULTIPLE-BEAM ANTENNA FREQUENCY REUSE CAPACITY AND INTERBEAM ISOLATION ANALYSIS: AXISYMMETRIC PARABOLIC REFLECTOR AND OFFSET-PARABOLIC REFLECTOR

In order to radiate multiple-zone coverage beams from a single antenna aperture, a multi-element feed system could be utilized to illuminate a parabolic reflector. Reflectors constitute one of the most widely used classes of large antennas. A reflector itself is quite broadband, limited at upper frequencies by its roughness. The roughness of the surface causes phase errors in the aperture field of the antenna, resulting in sidelobe level increase and peak gain decrease.

5.1 CHARACTERISTICS OF THE AXISYMMETRIC AND OFFSET-PARABOLIC REFLECTORS

Symmetrical front-fed parabolic reflectors suffer from high blockage due to feeds, feed trusses, and transmission lines. Most of the degradation in the performance of this type of antenna is due to blockage. Compared to its full-paraboloidal counterpart, the usage of an offset-reflector offers a number of advantages. The offset-reflector avoids aperture-blocking effects, reduces the reflector reaction upon the primary-feed, and leads to the use of larger focal-length to diameter ratios (F/D_p) while maintaining an acceptable structural rigidity [7]. As a consequence, the offset-reflector reduces the radiation scattering effects which results in a loss of system gain and the general degradation in the suppression of sidelobes. Also, the primary-feed VSWR can be made to be essentially independent of the reflector and can employ relatively larger radiating apertures which, in the case of multiple-element primary-feeds, will result in lower direct mutual coupling

between adjacent feed elements. These inherent advantages of the offset-reflector make the configuration attractive for use as a multiple-beam antenna. There are other advantages and disadvantages of these two reflector antennas but a rigorous comparison is beyond the scope of these notes. Figures 16 and 17 show an axisymmetric parabolic reflector antenna and the offset-parabolic reflector reference geometry.

In these reflector antennas, off-axis (scanned) beam operation results in appreciable performance degradation. This degradation is strongly related to the focal length over diameter (F/D_p) ratio of the reflector and to the aperture illumination function. Since the primary feed is made up of a multi-element arrangement, it is important to determine the effects of the off-axis location of the elements upon the antenna radiation characteristics. The principal effect of an off-axis location of the primary-feed, as the beam is scanned off the reflector axis, is in the formation of co-polarized comalobes on the side closer to the reflector axis. Other deteriorations caused by scanning the beam are comprised of beam-maximum scan loss, beam broadening, and main beam-maximum deviation. Software has been developed by Dr. Y. Rahmat-Samii of JPL [8] which takes these scan properties into account and calculates the axisymmetric and offset-parabolic reflector antenna patterns very accurately. In this report, in the case of axisymmetric reflector beam patterns, it is assumed that all beams have the same pattern and no consideration has been given to the pattern degradations caused by off-axis beam operation. This is due to the fact that the JPL developed software was not available at the time of axisymmetric reflector multiple-beam antenna study. However, for offset-reflector beam patterns, the JPL developed software was used to obtain the beam degradations due to the off-axis beam

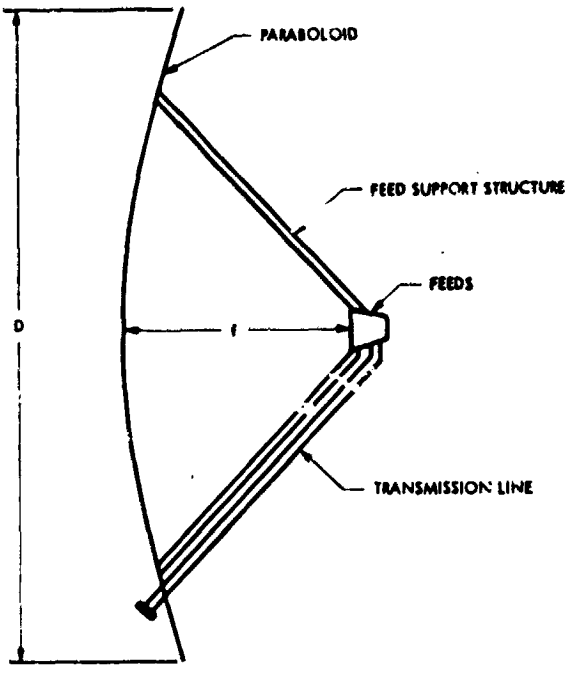

Figure 16. An Axisymmetric Parabolic Reflector Antenna

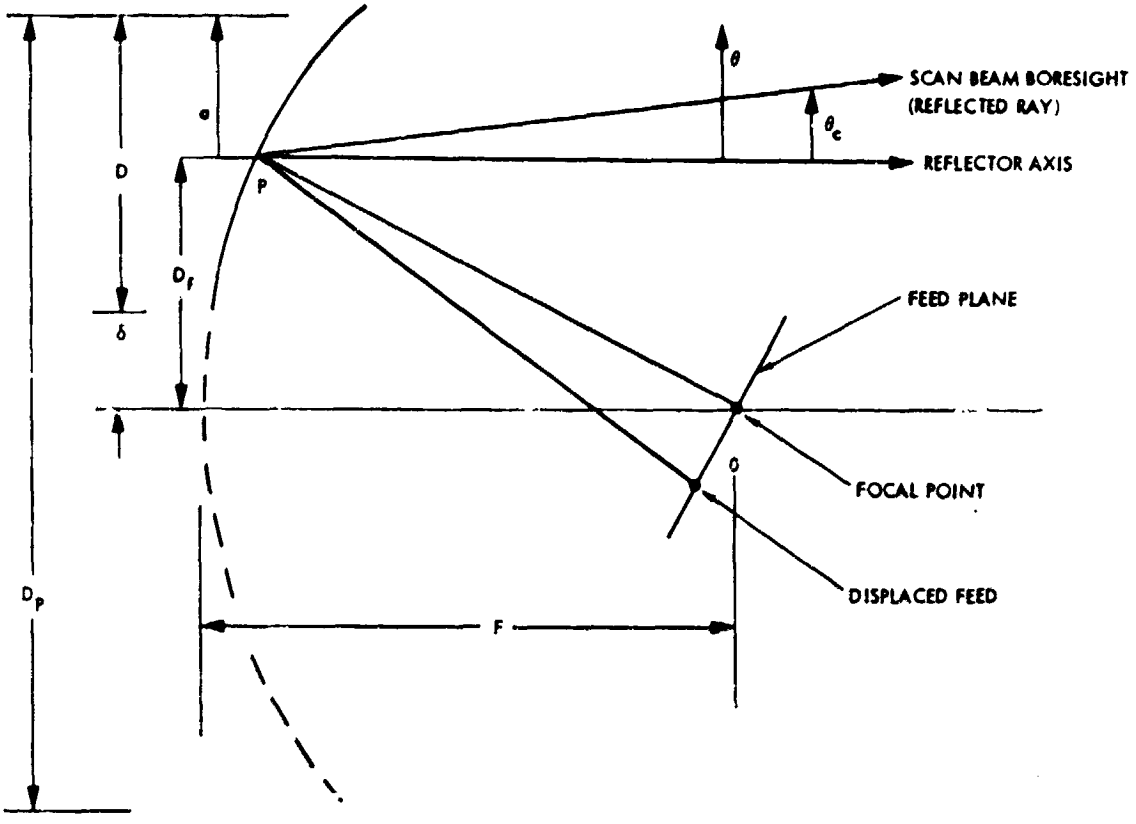

Figure 17. Offset-Parabolic Reflector Geometry

operation for each individual beam and to calculate the beam pattern model for all beams.

5.2 FREQUENCY REUSE CAPACITY AND INTERBEAM ISOLATION ANALYSIS: RESULTS FOR AXISYMMETRIC PARABOLIC REFLECTOR

The analysis done for axisymmetric parabolic reflector is included in this section.

5.2.1 Beam Pattern Model for Axisymmetric Reflector Multiple-Beam Antennas

The beam patterns used in the axisymmetric reflector case are very simple. The patterns are modified versions of the reference pattern for satellite transmitting antenna recommended at WARC-77 and CCIR(78) [1]. These model patterns possess an exponential main beam with linear sidelobe boundaries away from the main beam. Figure 18 shows these beam patterns with the following functional form:

$$
\begin{aligned}
G(\theta) &= -12\,\theta^2 && 0 \le \theta < \theta_1, \\
&= -K && \theta_1 \le \theta \le 3.16, \\
&= -C - 25\log_{10}\theta && 3.16 < \theta,
\end{aligned}
$$

where

$G(\theta)$ is the normalized gain in dB,

θ is the off-axis angle in beamwidths, and the constants K, C, and θ_1 were obtained from Figure 18 and are shown in Table 4.

These pattern models do not include degradations due to the scanned beam operation and it is assumed that all beams possess identical patterns which are circularly symmetric. An analysis, for a 100 wavelength axisymmetric

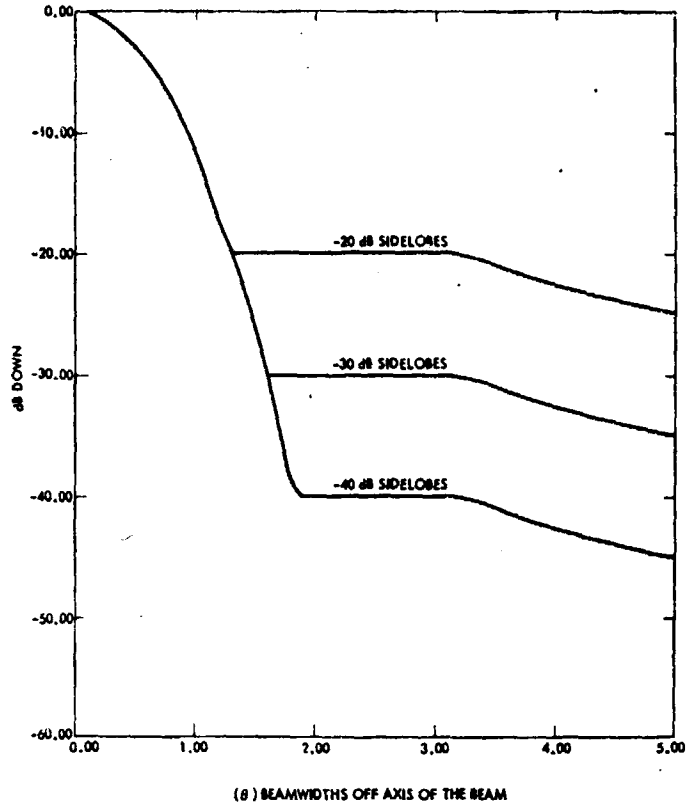

Figure 18. Modified Versions of the Reference Pattern for Satellite Transmitting Antenna Recommended at WARC-77 and CCIR(78). Modification is in the variation of sidelobe level.

TABLE 4

Exponential Pattern Function Constants

Sidelobe level, K (dB)	θ_1 (BW)	C (dB)
20	1.29	7.5
25	1.44	12.5
30	1.58	17.5
35	1.71	22.5
40	1.83	27.5

reflector antenna with $F/D_p = 1$ and varying illumination taper, done by the JPL developed software, shows that it is theoretically possible to achieve beam patterns with sidelobe envelopes very close to the sidelobe envelopes shown in Figure 18. However, since the beam patterns for each individual beam and the pattern degradations caused by off-axis beam operation were not calculated, it was assumed that all beams have the same pattern (i.e., one of the patterns shown in Figure 18).

5.2.2 Frequency Reuse Capacity and Interbeam Isolation

The relation between the number of beams and the number of frequencies for beams equally spaced in a triangular grid was described in 4.2. The relationship defines a discrete combination of a number of beams and a number of frequencies which is used to calculate a specific value of carrier-to-interference power ratio (C/I). The C/I calculation is repeated for the various allowed combinations of number of beams and number of frequencies, and the results can then be displayed as shown in Figure 19. In this figure, the C/I values of the multiple beam antenna systems are graphed as a function of number of beams. Every curve corresponds to a specific number of frequencies which was used to evaluate the C/I performance. It can be seen that the primary factor in the C/I performance level, interbeam isolation, is the frequency reuse factor (frequency reuse factor is defined as the total number of beams divided by the number of frequencies).

5.2.3 Sidelobe Level Analysis

Figure 19 was shown for a modified CCIR reference pattern with sidelobes starting at -20 dB level. Figures 20, 21, 22 and 23 were obtained for the

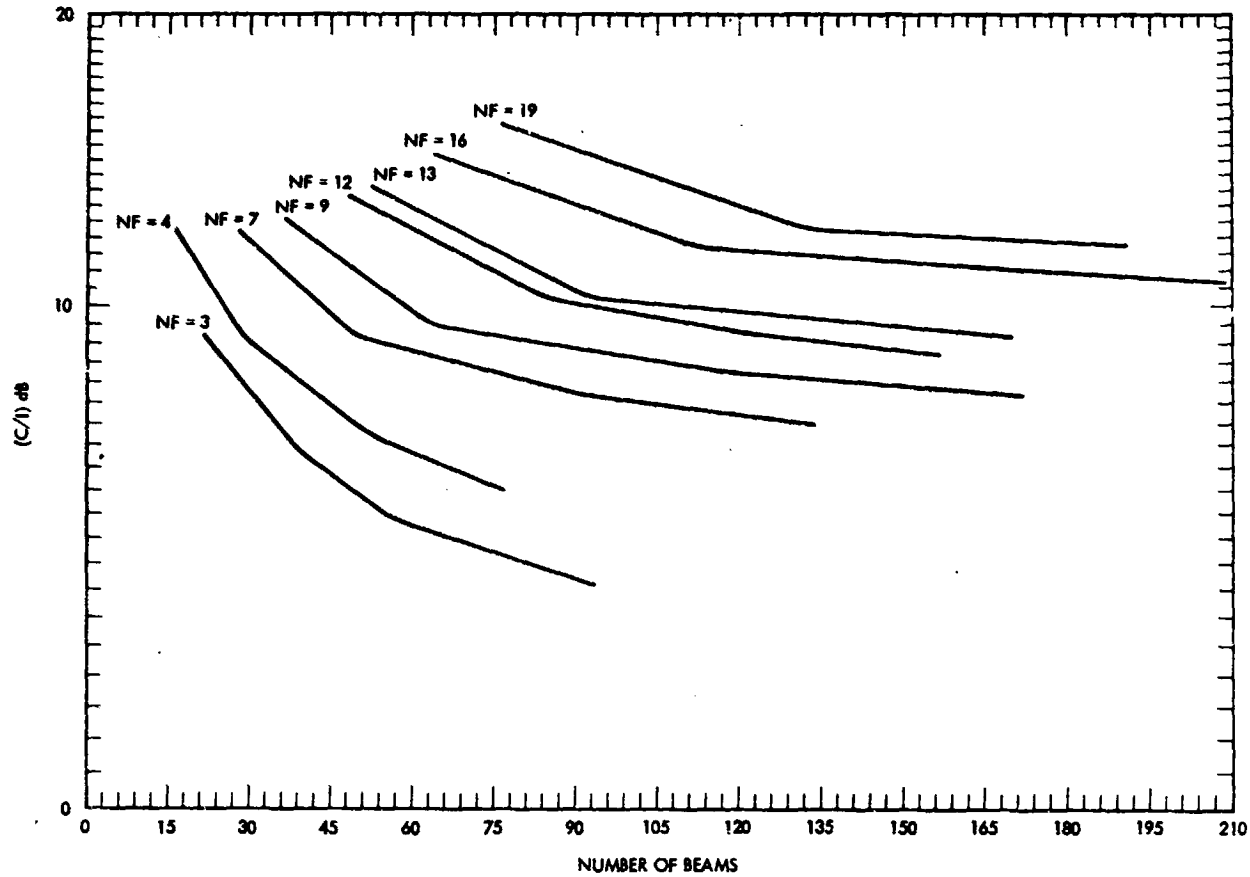

Figure 19. Frequency Reuse Capacity, Axisymmetric Reflector
Modified CCIR reference pattern with -20 dB sidelobes
Calculation Point: -3 dB down from peak of the main beam
Beam Separation: 1 HPBW of the main beam

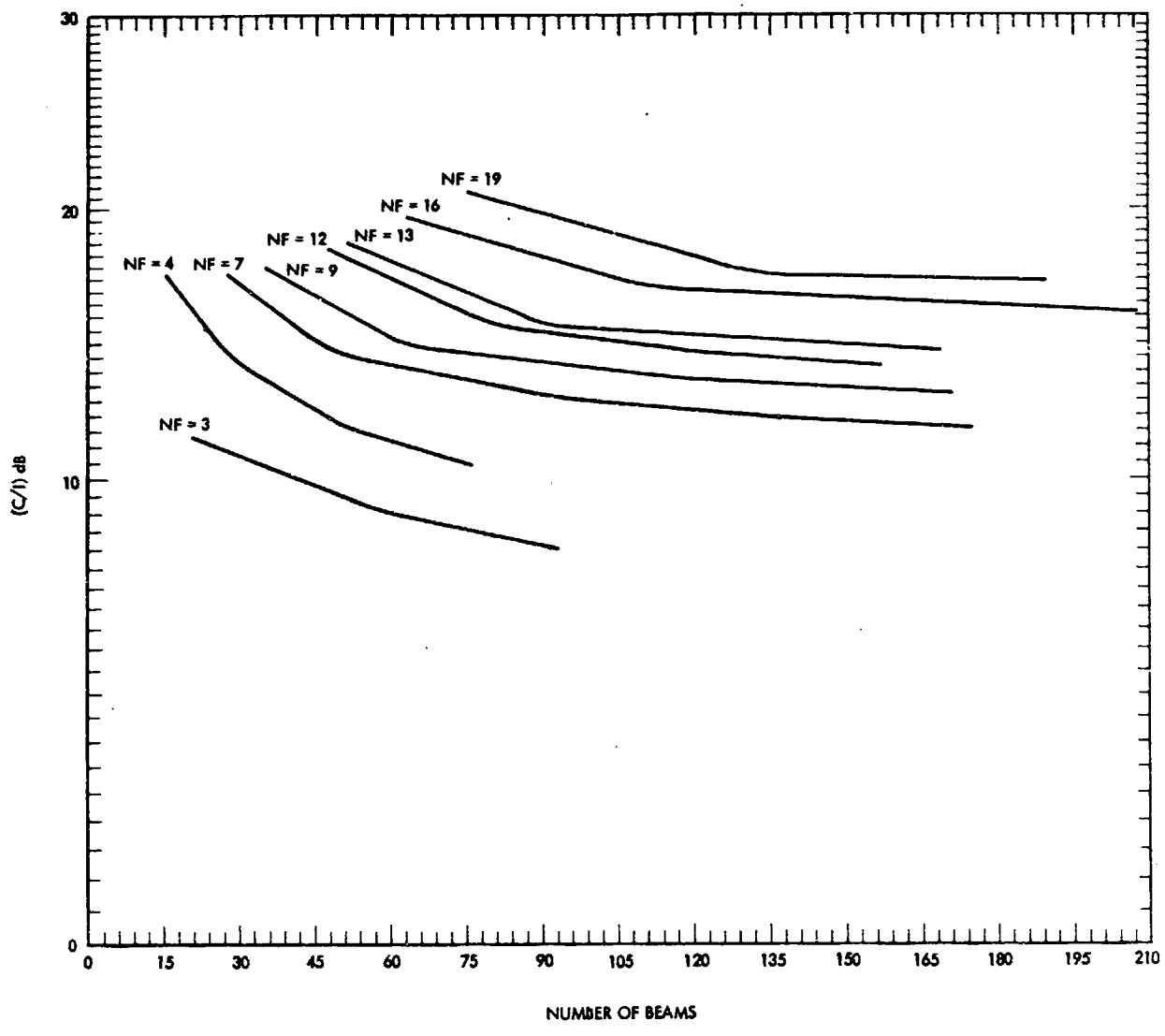

Figure 20. Frequency Reuse Capacity, Axisymmetric Reflector
Modified CCIR reference pattern with -25 dB sidelobes
Calculation Point: -3 dB down from peak of the main beam
Beam Separation: 1 HPBW of the main beam

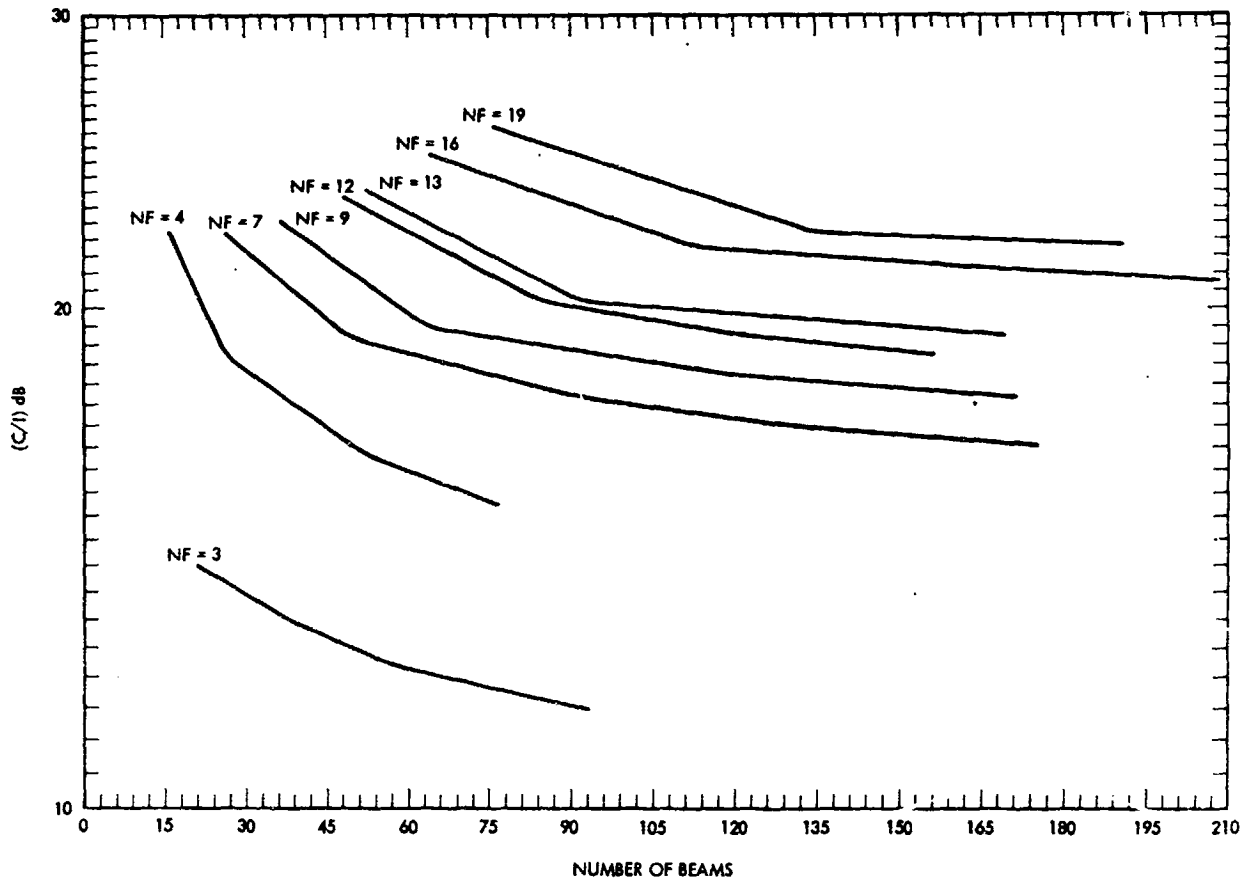

Figure 21. Frequency Reuse Capacity, Axisymmetric Reflector
Modified CCIR reference pattern with -30 dB sidelobes
Calculation Point: -3 dB down from peak of the main beam
Beam Separation: 1 HPBW of the main beam

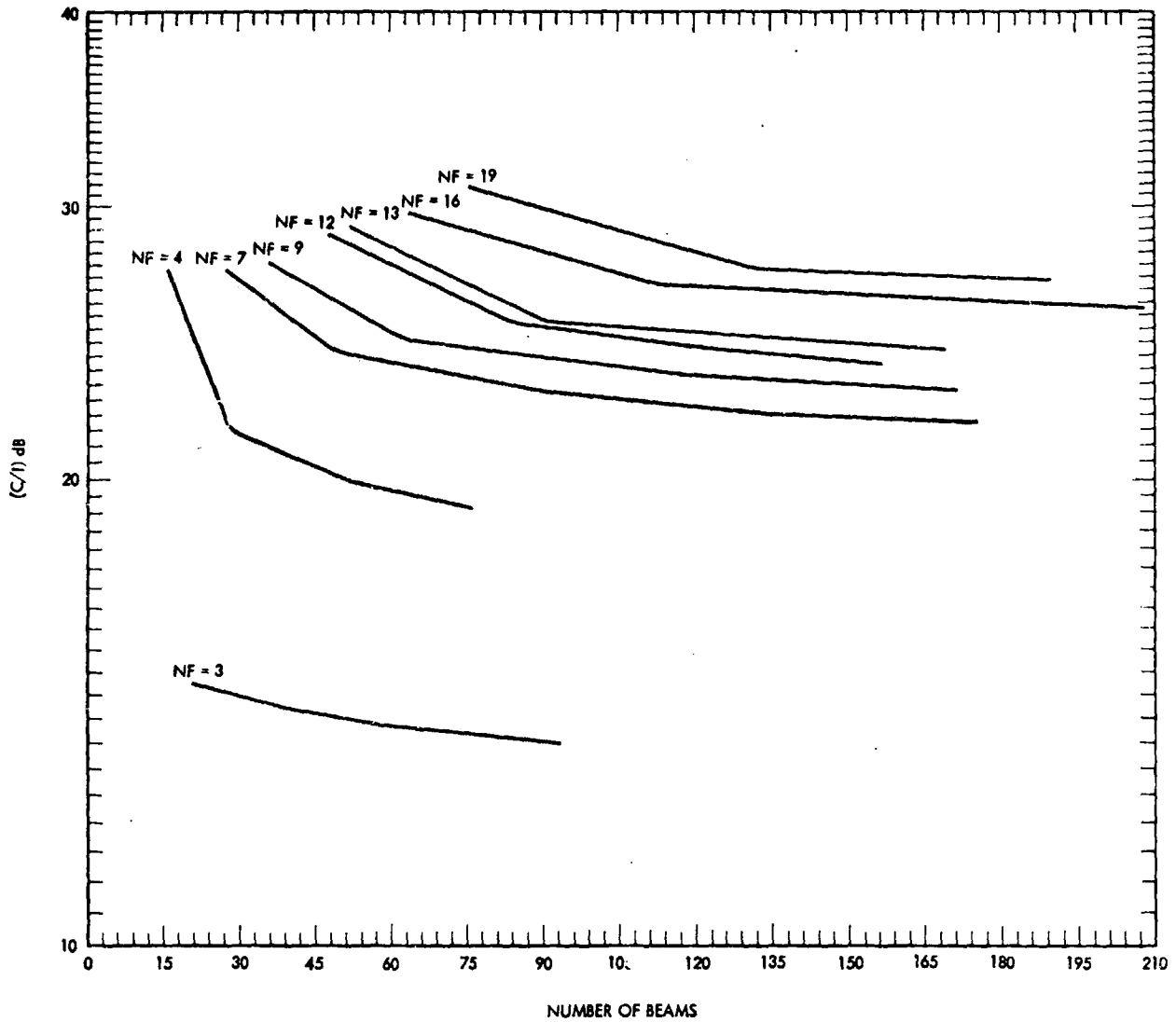

Figure 22. Frequency Reuse Capacity, Axisymmetric Reflector
Modified CCIR reference pattern with -35 dB sidelobes
Calculation Point: -3 dB down from peak of the main beam
Beam Separation: 1 HPBW of the main beam

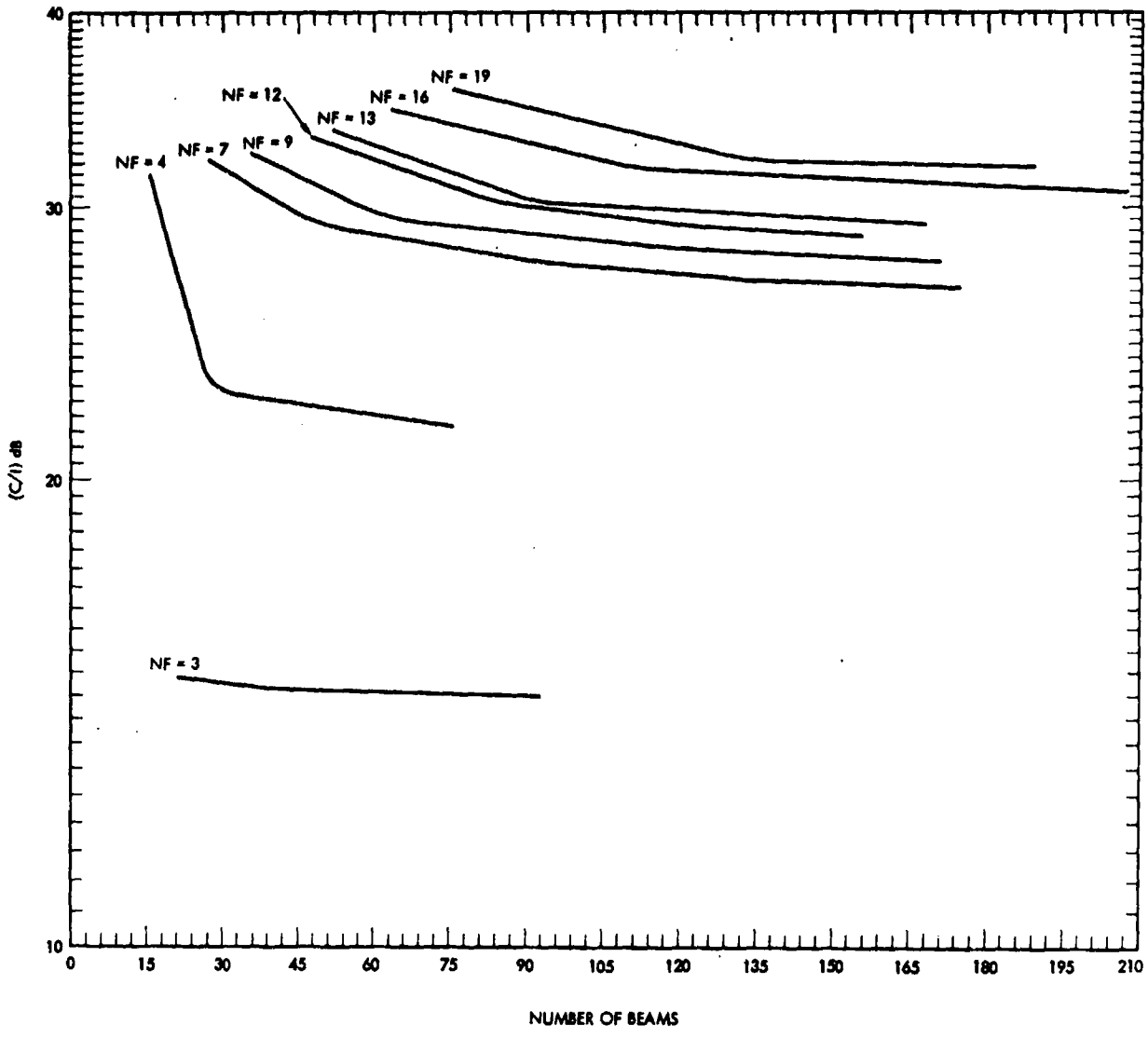

Figure 23. Frequency Reuse Capacity, Axisymmetric Reflector
Modified CCIR reference pattern with -40 dB sidelobes
Calculation Point: -3 dB down from peak of the main beam
Beam Separation: 1 HPBW of the main beam

same beam pattern with the value of sidelobe envelope varying from -25 dB to -40 dB. From these curves, it can be seen that a change in number of frequencies from 3 to 4 causes a considerable change in the C/I value (about 8-17 dB) for sidelobe levels of -30 dB and lower. But, for example, a change from 12 to 13 frequencies does not cause any appreciable change as the sidelobe levels are varied. So as the number of frequencies increases, the frequency reuse factor becomes less sensitive to it. Figures 24 and 25 show the effect of different sidelobe levels when a different number of frequencies is employed and compares the C/I values obtained for these different sidelobe levels. It can be seen that the sidelobe level has a more noticeable effect for larger number of beams when smaller number of frequencies are used as shown in Figure 24. Overall, the sidelobe level has a much greater effect when a larger number of frequencies is used (see Figure 25).

5.2.4 Crossover Level and Footprint Level Sensitivity

In Section 4.2, it was explained that an optimum layout of the beams is achieved by dividing the total number of beams into groups of beams such that each beam in a group utilizes a different frequency-band. A single frequency-band can be used only by one beam in each group and the number of cochannel beams can be as large as the number of groups. This type of beam layout insures the fact that no two adjacent beams are on the same frequency. Therefore, the usual considerations of the crossover level of two adjacent beams could not be as meaningful in this case. But, for instance, in the case of mobile satellite services, it is required to have continuous coverage beams and C/I values should be known at the coverage area boundaries (see Figure 4). So it is important to know the C/I variations at these boundaries as the beam spacing is varied. Figure 26 shows the relation between the C/I

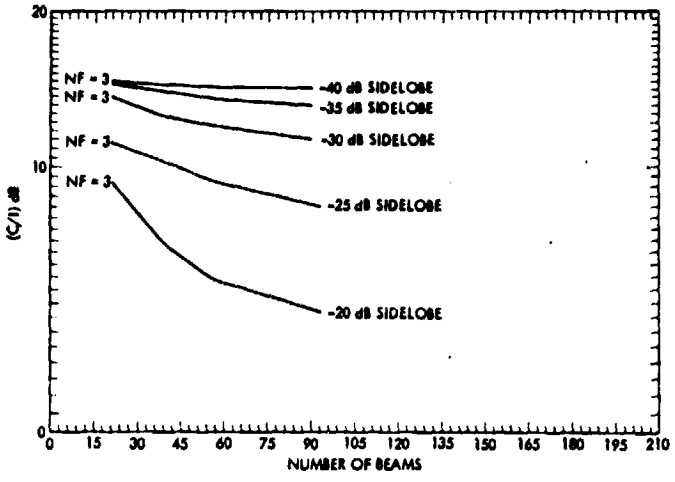

Figure 24. Frequency Reuse Capacity, Axisymmetric Reflector
Modified CCIR reference pattern
Comparison of (C/I) values for five sidelobe levels,
3 frequencies
Calculation Point: -3 dB down from peak of the main beam
Beam Separation: 1 HPBW of the main beam

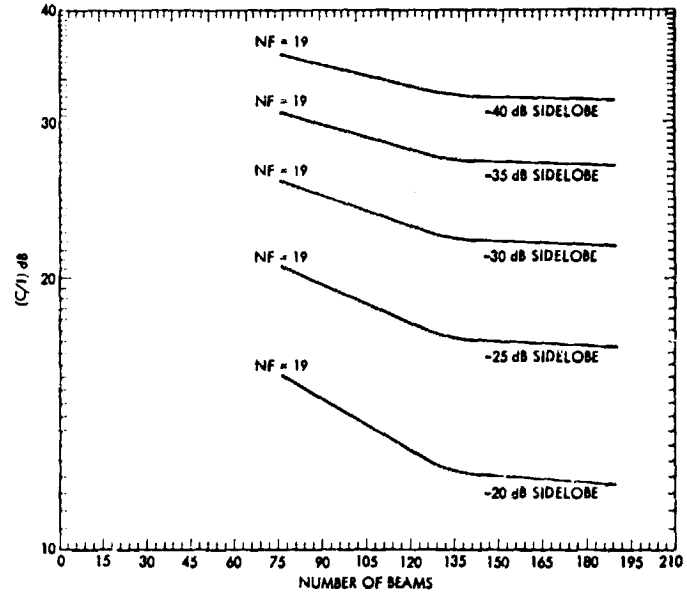

Figure 25. Frequency Reuse Capacity, Axisymmetric Reflector
Modified CCIR reference pattern
Comparison of (C/I) values for five sidelobe levels,
19 frequencies
Calculation Point: -3 dB down from peak of the main beam
Beam Separation: 1 HPBW of the main beam

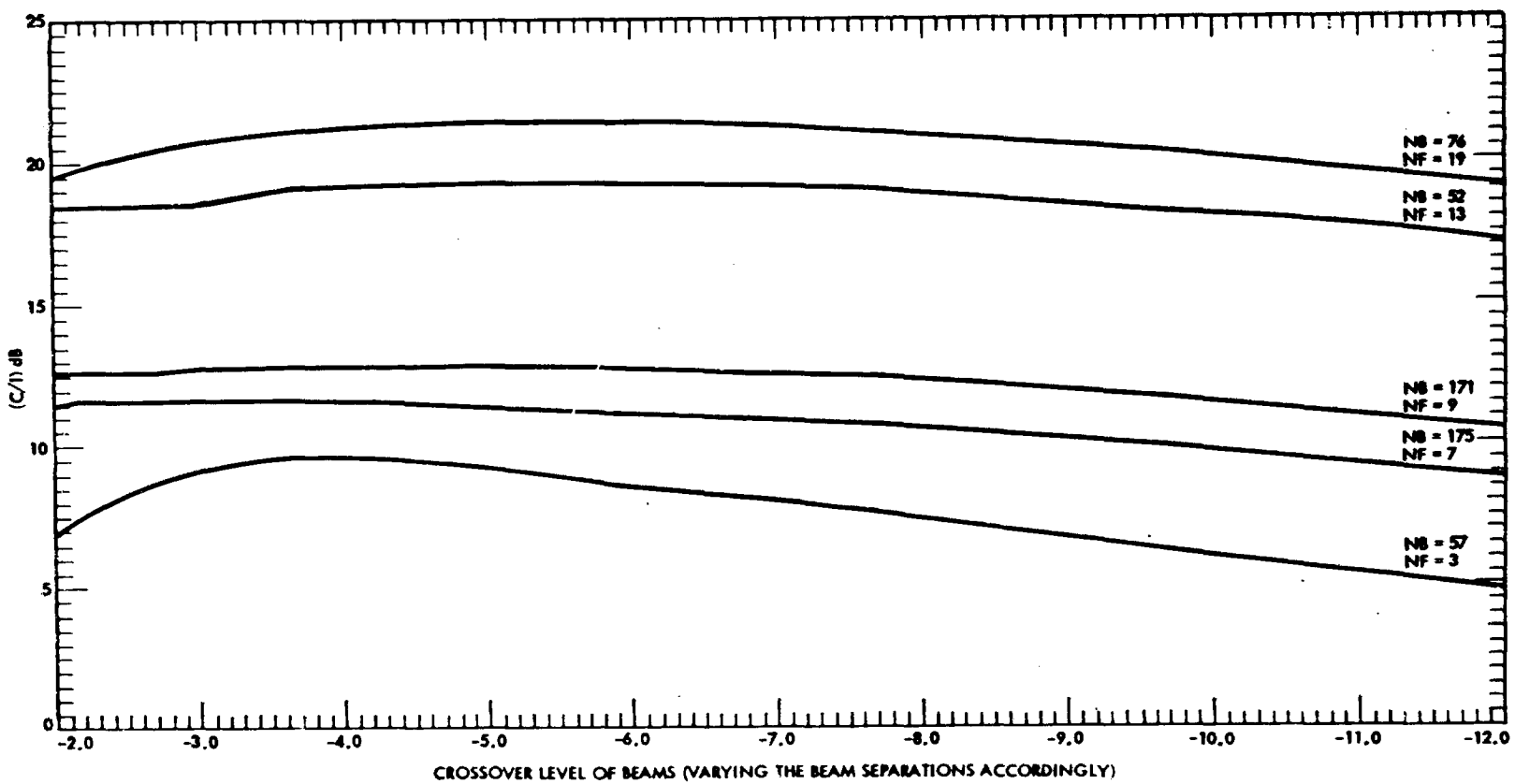

Figure 26. Crossover Level Sensitivity, Axisymmetric Reflector
Modified CCIR reference pattern with -25 dB sidelobes
Calculation Point: See Table 3
Beam Separation: See Table 3

and crossover level for the modified CCIR reference pattern with sidelobes starting at -25 dB level. Table 5 shows the relationship between the beam separation values, distance between the centers of two adjacent beam, and the footprint levels at the crossover points for the modified CCIR reference pattern with -25 dB sidelobes. Notice that the calculation point is located at the midway point of the line between the center of the desired beam and the center of the adjacent beam. In Figure 26, C/I values as a function of the beam crossover levels are given for five multiple-beam antenna systems with different number of frequencies and number of beams. Again, notice that the C/I values are relatively insensitive to the crossover levels of between -2 to -7 dB for very large number of beams and -5 to -7 dB for smaller number of beams with higher number of frequencies. In this case, for an axisymmetric reflector antenna, the optimum crossover level is dependent on the number of beams and frequencies.

In the Final Acts of the 1977 International Telecommunication Union Broadcasting Satellite Conference, Annex 8, the beam area was defined as the area on the earth's surface corresponding to the -3 dB points on the satellite radiation pattern, "The area delineated by the intersection of the half-power beams of the satellite transmitting antenna with the surface of the earth." Also, it is mentioned that for a service area when the maximum dimension as seen from the satellite position is more than 0.6° (the agreed minimum practicable satellite antenna half-power beamwidth), the beam area would almost coincide with the coverage area. If the maximum dimension is less than 0.6°, there could be a significant difference between the beam area and the coverage area. In the case of U.S. coverage the maximum dimension as seen from the satellite position is around 7.3°, but for a multiple-beam antenna with large number of beams (i.e., 75 beams) this maximum dimension for

TABLE 5

Relationship Between the Crossover Levels and Beam Separation Values for Modified CCIR Reference Pattern (-25 dB Sidelobes)

Beam Separation (HPBW)	Calculation Point (HPBW)	Crossover Level (dB)
0.80	0.40	-1.92
0.85	0.425	-2.17
0.90	0.45	-2.43
0.95	0.475	-2.71
1.00	0.50	-3.00
1.10	0.55	-3.63
1.20	0.60	-4.32
1.30	0.65	-5.07
1.40	0.70	-5.88
1.50	0.75	-6.75
1.60	0.80	-7.68
1.80	0.90	-9.72
2.00	1.00	-12.00

individual beams is less than or equal to 0.6°. For this reason the C/I values, in Figures 19-23, were evaluated at -3 dB footprint level of the main beam. However, since the maximum dimension as seen from the satellite by the individual beams could be less than 0.6°, the relationship between the C/I performance of the system, with constant beam separations, and the desired beam footprint level should be analyzed. Figures 27 and 28 show the relationship between the C/I values, obtained for the modified CCIR pattern with different sidelobe levels, and the footprint level of the desired beam

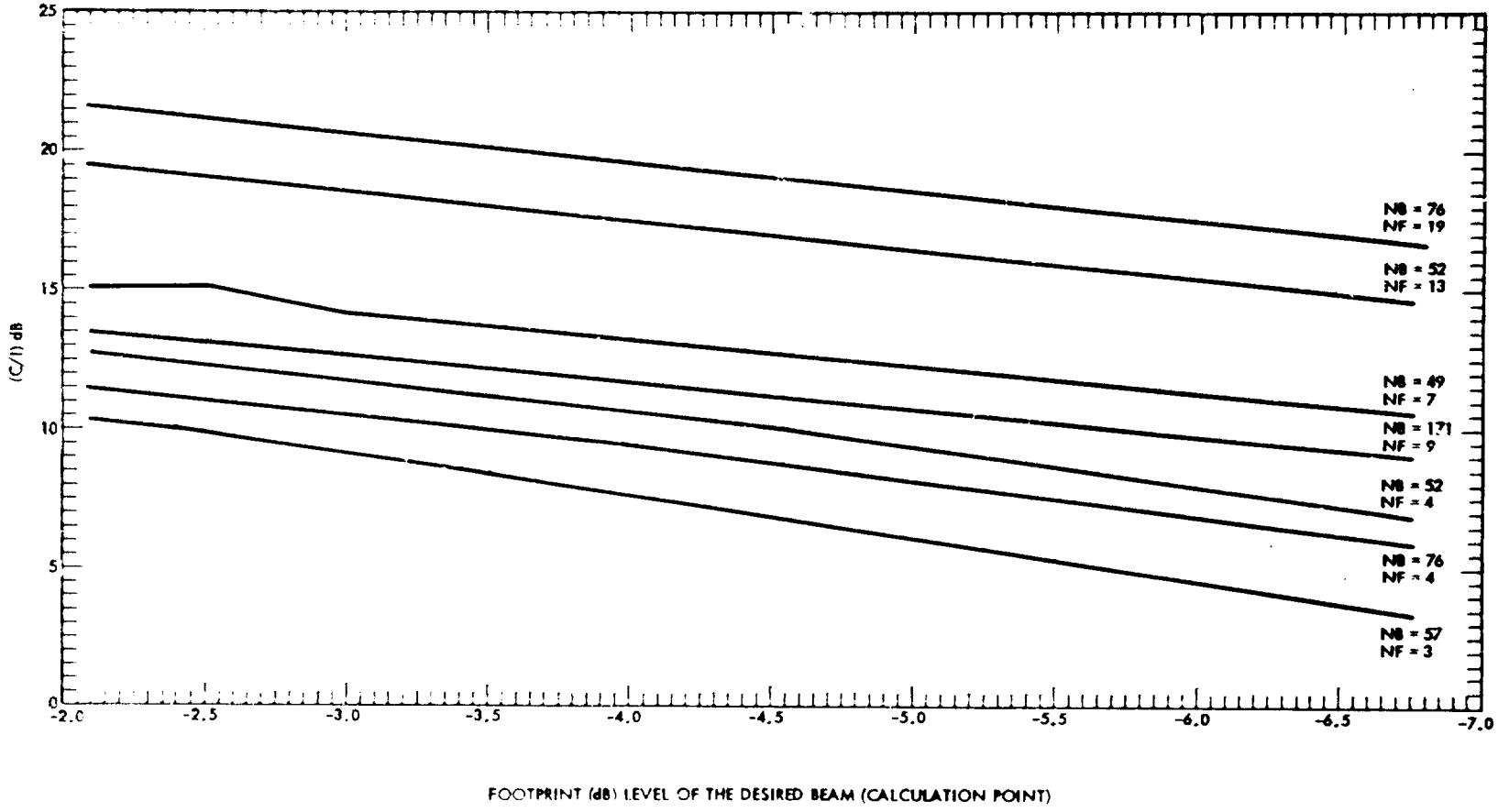

Figure 27. (C/I) Performance Calculated at Different Footprint (dB) Levels of the Desired Beam, Axisymmetric Reflector
Modified CCIR reference pattern with -25 dB sidelobes
Beam Separation: 1 HPBW of the main beam

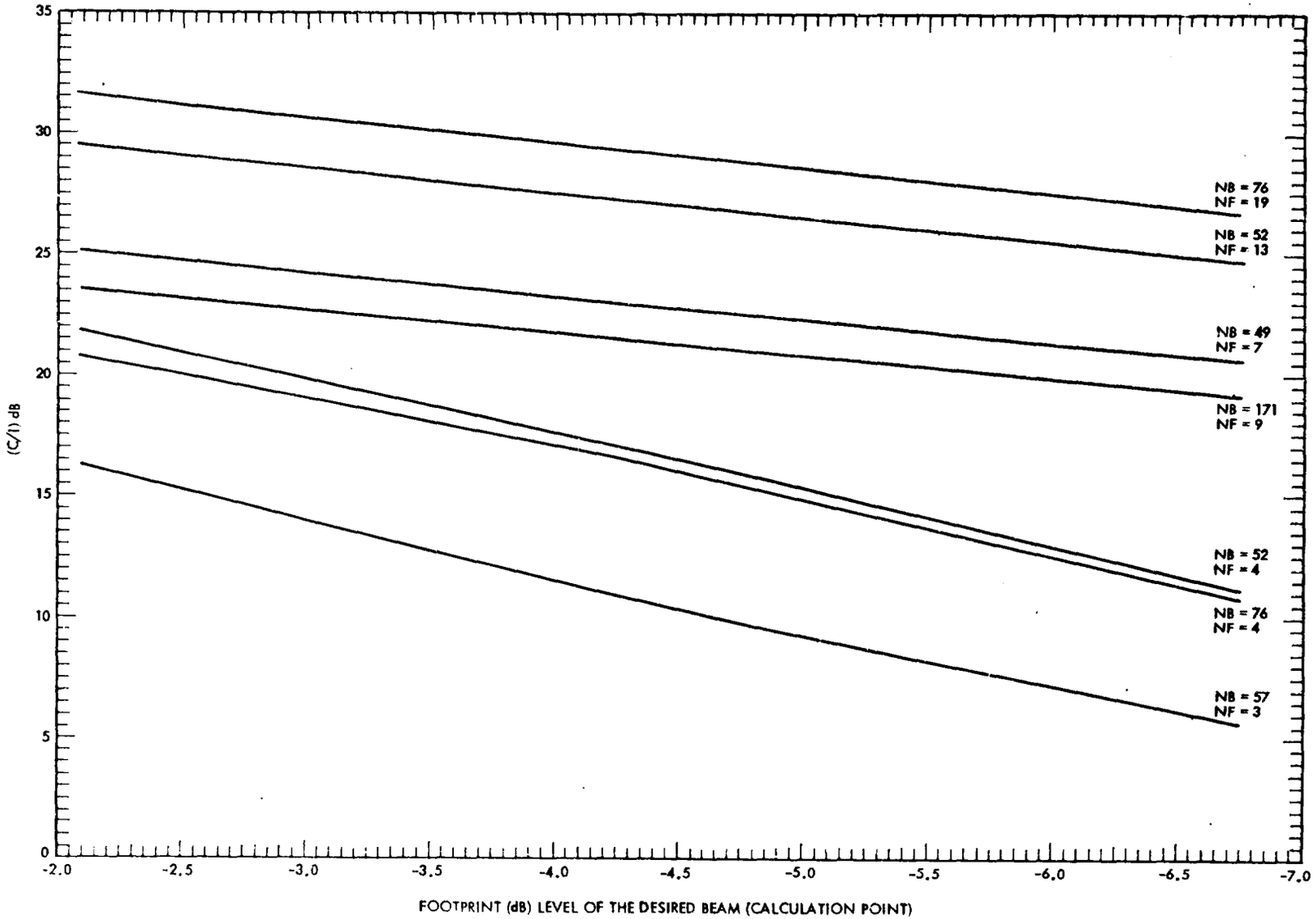

Figure 28. (C/I) Performance Calculated at Different Footprint (dB) Levels of the Desired Beam, Axisymmetric Reflector
Modified CCIR reference pattern with -35 dB sidelobes
Beam Separation: 1 HPBW of the main beam

for different numbers of beams and frequencies. Figure 29 shows the comparison made to see the effects of the variations of the footprint level on the C/I performance as the sidelobe levels are varied. It could be seen that in all the cases the C/I values are almost linearly decreasing function of decreasing footprint level (or increasing footprint area).

5.2.5 Beam Spacing

It was mentioned that the minimum separation between the feeds is limited by the mutual coupling between the elements and the physical size of the feeds. On the optimal focal plane, feeds should be placed as close as possible to the reflector focal point; so the beam degradations due to the off-axis location of the primary-feeds are minimized.

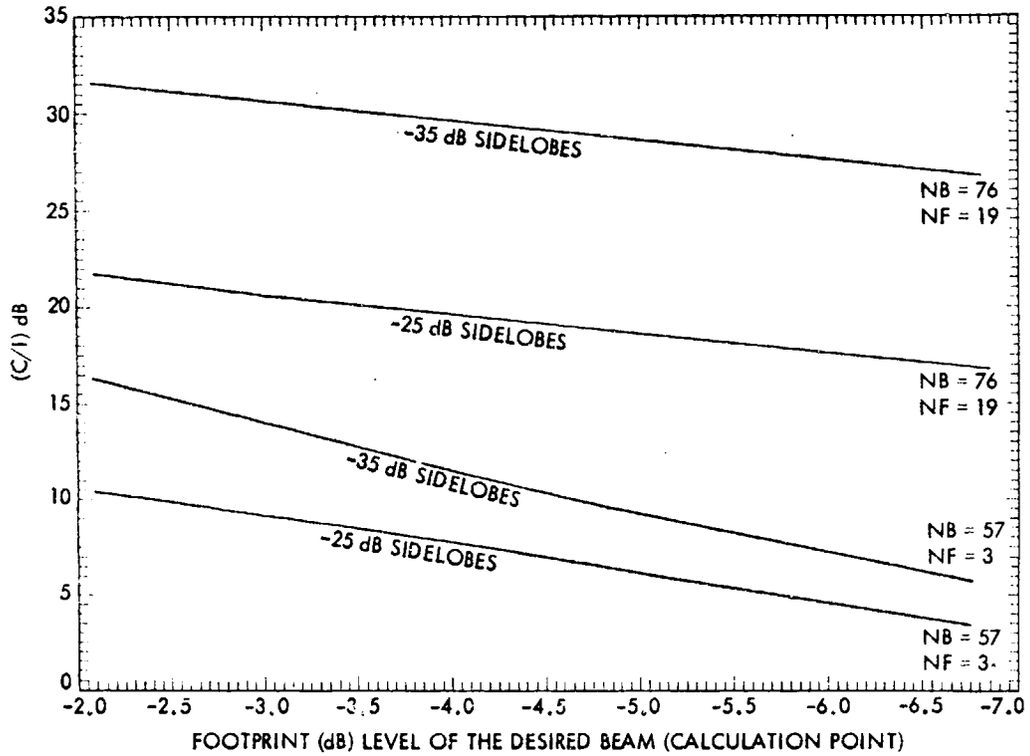

Figure 29. (C/I) Performance Calculated at Different Footprint (dB) Levels of the Desired Beam, Comparison for 2 Sidelobe Levels Modified CCIR reference pattern, axisymmetric reflector Beam Separation: 1 HPBW of the main beam

If a "complex-feed" design is used, as opposed to the "simple-feed" approach, there are certain conditions to be met [2]. The complex-feed concept effectively combines certain phased-array techniques with reflector-antenna techniques. The primary advantage of the complex-feed design is in its ability to achieve limited beam-steering or generate closely-spaced beams. This is due to the fact that in a complex-feed a number of elements may be employed to generate each radiated beam and each feed element may contribute to more than one radiated beam. Since the shape of the feed radiation pattern is governed largely by the combined array characteristics of the multiple elements, rather than by the radiation characteristics of the individual feeds, the avoidance or suppression of the feed-array grating-lobe effects becomes extremely important. The maximum separation between the feed elements is constrained by the generation of grating lobes in the feed radiation pattern which will exist within the spatial solid-angle subtended by the reflector. It has been shown [2] that in order to provide closely-spaced beams without generation of grating lobes in the feed radiation-pattern, the interelement spacing must be less than

$$\delta = \frac{\lambda}{2 \sin \theta^*} ,$$

where δ is the inter-element spacing and θ^* is the maximum half-angle subtended by the reflector at the geometric focus.

Since the relative position of the feeds, "simple feeds", on the optimal focal plane determines the relative location of the beams within the coverage area, the C/I performance of the system, with a constant footprint level, as a function of beam spacing was studied. In Figures 30 and 31, the results are shown for seven multiple-beam antenna systems with different number of beams

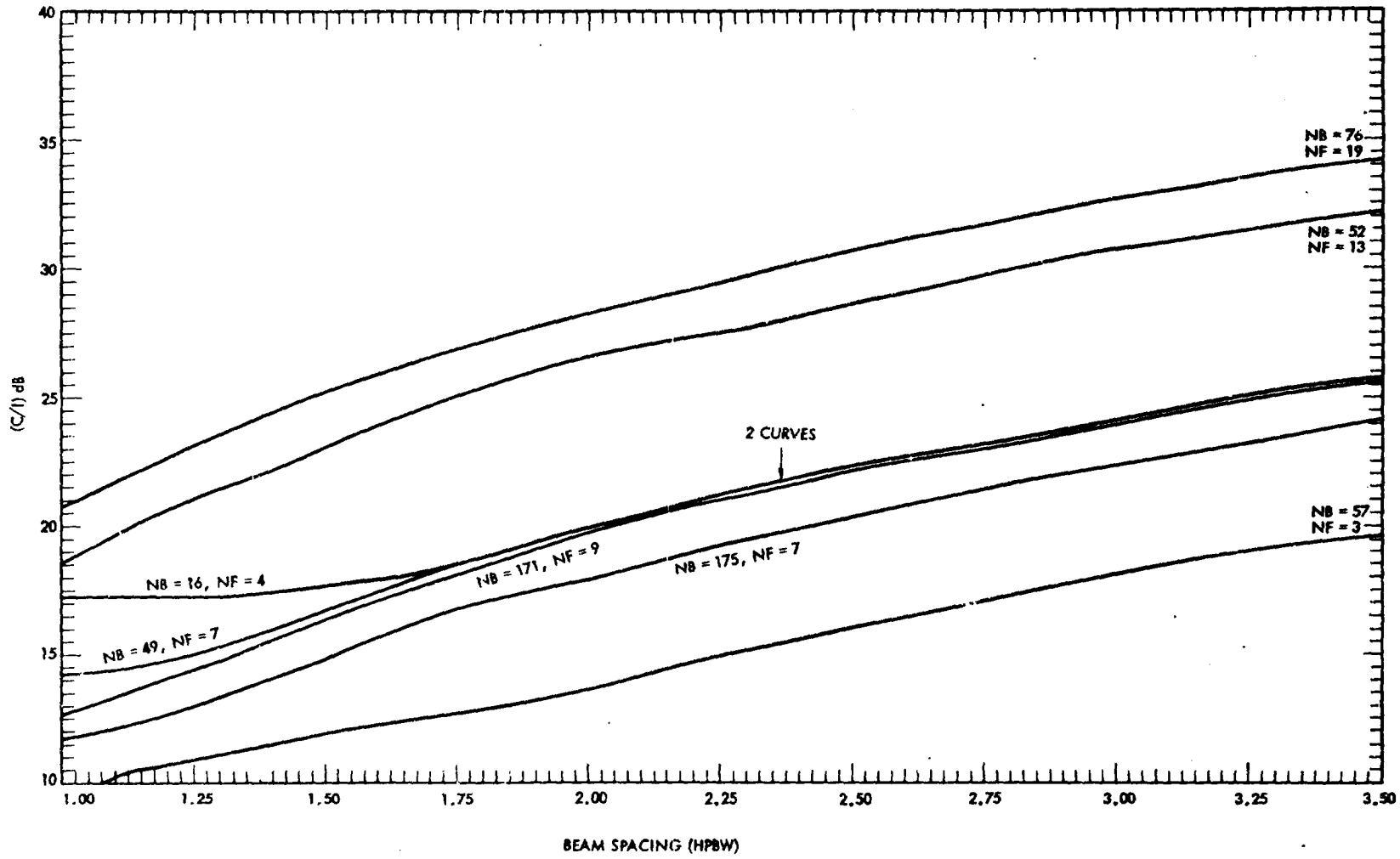

Figure 30. (C/I) Performance as a Function of Beam Spacing (HPBW)
Modified CCIR reference pattern with -25 dB sidelobes,
axisymmetric reflector
Calculation Point: -3 dB down from peak of the main beam

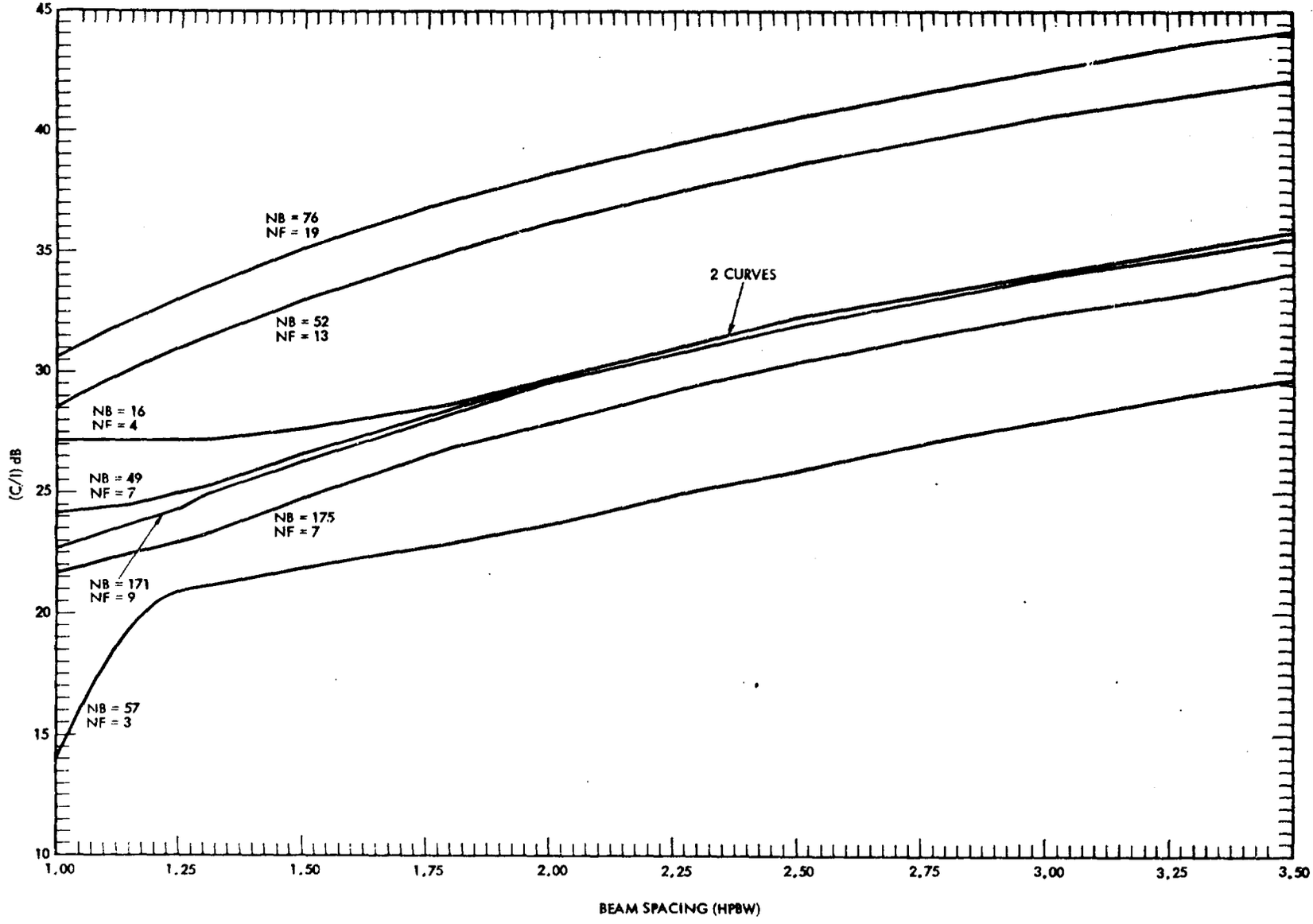

Figure 31. (C/I) Performance as a Function of Beam Spacing (HPBW)
Modified CCIR reference pattern with -35 dB sidelobes,
axisymmetric reflector
Calculation Point: -3 dB down from peak of the main beam

and frequencies. A comparison of the effects of beam spacing variations on the C/I performance as the sidelobe levels are varied is shown in Figure 32. It should be of interest to remember that a specific combination of beam spacing variations and footprint level variations generates the crossover level variations shown in Figure 26.

5.2.6 Conclusions

The results presented here show that the sidelobe characteristics and beam spacing are the primary influence on frequency reuse capacity of a multiple-beam antenna with a specific number of beams and frequencies, as expected. However, as the number of frequencies increases, the frequency reuse factor becomes less sensitive to the sidelobe levels, but the C/I performance of the system improves (see 5.2.3). Also, it has been shown that the sidelobe levels have a more noticeable effect for larger number of beams when smaller number of frequencies are used.

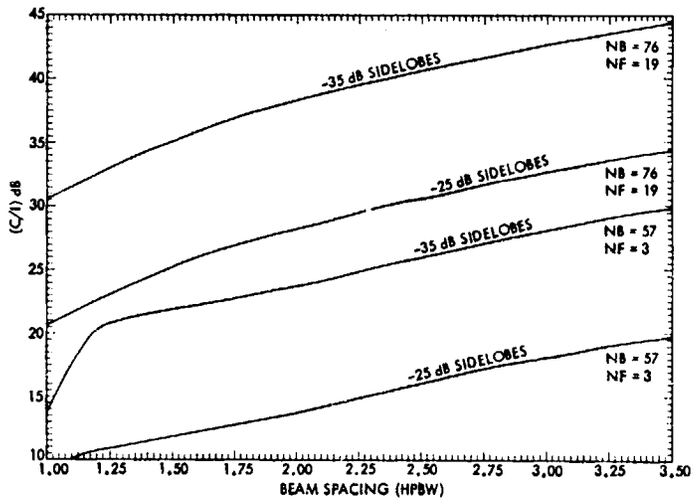

Figure 32. (C/I) Performance as a Function of Beam Spacing (HPBW)
Comparison for 2 sidelobe levels, axisymmetric reflector
Modified CCIR reference pattern
Calculation Point: -3 dB down from peak of the main beam

The other important fact discovered for the axisymmetric reflector multiple-beam antenna, with identical beam patterns, is that the optimum crossover level is dependent on the number of beams and frequencies. The relationship between the interbeam isolation values and decreasing footprint levels of the desired beam was shown to be an approximately linearly decreasing function. For increasing values of beam spacing, the C/I values have an approximately linear increase.

5.3 FREQUENCY REUSE CAPACITY AND INTERBEAM ISOLATION ANALYSIS: RESULTS FOR OFFSET-PARABOLIC REFLECTOR

In this section the results of the analyses done for offset-parabolic reflectors are explained. The basic approach to find the frequency reuse factor and interbeam isolation for offset-parabolic reflectors is the same as before with the exception of the more sophisticated beam pattern models as discussed below.

5.3.1 Beam Pattern Model for Offset-Parabolic Reflector Multiple-Beam Antennas

It was discussed that an off-axis location of the primary-feed causes deteriorations in the beam radiation-pattern, which are comprised of beam-maximum scan loss, beam broadening, main beam-maximum deviation, and most importantly the formation of co-polarized comalobes on the side closer to the reflector axis.

In Figure 17, the feed is displaced on the optimal plane, which is normal to the line joining the focal point 0 to the center of reflector P. In each case the feed is tilted in a manner that its beam boresight axis goes through the Point P. In the present analysis, the patterns are assumed to be circularly symmetric about the scanned beam boresight, and the scan properties

are assumed to depend only on the angle between the scanned beam boresight and the reflector axis (i.e., the scan angle). It was mentioned that for a scanned beam, sidelobes closer to the reflector axis have the most degradation. In addition, it has been shown [9] that when the primary-feed is displaced downward in the optimal plane (see Figure 17), or the beam is scanned in a counterclockwise manner with respect to the reflector axis, this would provide the most pattern degradation. These "worst case" sidelobes were used to obtain the sidelobe envelope coefficient for the pattern model. A pictorial description of the beam radiation-pattern model for the offset-reflector case is shown in Figure 33.

The theoretical model for the main beam shape and sidelobe envelope of a scanned beam, offset-reflector scan, has two primary simplifying assumptions:

(1) The far-field pattern is only a function of the beam scan angle, θ_c, in the plane of symmetry, and

(2) The far-field pattern is circularly symmetric about the scanned beam boresight.

In Figure 33, the main beam function is composed of

$$G_M(\theta, \theta_c) = G_p(\theta_c) + G_s(\theta, \theta_c) \text{ (dB)},$$

where

$G_p(\theta_c)$ = scan loss at a scan angle θ_c,

$G_s(\theta, \theta_c)$ = main beam pattern relative to its peak at $\theta = \theta_c$, and

θ = pattern angle measured relative to reflector axis.

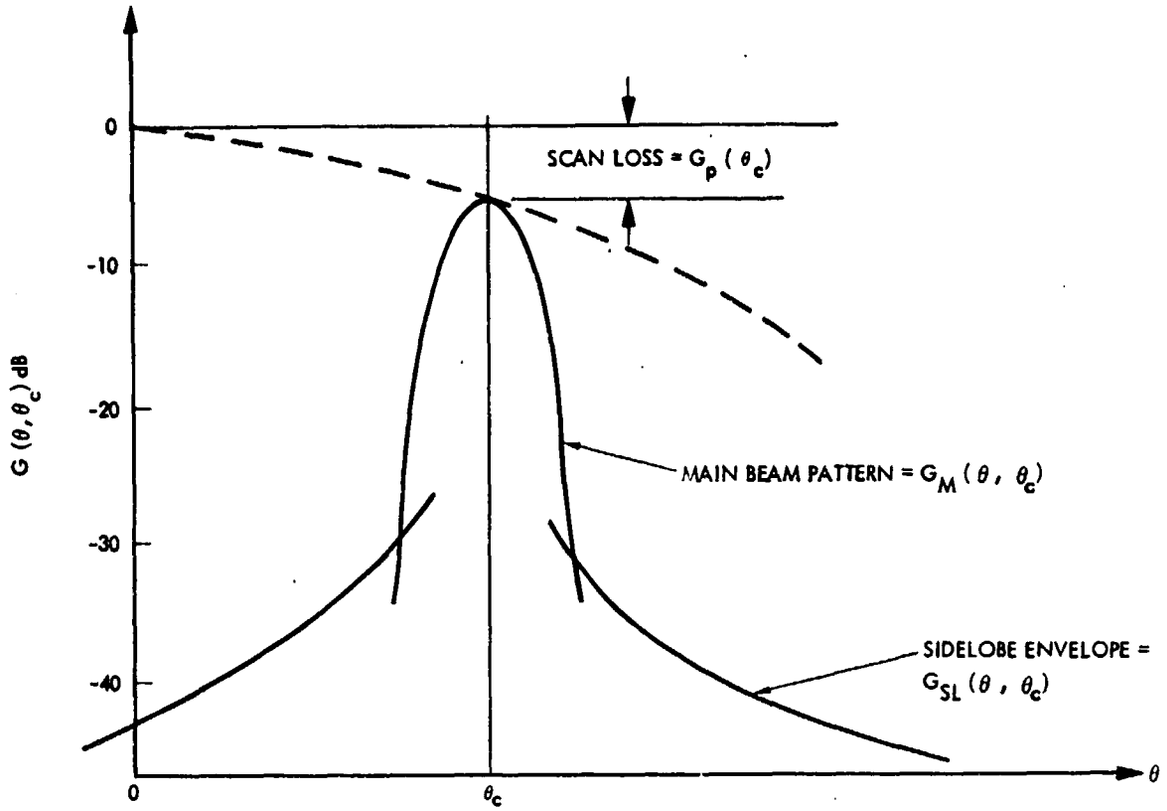

$$G_M(\theta, \theta_c) = G_p(\theta_c) + G_s(\theta, \theta_c) \text{ dB}$$

$$G_s(\theta, \theta_c) = -12 \left[\frac{(\theta - \theta_c)}{\Theta_o(\theta_c)}\right]^2 \text{ dB} \qquad \Theta_o(\theta_c) = B(\theta_c)\,\Theta_o(O)$$

$$G_{SL}(\theta, \theta_c) = 20 \log \left[\frac{K(\theta_c)}{(ka \sin |\theta - \theta_c|)^{3/2}}\right] \text{ dB}$$

WHERE $ka = \pi D/\lambda$

Figure 33. Scanned Beam Geometry

$G_M(\theta, \theta_c)$ is normalized in dB relative to $G_M(\theta, 0) = 0$ dB. Since the offset-reflector is not a symmetric configuration, $G_M(\theta, \theta_c)$ will not be a symmetric function of θ or θ_c. However, for initial simplicity it was assumed that the scanned main beam is a symmetric Gaussian function centered at $\theta = \theta_c$,

$$G_s(\theta, \theta_c) = -12\left(\frac{\theta - \theta_c}{\Theta_o(\theta_c)}\right)^2 \text{ dB},$$

where Θ_o is a function of θ_c and $\Theta_o(\theta_c)$ is the -3 dB beamwidth of the beam at a scan angle, θ_c. The beam will broaden as the beam is scanned off-axis, so

$$\Theta_c(\theta_c) = B(\theta_c)\ \Theta_o(0)\ ,$$

where $B(\theta_c)$ is the beam broadening function, and $\Theta_o(0)$ is the on-axis beamwidth. In the development of the beam pattern model, the radiation-patterns of the offset-parabolic antenna, for different aperture sizes and illumination functions, were calculated by the use of the JPL developed software. Then, by a study of these far-field radiation-patterns [8], the scan loss function and the beam broadening function were theoretically derived.

The sidelobe pattern function is an approximation to the upper bound of the sidelobe peaks. From the results given in Reference [9], it can be

demonstrated that the far-field E-field of an offset-reflector can be represented in the form

$$E \approx \sum_{m=0}^{M} \sum_{n=0}^{N} K_{mn} \frac{J_{n+2m+1}(ka \sin \Psi)}{ka \sin \Psi} ,$$

where $\Psi = |\theta - \theta_c|$ is a small angle (less than 6^o), $ka = \pi D/\lambda$ and D is the reflector diameter (see Figure 17). At large angles off the beam boresight, Ψ is large, and the first term, (m=0, n=0), predicts the sidelobe upper bound fairly accurately. Therefore,

$$E \approx K_{oo} \frac{J_1(ka \sin \Psi)}{ka \sin \Psi} \approx \frac{K_{oo}}{(ka \sin \Psi)^{3/2}} ,$$

where for the second approximation the large argument approximation [10] $J_1(x) \approx x^{-1/2}$ is used. Thus the sidelobe power pattern envelope in dB takes the form

$$G_{SL}(\theta, \theta_c) = 20 \log_{10} \left[\frac{K_{oo}}{(ka \sin \Psi)^{3/2}} \right] (dB) .$$

As the beam is scanned off the reflector axis, the sidelobes closer to the reflector axis, $\theta < \theta_c$, will be higher than the sidelobes away from the reflector axis, $\theta > \theta_c$. Therefore, the factor K_{oo} in the numerator of the sidelobe envelope function is actually a function of θ_c,

$$K_{oo} = K(\theta_c) .$$

In fact, two functions are needed, one for each side of the scanned beam boresight. However, in the present analysis, the patterns are assumed to be circularly symmetric about the scanned beam boresight and only the "worst case" sidelobes were used to obtain the sidelobe envelope coefficient, K_{oo}, of the sidelobe envelope function.

In order to derive the empirical functions which are the scan loss function, beam broadening function, and sidelobe envelope function, the JPL developed software was used to generate many examples of far-field patterns for the scanned beams. These data were obtained for a number of offset-parabolic reflectors of varying reflector dimensions and illumination function. The first example is an extreme case of a very large reflector with $D/\lambda = 1866.67$, and $F/D_p = 1$, where D, D_p, and F are shown in Figure 17, and a -10 dB edge taper. In this case the functions obtained for the beam broadening function, $B(\theta_c)$, scan loss function, $G_p(\theta_c)$, and the sidelobe level coefficients, $K(\theta_c)$, are shown in Figures 34-36. In Figure 36, note that the upper curve is for the "near" sidelobes and the lower curve is for the "far" sidelobes. In order to demonstrate the accuracy of the sidelobe envelope model, the model output is superimposed on patterns generated by the JPL developed software (also available in [9]). This is shown in Figures 37 and 38. In both cases, the "far" sidelobe approximation is very accurate beyond the first sidelobe. As expected, the "near" sidelobe approximation is good beyond the second or third sidelobe. The reason that the first few "near" sidelobes are not approximated accurately, is because the scanning operation modifies the phase distribution in the reflector aperture and this modification has more impact on the fields closer to the reflector axis.

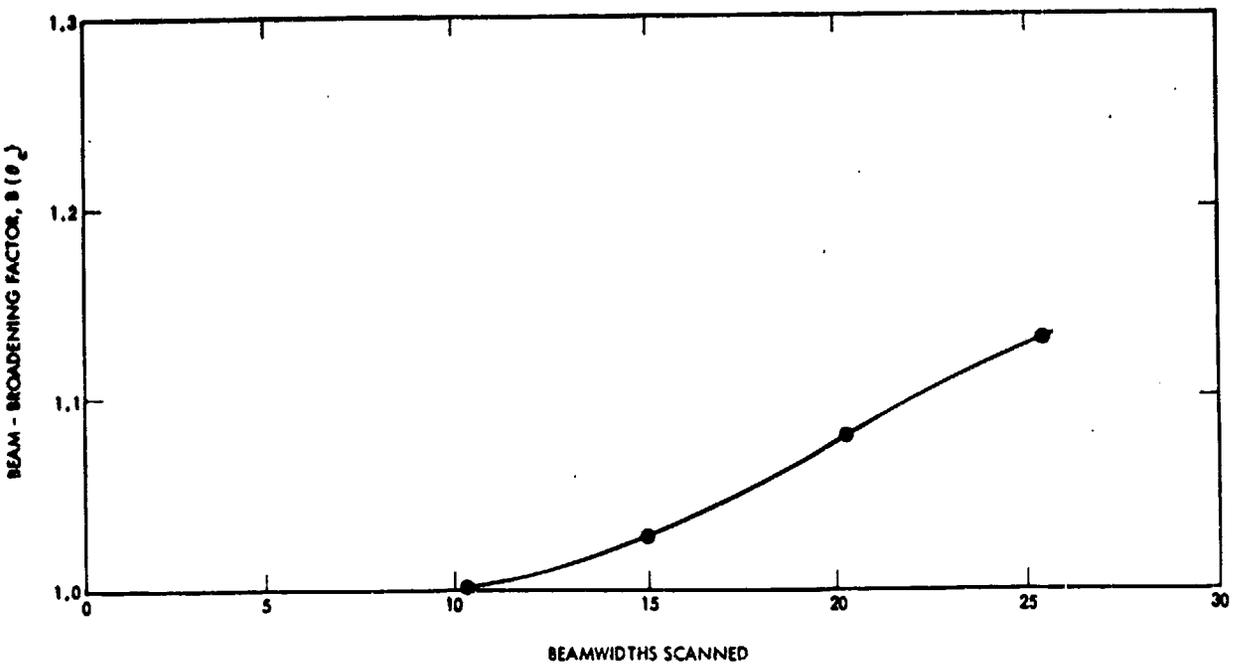

Figure 34. Beam-Broadening Factor. D = 1866.67 wavelengths, F/D_p = 1, and -10 dB taper offset-parabolic reflector.

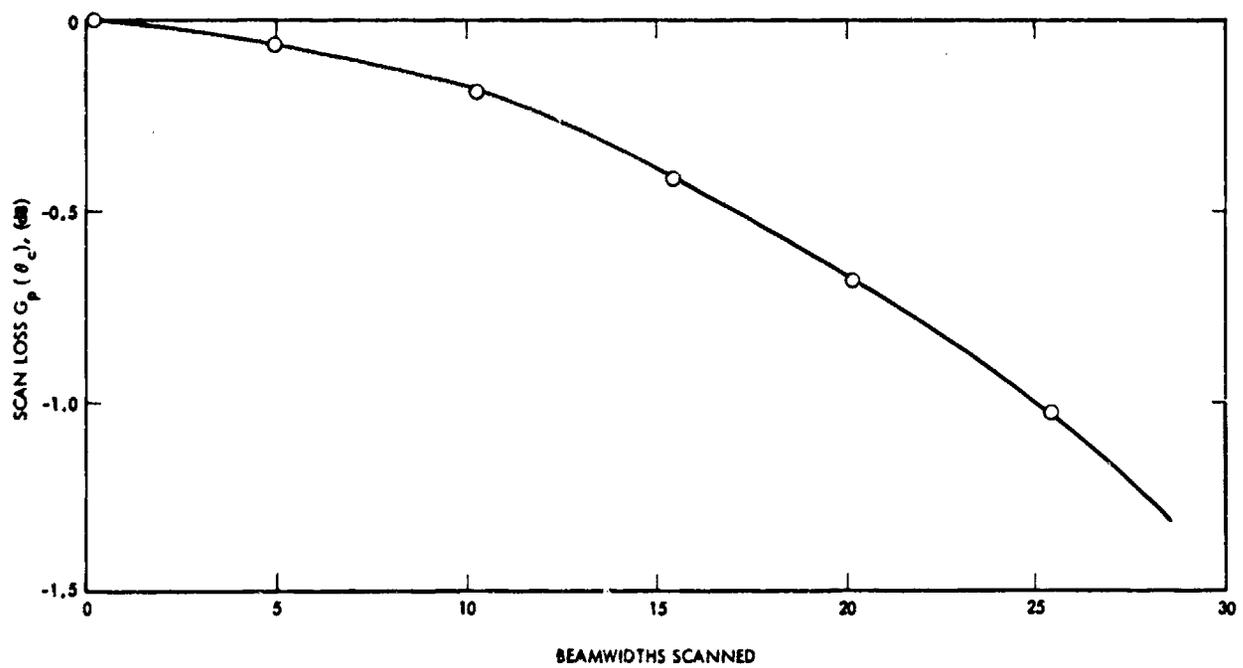

Figure 35. Scan Loss Function. D = 1866.67 wavelengths, F/D_p = 1, and -10 dB taper offset-parabolic reflector.

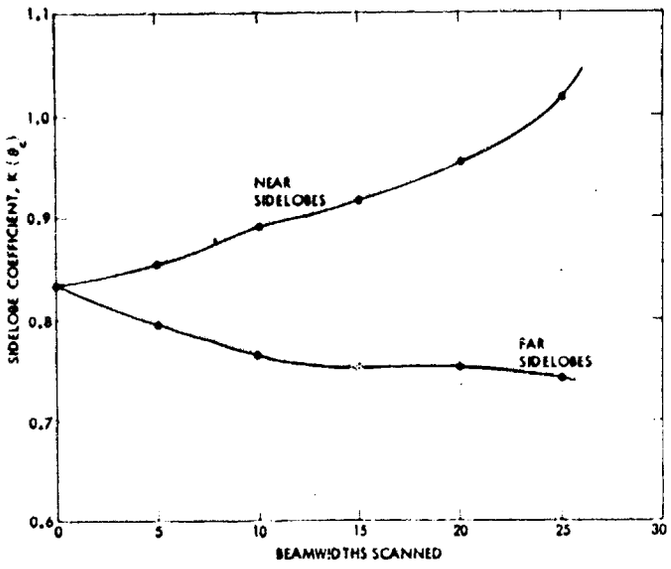

Figure 36. Sidelobe Envelope Coefficient Function. D = 1866.67 wavelengths, F/D_p = 1, and -10 dB taper offset-parabolic reflector.

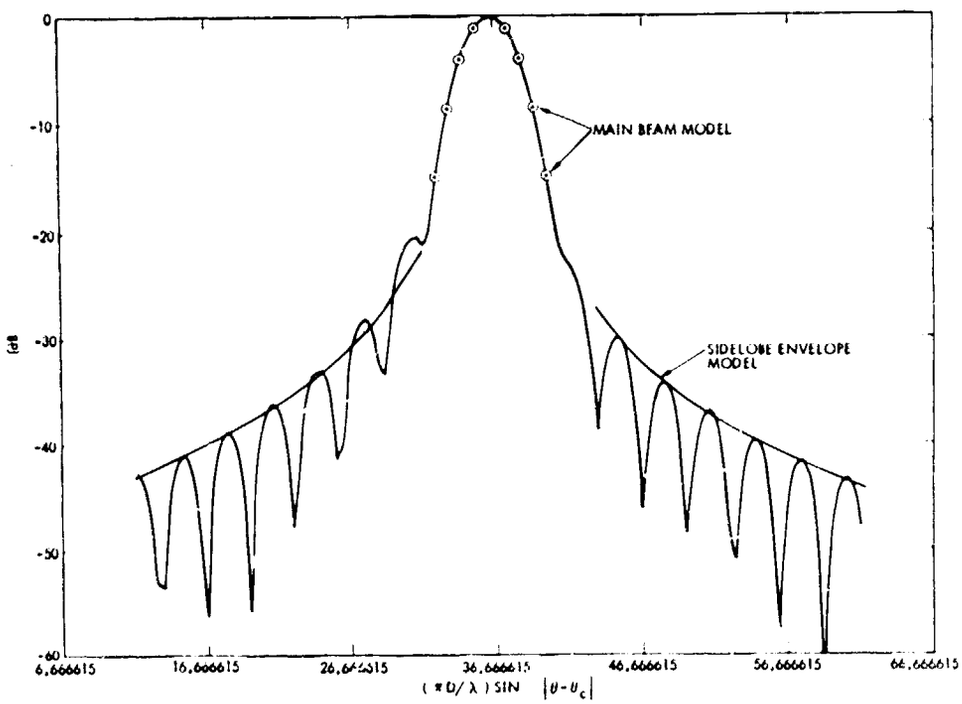

Figure 37. The Model Output Superimposed on Patterns Generated by the JPL Developed Software: D = 1866.67 wavelengths, F/D_p = 1, -10 dB taper, and θ_c = 10.2 beamwidths.

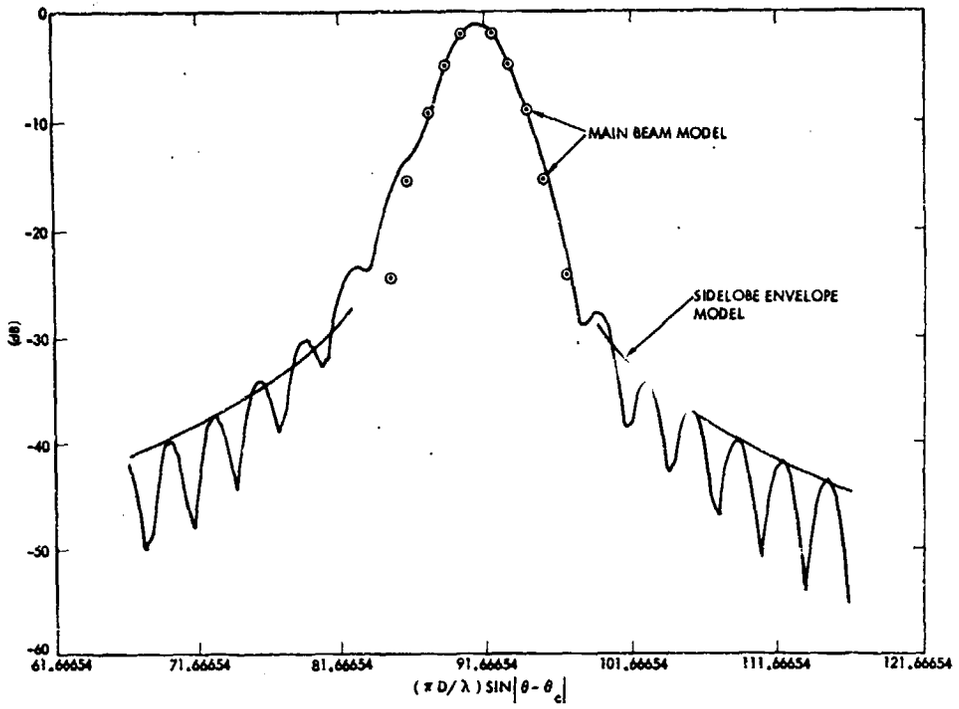

Figure 38. The Model Output Superimposed on Patterns Generated by the JPL Developed Software: D = 1866.67 wavelengths, F/D_p = 1, -10 dB taper, and θ_c = -25.5 beamwidths.

The transition point between the main beam and the side lobe envelope is assumed, for simplicity, to be where the main beam gain is less than -20 dB. Thus, in the model program, if the calculated value for $G_M(\theta, \theta_c)$ is greater than -20 dB, then the value of $G_M(\theta, \theta_c)$ is used. However, if the calculated value is less than -20 dB, then the value of G_{SL} is calculated, and after a comparison the larger of the two values is used. This will insure the use of an upper bound in the transition region.

Additional beam pattern models were obtained by the use of JPL developed software for three cases of 100 wavelength diameter offset-reflectors with a -10 dB edge taper for F/D_p's of 0.5 and 1.0, and with a -15 dB edge taper for F/D_p of 1.0. The data obtained by the use of the software are plotted as a function of the beam scan angle and include the scan loss function, beam

broadening function, and the sidelobe level coefficients. This is shown in Figures 39-41 for the three cases. It can be seen that the scan loss is drastically reduced by using a larger F/D_p, particularly at large scan angles. This same effect was noted in reference [9]. The effect of decreasing the feed taper from -10 dB to -15 dB on the scan loss is not noticeable, as expected. In Figure 40, the beam broadening factor shows the most severe beam degradation, at large scan angles, for F/D_p of 0.5. As for the sidelobe performance away from the main beam, Figure 41 shows that the F/D_p has very little effect for small scan angles, but the sidelobes are significantly higher at large scan angles for the smaller F/D_p. In addition, the reduction in taper from -10 dB to -15 dB reduces the sidelobe level, as expected.

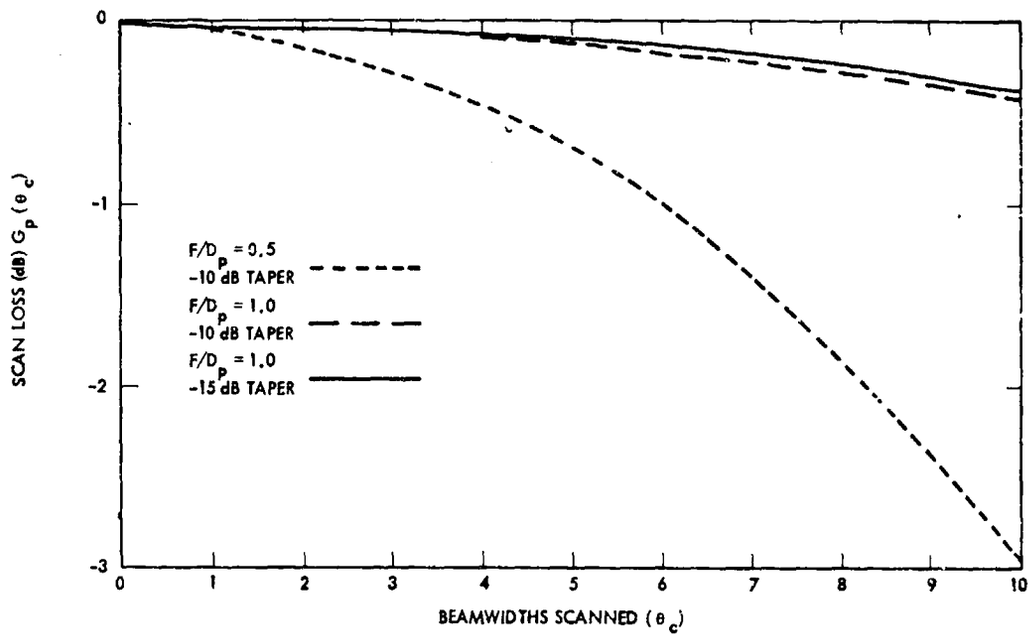

Figure 39. Scan Loss Function, 100 Wavelength Diameter Offset-Parabolic Reflector

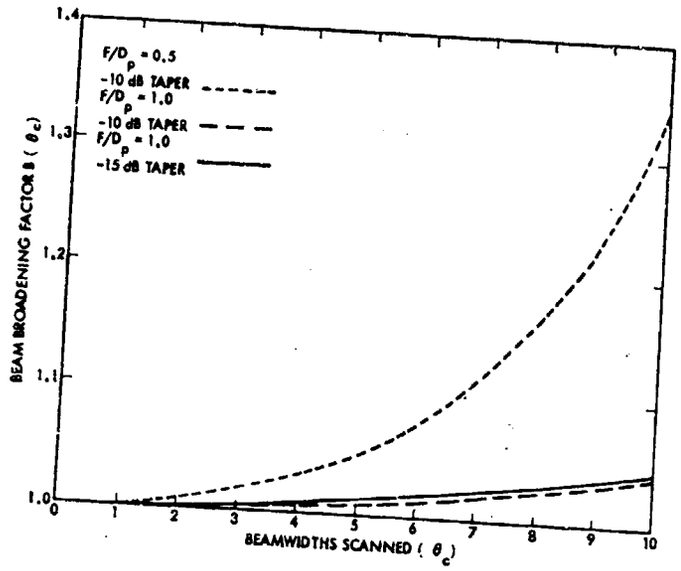

Figure 40. Beam Broadening Function, 100 Wavelength Diameter Offset-Parabolic Reflector

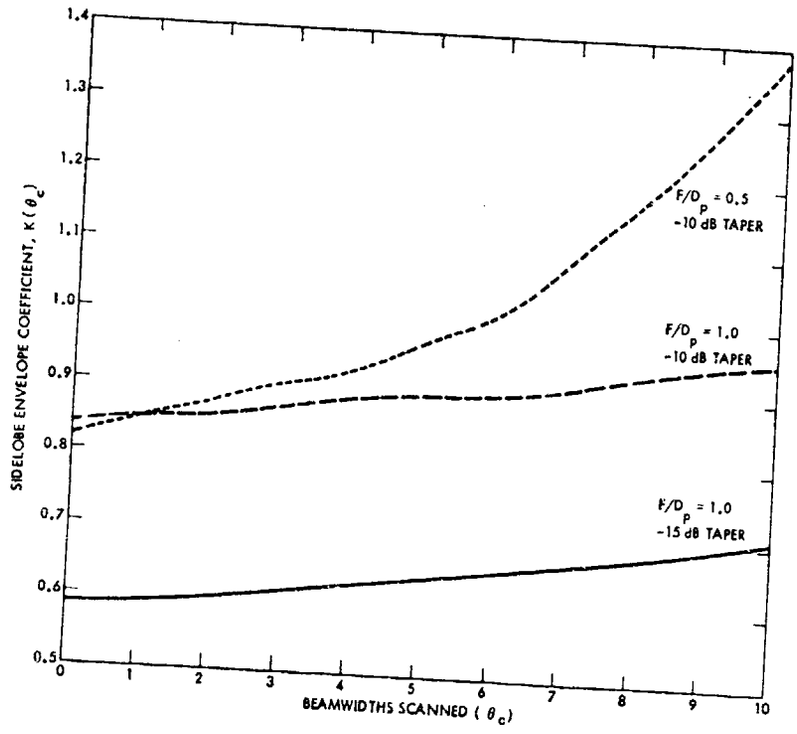

Figure 41. Sidelobe Envelope Coefficient Function, 100 Wavelength Diameter Offset-Parabolic Reflector

In Figures 42-50 the beam pattern model (dashed curves) has been compared to the JPL software generated theoretical patterns, for the three offset-reflector examples, from which the model data were empirically derived. In Figures 42-44, two features are evident. First, the main beam model should include the beam deviation factor (BDF) because it is a definite factor for smaller F/D_p's. At present time this model does not include the beam deviation factor and it has been assumed to be very close to unity. Secondly, the model is somewhat optimistic in the region of the first sidelobe/shoulder for large scan angles. It was anticipated that the transition region between the sidelobe envelope and the main beam would be where the beam model would show the worst approximation. Thus, for small values of F/D_p, for beam scan angles larger than 5 beamwidths the model is slightly better than the "worst case" in the transition region between the sidelobe envelope and the main beam, and is slightly worse than the "worse case" for sidelobes at large angles off the beam boresight, θ .

Figures 45-50 show how well the model approximates the theoretically calculated patterns for F/D_p of 1.0. These figures show that the main beam model is very accurate to at least 10 dB below the peak gain. The beam deviation factor is very close to unity in all cases. The envelope approximation is also very good outside the second sidelobe. As before, the region near the first sidelobe is where the model is least accurate, but it is much more accurate than the model for F/D_p of 0.5. The decrease in edge taper from -10 to -15 dB improves the scanned beam performance and also reduces

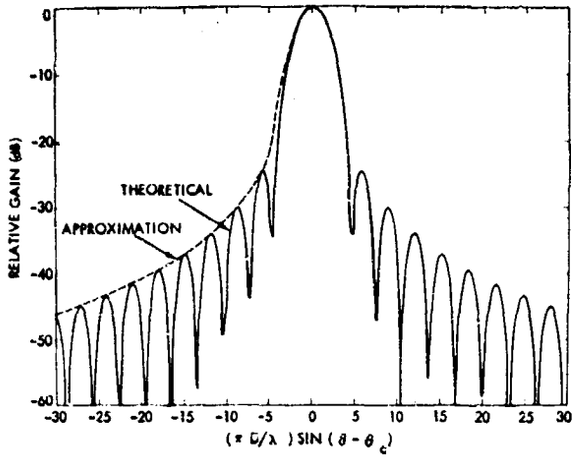

Figure 42. Comparison of the Beam Pattern Model and the JPL Software Generated Theoretical Pattern for Offset-Parabolic Reflector with D = 100 wavelengths, F/D_p = 0.5, -10 dB taper, and θ_c = 0 beamwidths

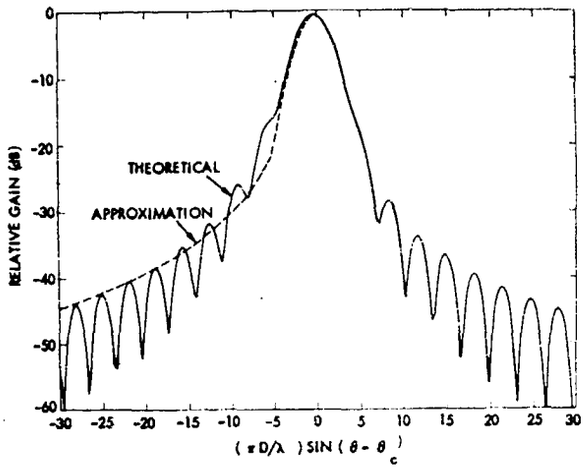

Figure 43. Comparison of the Beam Pattern Model and the JPL Software Generated Theoretical Pattern for Offset-Parabolic Reflector with D = 100 wavelengths, F/D_p = 0.5, -10 dB taper, and θ_c = 5 beamwidths

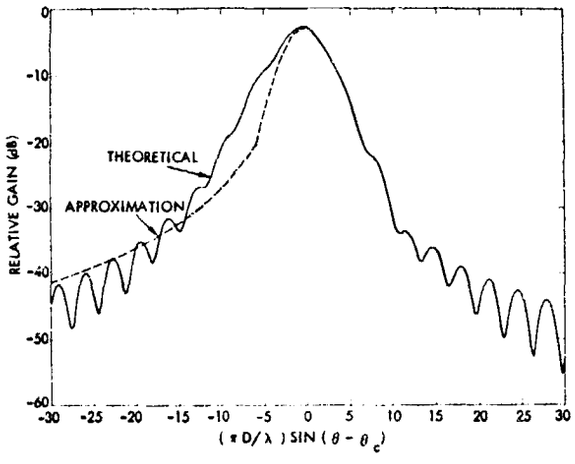

Figure 44. Comparison of the Beam Pattern Model and the JPL Software Generated Theoretical Pattern for Offset-Parabolic Reflector with D = 100 wavelengths, F/D_p = 0.5, -10 dB taper, and θ_c = 10 beamwidths

Figure 45. Comparison of the Beam Pattern Model and JPL Software Generated Theoretical Pattern for Offset-Parabolic Reflector with D = 100 wavelengths, F/D_p = 1.0, -10 dB taper, and θ_c = 0 beamwidths

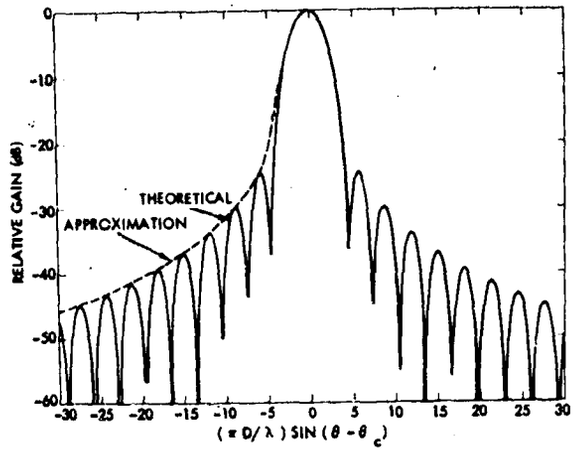

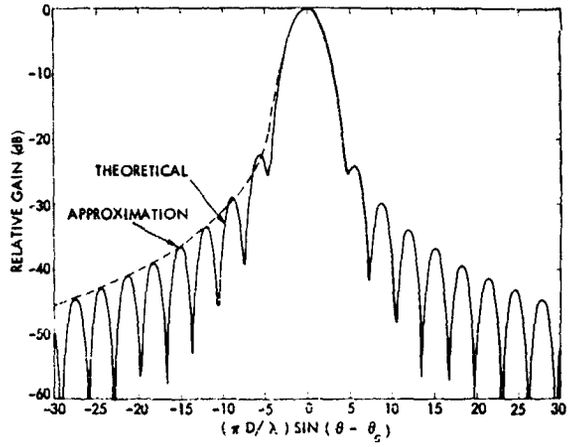

Figure 46. Comparison of the Beam Software Generated Theoretical Pattern for Offset-Parabolic Reflector with D = 100 wavelengths, F/D_p = 1.0, -10 dB taper, and θ_c = 5 beamwidths

Figure 47. Comparison of the Beam Pattern Model and the JPL Software Generated Theoretical Pattern for Offset-Parabolic Reflector with D = 100 wavelengths, F/D_p = 1.0, -10 dB taper, and θ_c = 10 beamwidths

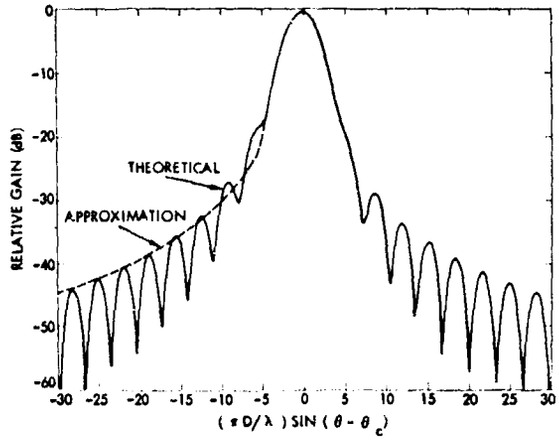

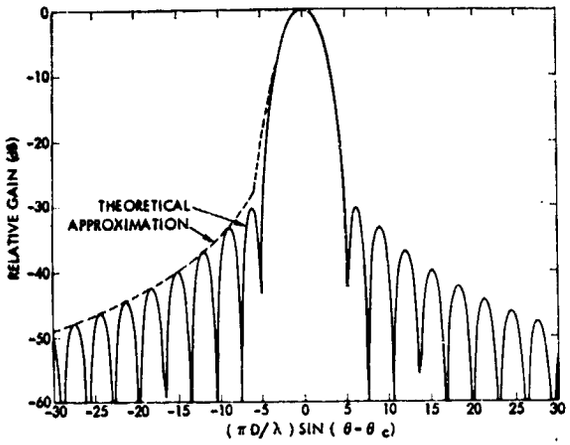

Figure 48. Comparison of the Beam Pattern Model and the JPL Software Generated Theoretical Pattern for Offset-Parabolic Reflector with D = 100 wavelengths, F/D_p = 1.0, -15 dB taper, and θ_c = 0 beamwidths

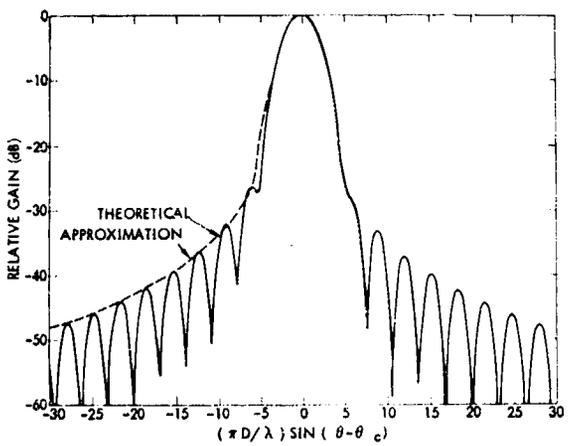

Figure 49. Comparison of the Beam Pattern Model and the JPL Software Generated Theoretical Pattern for Offset-Parabolic Reflector with D = 100 wavelengths, F/D_p = 1.0, -15 dB taper, and θ_c = 5 beamwidths

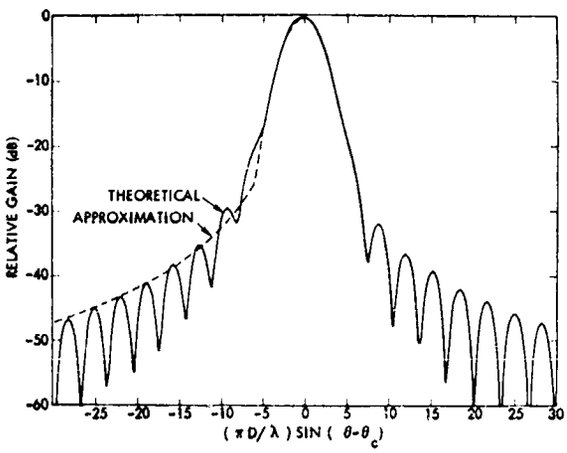

Figure 50. Comparison of the Beam Pattern Model and the JPL Software Generated Theoretical Pattern for Offset-Parabolic Reflector with D = 100 wavelengths, F/D_p = 1.0, -15 dB taper, and θ_c = 10 beamwidths

the difference between the theoretically calculated patterns and the beam pattern model. As a general comment, for the cases considered here, the offset-reflector diameter is 100 wavelengths which corresponds to a 7.5 meter antenna at a 4 GHz or a 2.5 meter antenna at 12 GHz.

In this analysis, it was assumed that the desired beam is the beam generated by the feed at the focal point of the reflector antenna, $\theta_c = 0$. This assumption insures a type of symmetry around the desired beam by the interfering beams and gives a possible "worst case" for the interbeam isolations within the coverage area. The disadvantage of this assumption is that the scan loss is somewhat large at large scan angles and it is possible to have the "worst case" isolations for the desired beams with largest beamwidths scanned. This is specially true for the offset-reflectors with smaller F/D_p's as discussed before. However, it should be noticed that the beam broadening factor and sidelobe coefficients are also largest at large scan angles. Thus, it seems that the "worst case" isolation is for the desired beam generated by the feed at the focal point of the reflector, since for this beam the cochannel interfering beams have the highest sidelobe levels. In general, only a thorough analysis, by considering the C/I performances of the foregoing possibilities would show the "worst case" interbeam isolation within the coverage area.

5.3.2 Frequency Reuse Capacity and Interbeam Isolation

In order to obtain the frequency reuse factors for the offset-reflector multiple beam antennas, the C/I calculation is repeated for the various allowed combinations of number of beams and number of frequencies, as done in the axisymmetric reflector case. The results for a 100 wavelength diameter

offset-reflector, with F/D_p of 1 and -15 dB edge taper, are shown in Figure 51. Again, every curve corresponds to a specific number of frequencies which was used to evaluate the C/I performance. It can be seen that the primary factor in the C/I performance level is the frequency reuse factor. A change in number of frequencies from 3 to 4 causes a considerable change in the C/I value (about 5-7 dB), but a change from 12 to 13 causes a smaller change of about 1 dB. So as the number of frequencies increases, the C/I value becomes less sensitive to it.

5.3.3 Sidelobe Level Analysis

Figure 51 was obtained for a beam pattern model with sidelobes starting at -30 dB level. In order to study the effects of some wide variations of sidelobe levels upon the C/I performance of the system, the beam pattern models shown in Figures 45-47 were modified and used. Figures 45-47 show the beam pattern models generated for an offset-parabolic reflector with 100 wavelength diameter, F/D_p of 1.0, and a -10 dB edge taper. These beam pattern models have sidelobe envelopes starting at about -25 dB relative to the main beam-maximum. In this study of sidelobe effects, the sidelobe envelope for these beam pattern models were shifted up or down to create the variations of sidelobe level. Figure 52 shows the modification for variations of the sidelobe envelope for the beam pattern generated by the feed at the focal point of the reflector antenna (scan angle $\theta_c = 0$). For beams at other scan angles the same procedure was used and the sidelobe envelope of the degraded beam pattern was shifted up or down in order to obtain the desired level of the sidelobe envelope.

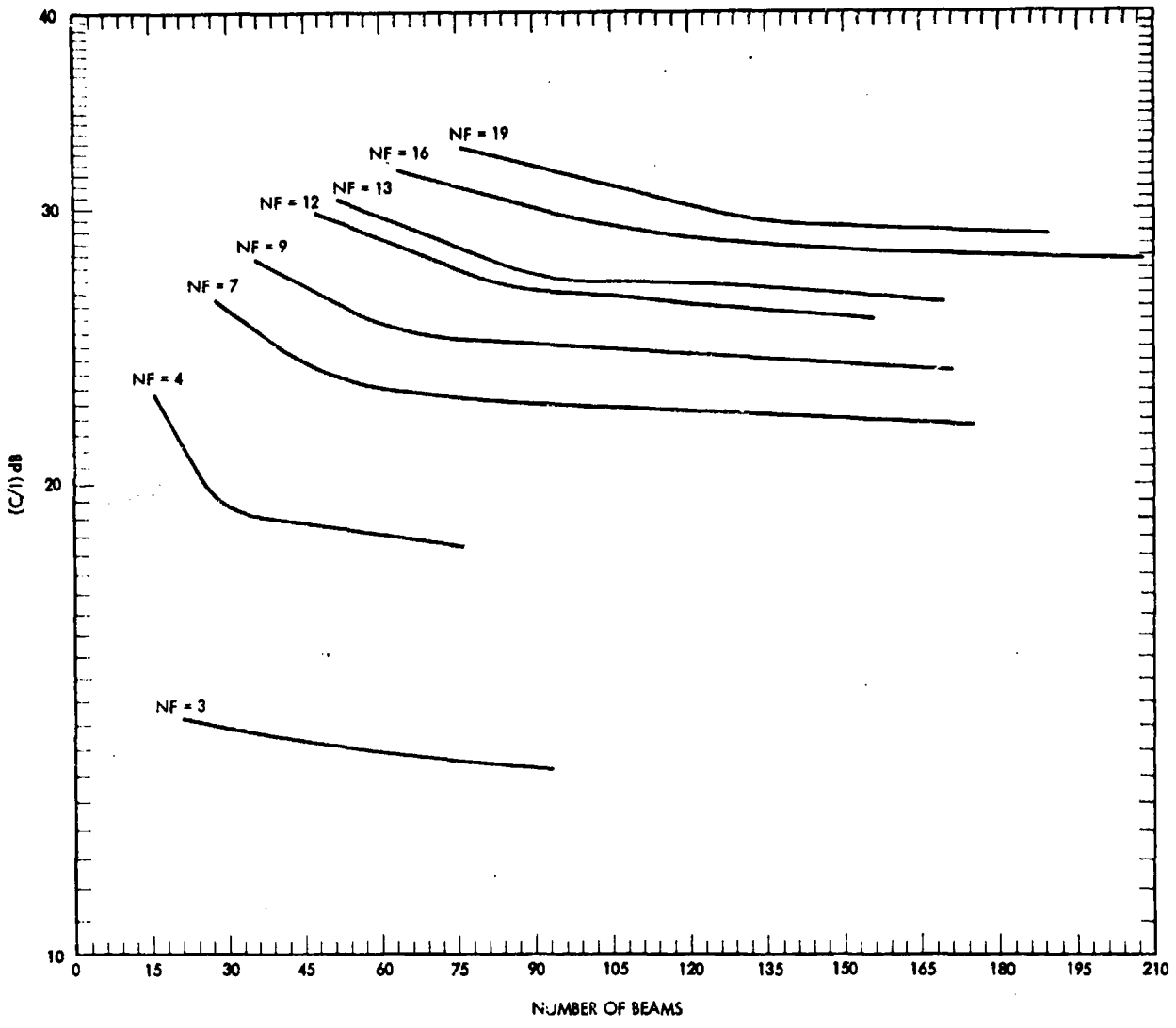

Figure 51. Frequency Reuse Capacity
Offset-Reflector Diameter = 100λ, F/D_p = 1.0,
-15 dB Taper and -30 dB Sidelobe Level
Calculation Point: -3 dB down from peak of the main beam
Beam Separation: 1 HPBW of the main beam

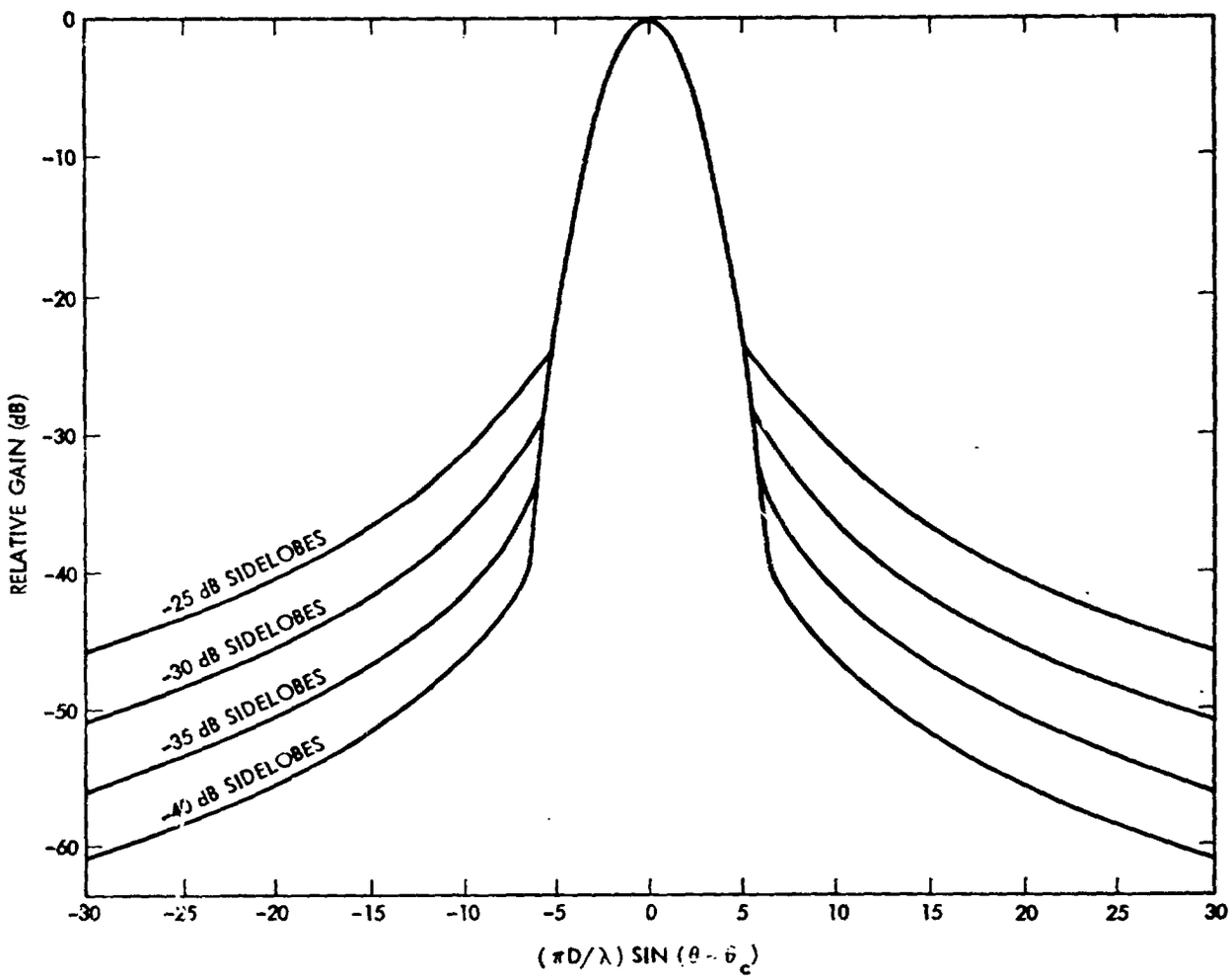

Figure 52. Type A patterns. This set of patterns are the Modified Versions of the pattern obtained for an offset-parabolic reflector with D = 100 wavelengths, F/D_p = 1.0, -10 dB taper, and θ_c = 0 beamwidths. Modification is in the variations of the -25 dB sidelobe envelope.

In order to avoid confusion, the beam patterns shown in Figure 52 were named type A patterns. This is due to the fact that, in practice, for an offset-parabolic reflector with the above mentioned dimensions and a -10 dB edge taper, it is not possible to have beam patterns with sidelobes starting at -30 dB, or lower, relative to the main beam-maximum.

Figures 53-55 show the C/I values obtained for a 100 wavelength diameter offset-reflector with beam patterns of type A. In these figures the value of sidelobe envelope was varied from -25 dB to -35 dB. Figure 56 compares the (C/I) values obtained for these different sidelobe levels and shows the effect of different sidelobe levels when a different number of frequencies is employed. It can be seen that the sidelobe level has a much greater effect when a larger number of beams and frequencies is used.

5.3.4 Illumination Taper Analysis

The primary advantage of illumination tapers (edge tapers) is the low sidelobe levels provided by them. It was shown that the use of illumination taper slightly improves the scan loss performance and causes sidelobe level reduction. Figure 57 shows a comparison of C/I levels for two different taper levels and three different frequencies. The comparison shows that a 5 dB decrease in the illumination taper, corresponding to a 5 dB decrease in sidelobe levels, causes a C/I improvement of about 1-4 dB. In Figure 57, a comparison of results obtained by a type A pattern with -30 dB sidelobes and -15 dB edge taper pattern with -30 dB sidelobes shows that the method used in 5.3.3 (employing the beam patterns of type A to study the effects of sidelobe level variations) could yield optimistic results by about 1 dB.

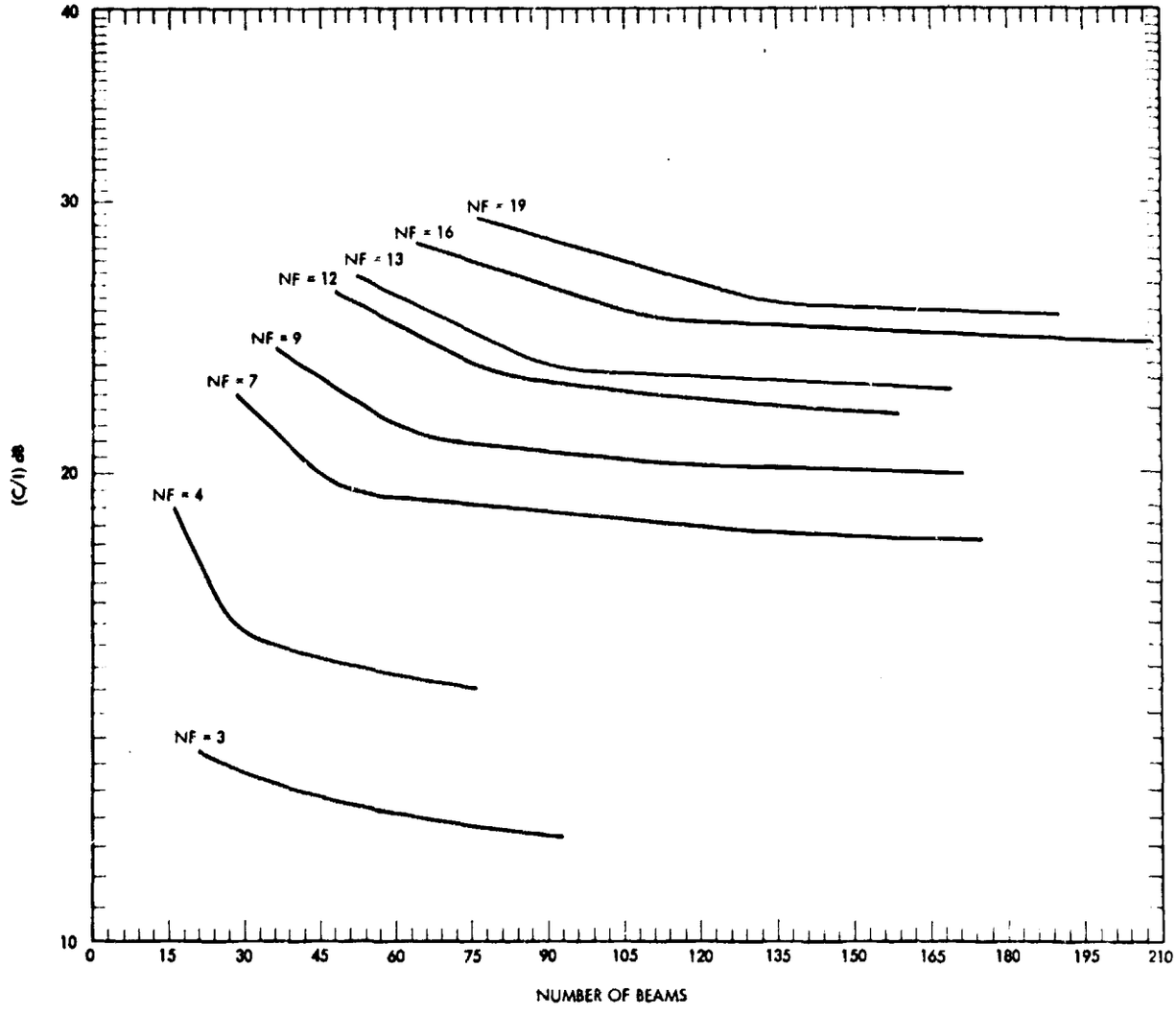

Figure 53. Frequency Reuse Capacity
Offset-Reflector Diameter = 100λ, F/D_p = 1.0,
-10 dB taper and -25 dB Sidelobe Level
Calculation Point: -3 dB down from peak of the main beam
Beam Separation: 1 HPBW of the main beam

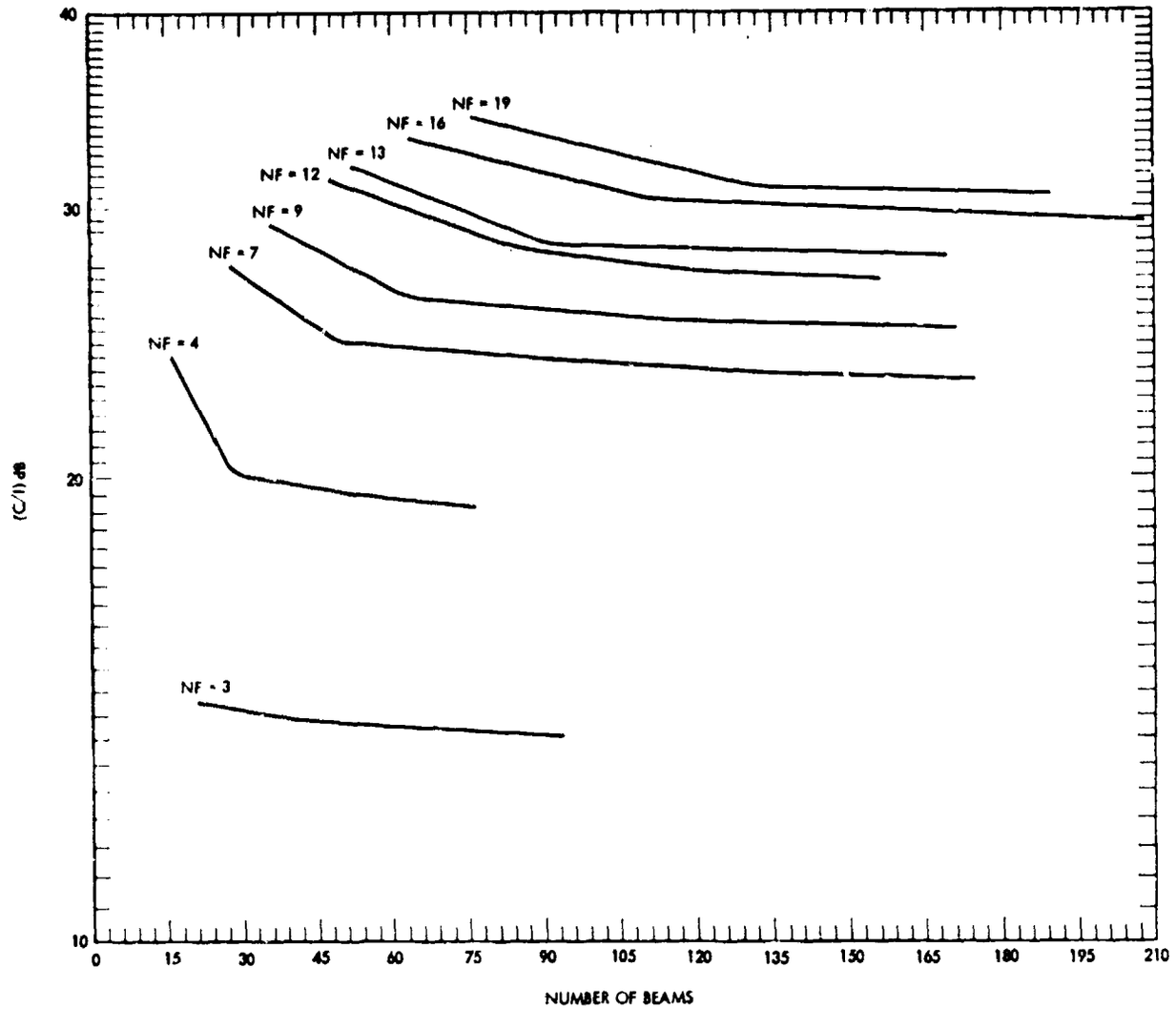

Figure 54. Frequency Reuse Capacity
Offset-Reflector Diameter = 100λ, F/D_p = 1.0,
Type A Pattern with -30 dB Sidelobe Level
Calculation Point: -3 dB down from peak of the main beam
Beam Separation: 1 HPBW of the main beam

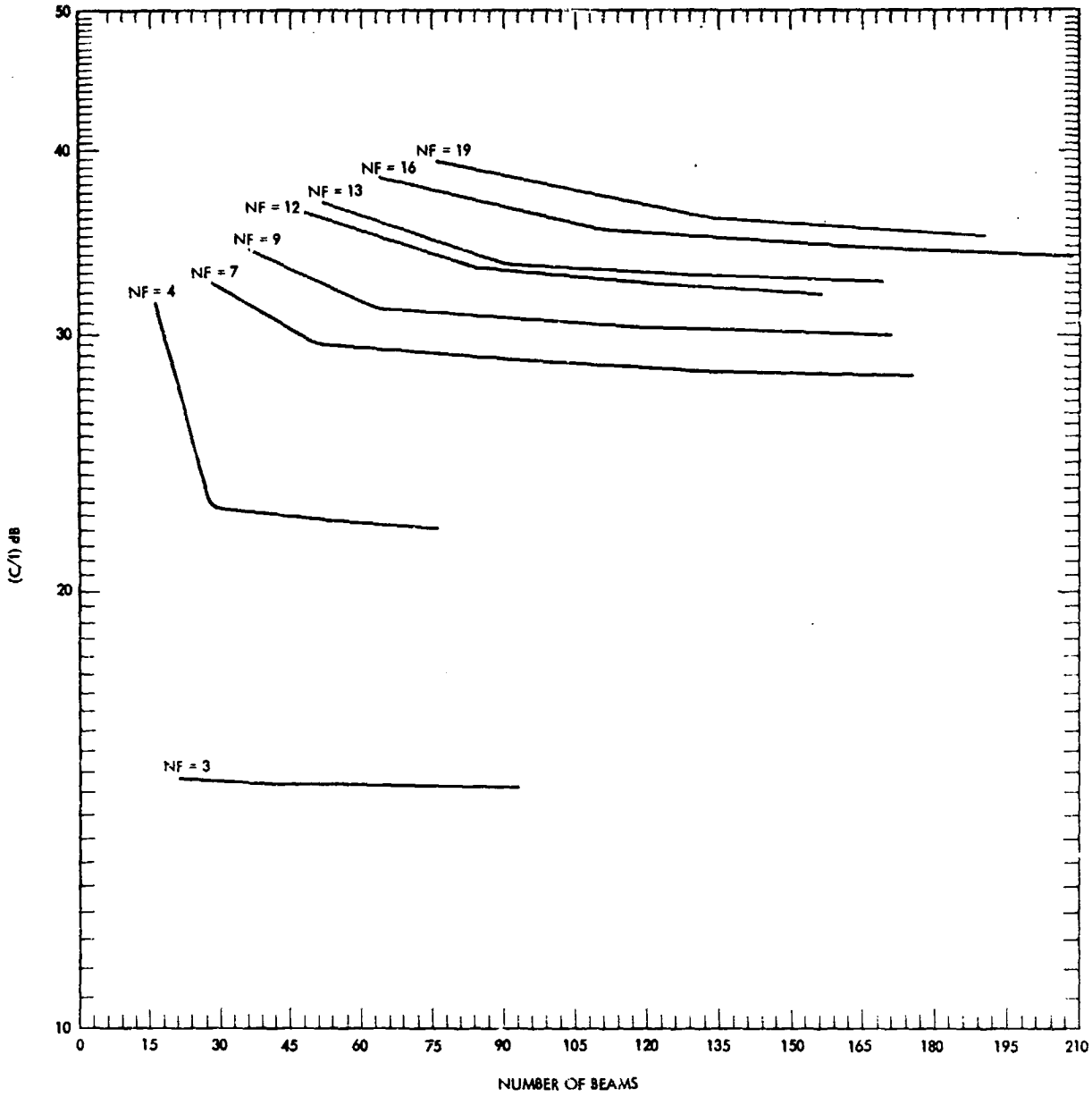

Figure 55. Frequency Reuse Capacity
Offset-Reflector Diameter = 100λ, F/D_p = 1.0,
Type A Pattern with -35 dB Sidelobe Level
Calculation Point: -3 dB down from peak of the main beam
Beam Separation: 1 HPBW of the main beam

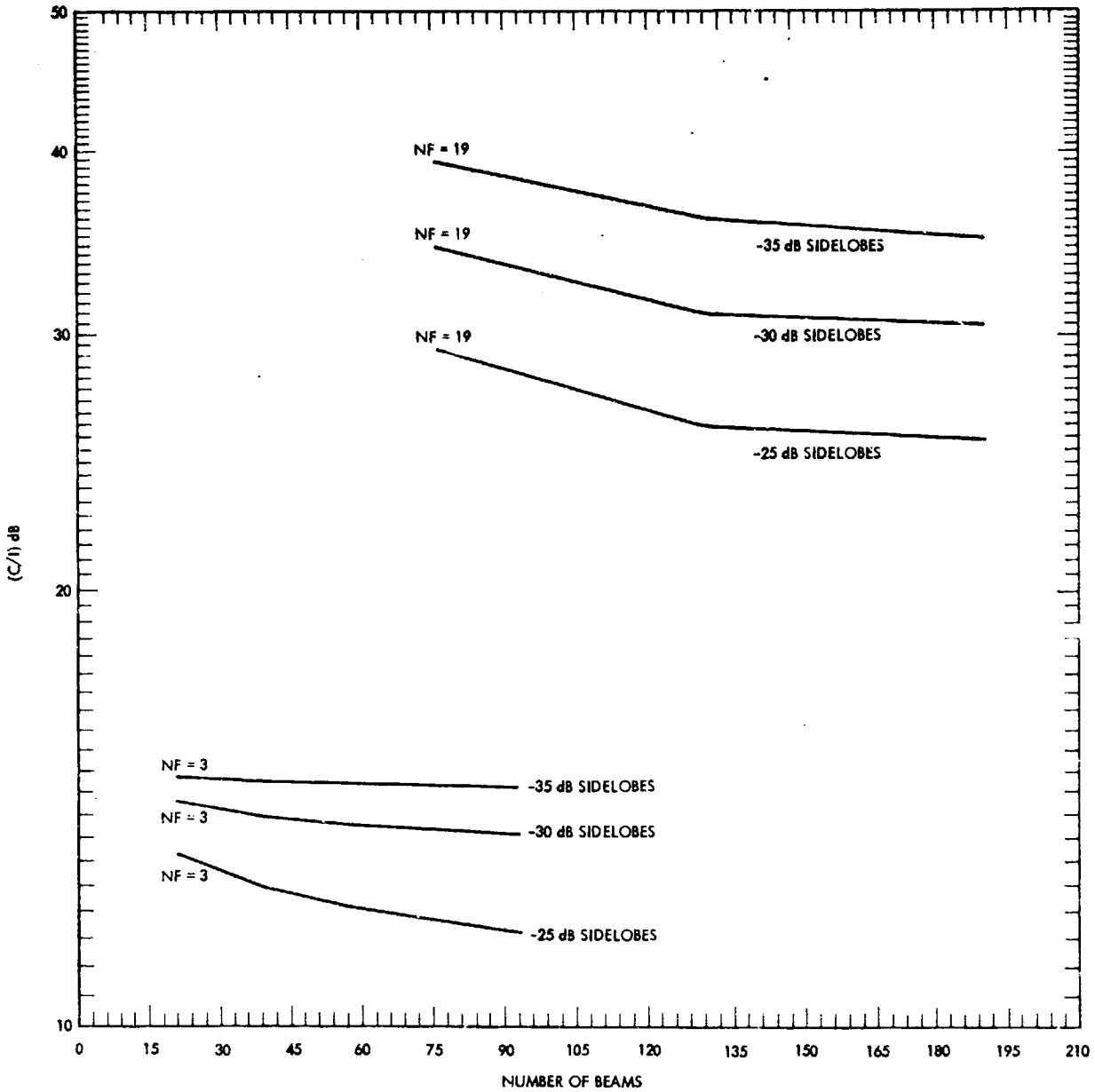

Figure 56. Comparison of (C/I) Values for Three Sidelobe Levels
Offset-Reflector Diameter = 100λ, F/D_p = 1.0,
Type A Patterns
Calculation Point: -3 dB down from peak of the main beam
Beam Separation: 1 HPBW of the main beam

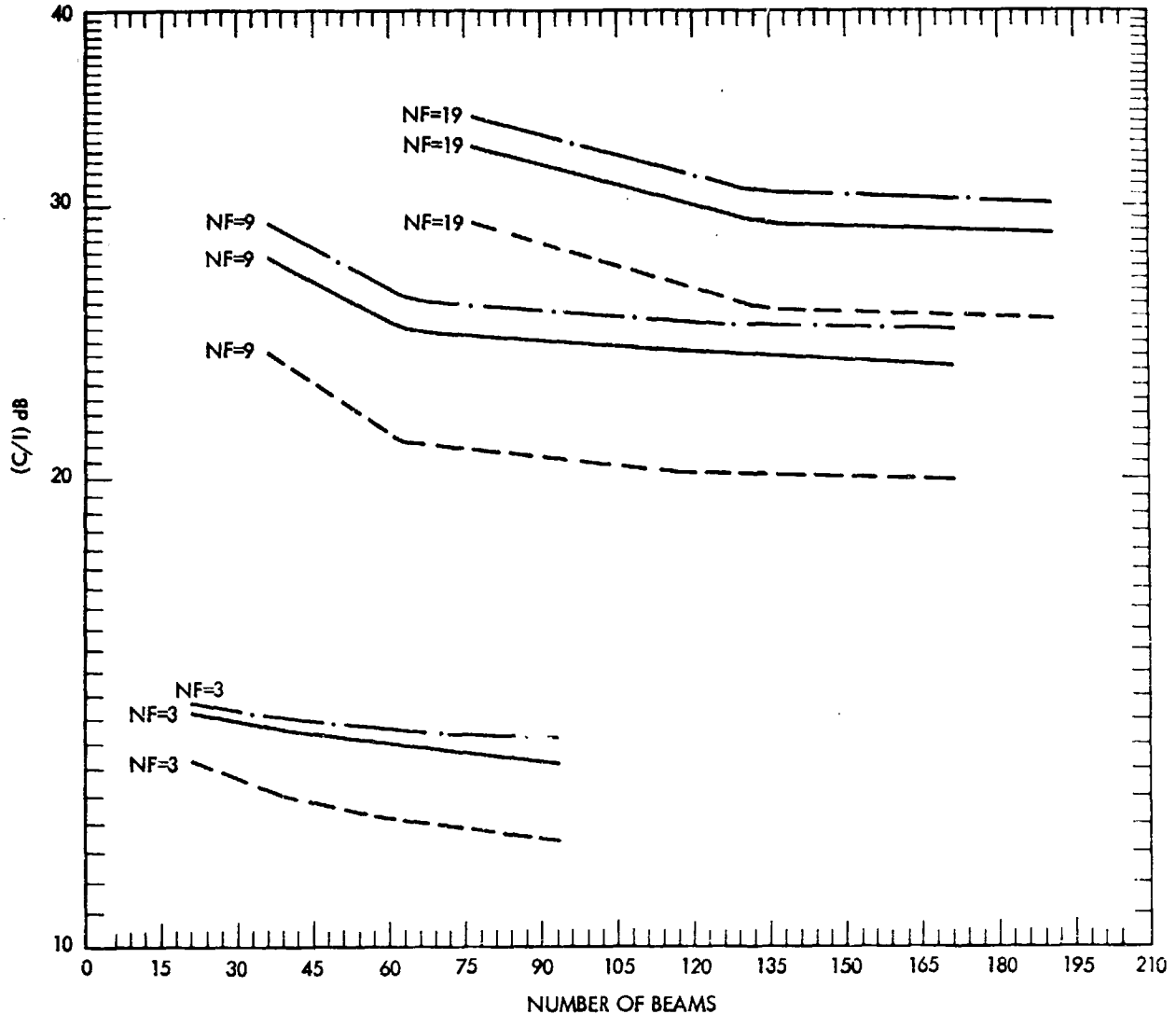

Figure 57. Comparison of (C/I) Performance for 2 Different Illumination Tapers and Type A Pattern
——— F/D_p = 1.0, -15 dB Taper and -30 dB Sidelobe Level
—.— F/D_p = 1.0, Type A pattern with -30 dB Sidelobe Level
----- F/D_p = 1.0, -10 dB Taper and -25 dB Sidelobe Level
Calculation Point: -3 dB down from peak of the main beam
Beam Separation: 1 HPBW of the main beam

5.3.5 Dimensional Considerations

It was discussed that the beam radiation pattern degradation is strongly related to the focal length over the parent paraboloid diameter (F/D_p) ratio of the offset-reflector and to the aperture illumination function. Also, it was shown that larger F/D_p's drastically reduce the scan loss, beam broadening factor, and the sidelobe envelope coefficients at large scan angles. In general, linearly polarized offset antennas will generate significant levels of cross-polar radiation unless the reflector has a large F/D_p ratio. However, for most applications it was found that the reflector depolarization lays below the copolarized sidelobe envelope. Hence, the offset-reflector depolarization does not preclude the use of this antenna in a low-sidelobe role. For smaller offset-reflectors, primary-feed spillover constitutes the main limitations on the overall sidelobe performance. These effects can be alleviated by good primary feed design and some use of shields or blinders about the antenna aperture [7]. Also, for a single linear polarization, good polarization purity can be restored by use of polarization-sensitive grids and a large F/D_p ratio is not necessary. In our analysis a single linear polarization, considering only the copolar patterns, is used. In terms of the C/I performance it was discovered that the performance was not affected by more than 1 dB when an F/D_p ratio of 1.0 was used in comparison to an F/D_p ratio of 0.5. Figure 58 shows the C/I values obtained for a 100 wavelength diameter offset-reflector with a -10 dB taper and $F/D_p = 0.5$. Figure 59 shows the comparison made for two different F/D_p ratios of 0.5 and 1.0. It can be seen that for different numbers of frequencies, the two different F/D_p ratios compared very closely in terms of the C/I performance. This is primarily due to the fact that the desired beam was assumed to be the beam generated at the focal point of the reflector and,

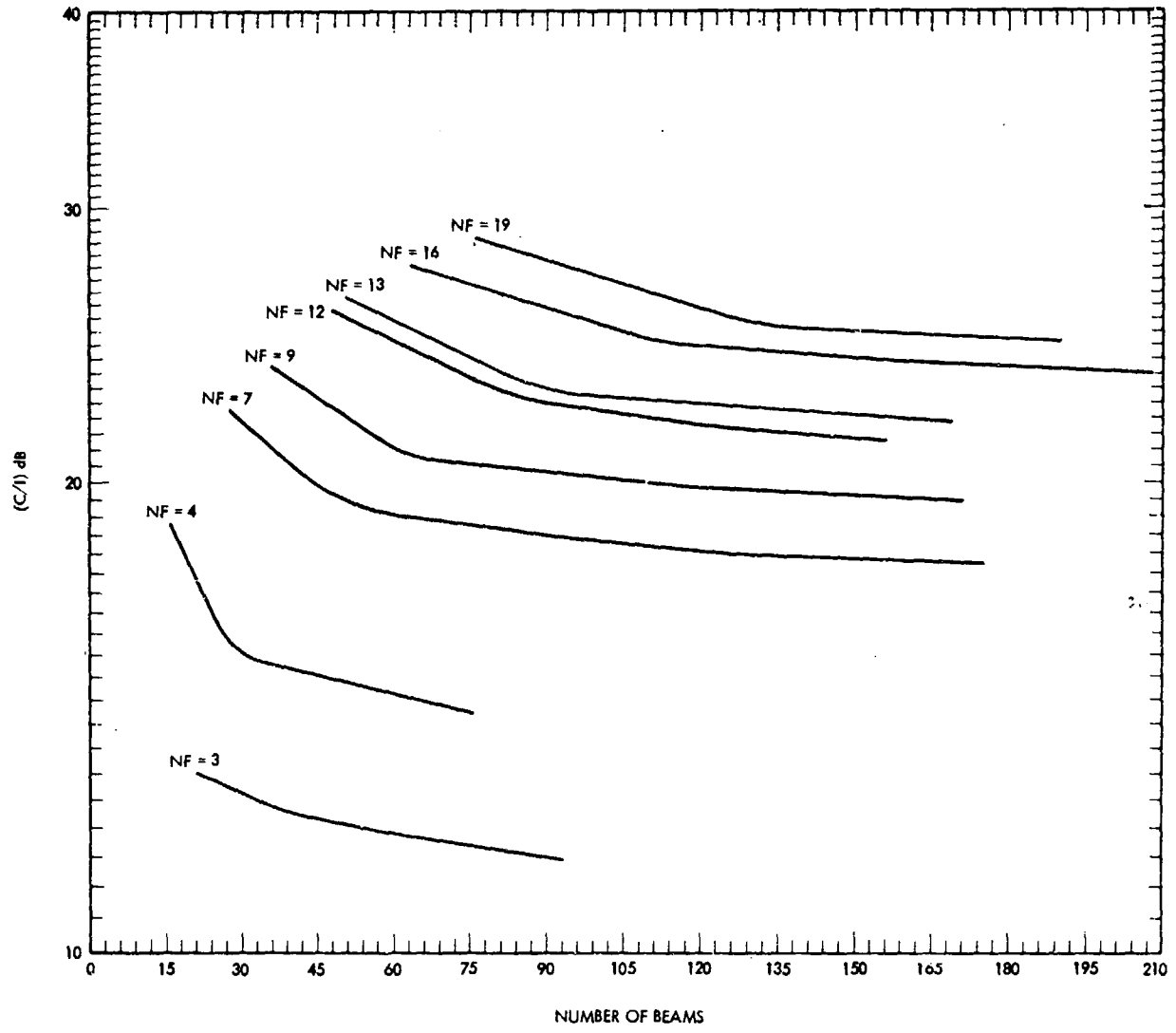

Figure 58. Frequency Reuse Capacity
Offset Reflector Diameter = 100λ, F/D_p = 0.5,
-10 dB taper and -25 dB Sidelobe Level
Calculation Point: -3 dB down from peak of the main beam
Beam Separation: 1 HPBW of the main beam

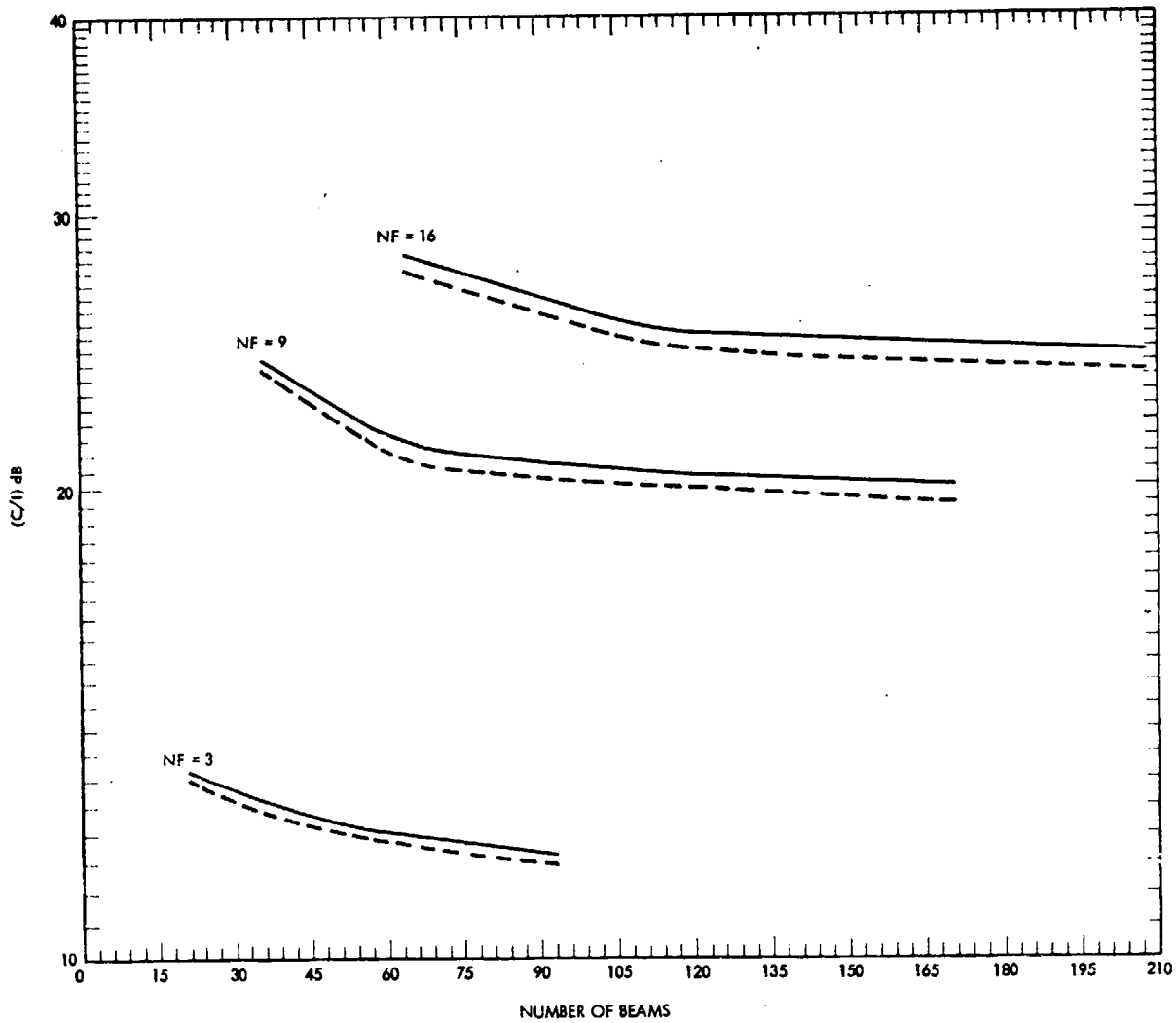

Figure 59. Comparison of (C/I) Performances for 2 Different Offset Reflector Sizes
Offset Reflector Diameter = 100λ
_____ F/D_p = 1.0, -10 dB Taper and -25 dB Sidelobe Level
----- F/D_p = 0.5, -10 dB Taper and -25 dB Sidelobe Level
Calculation Point: -3 dB down from peak of the main beam
Beam Separation: 1 HPBW of the main beam

therefore, does not incur any large scan losses for the smaller F/D_p. The difference in the C/I performances could be attributed to the increase of beam broadening factor and sidelobe coefficients for the smaller F/D_p at large scan angles.

5.3.6 Crossover Level and Footprint Level Sensitivity

The importance of knowing the C/I variations at different crossover levels in multiple-beam antenna applications was discussed in 5.2.4. Figure 60 shows the relation between the C/I and crossover level for a 100 wavelength diameter offset-reflector with a -10 dB taper and $F/D_p = 1.0$. The main beam function, the symmetric Gaussian function centered at $\theta = \theta_c$, for the offset-reflector case is the same as the main beam function, modified CCIR reference pattern, for the axisymmetric reflector case when $\theta_c = 0$ (the main beam of the desired beam generated at the focal point of the offset-reflector). Therefore, the relationship between the beam separation values, distances between the centers of two adjacent beams, and the footprint levels at the crossover boundaries is the same as that shown in Table 5. In Figure 60, C/I values as a function of the beam crossover levels are given for five multiple-beam antenna systems with different number of frequencies and number of beams. Notice that the C/I values have very small variations (0.1 dB) or no variations for crossover levels between -5 to -7 dB. It can be seen that the optimum crossover level is independent of the number of beams and frequencies and, in this case, is between -5 to -7 dB. This is an important result since the optimum crossover level was dependent on the number of beams and frequencies for the axisymmetric reflector antenna. Figures 61 and 62 show the relationship between the C/I values and the footprint level of the desired beam for different numbers of

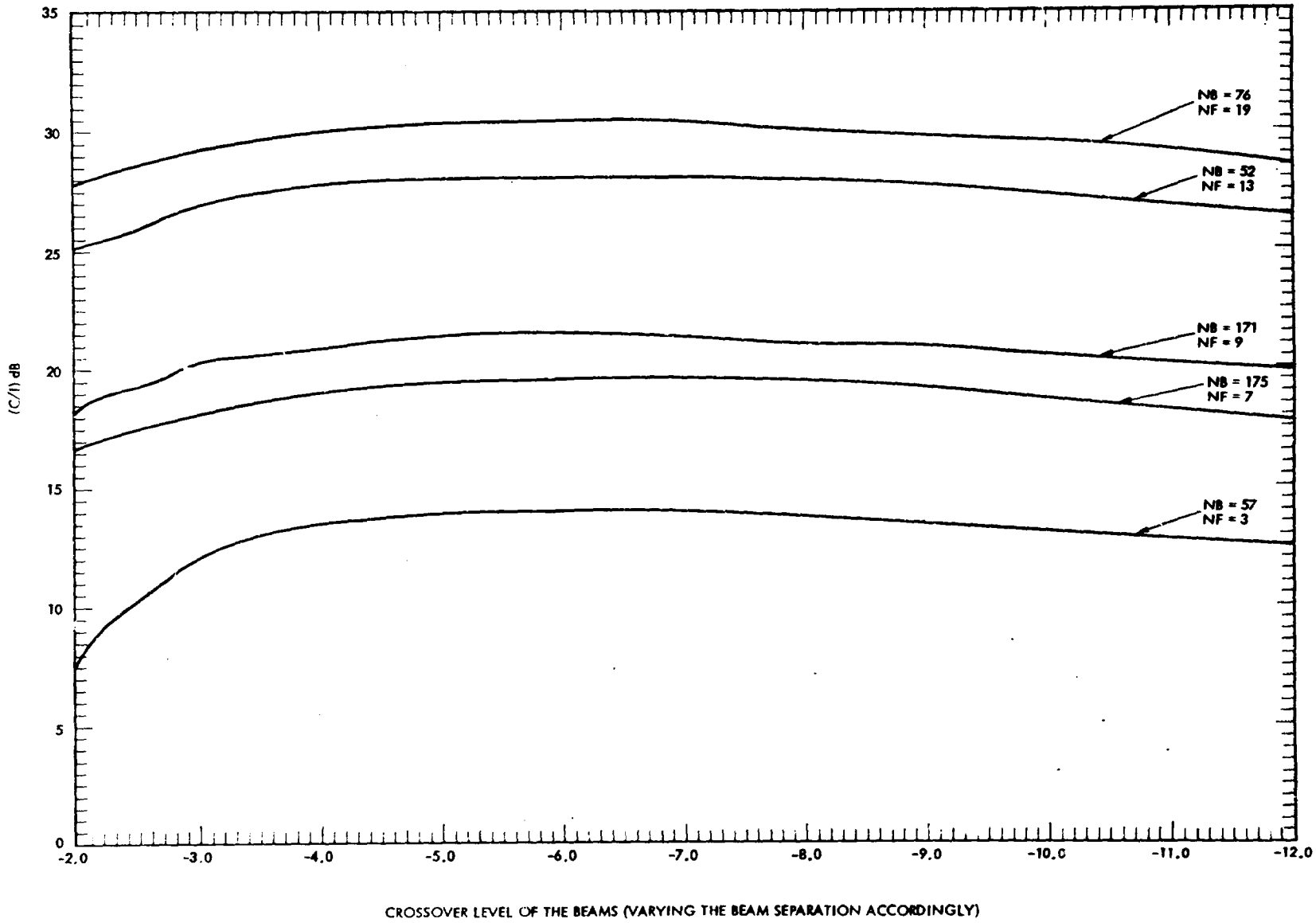

Figure 60. Crossover Level Sensitivity,
Offset-Reflector Diameter = 100 F/D_p = 1.0,
-10 dB Taper, -25 dB sidelobe level
Calculation Point: See Table 5
Beam Separation: See Table 5

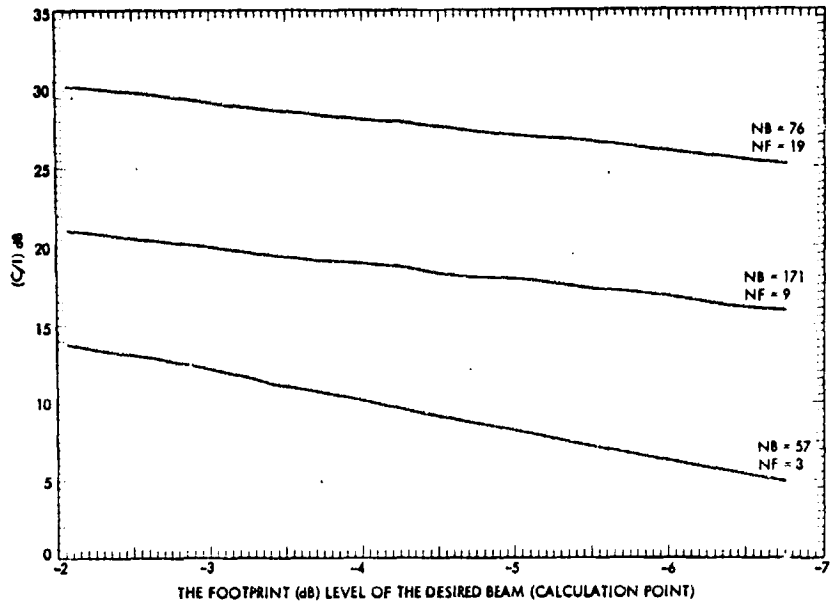

Figure 61. (C/I) Performance Calculated at Different Footprint (dB) Levels of the Desired Beam
Offset-Reflector Diameter = 100λ, F/D_p = 1.0,
-10 dB Taper, and -25 dB Sidelobe Level
Beam Separation: 1 HPBW of the main beam

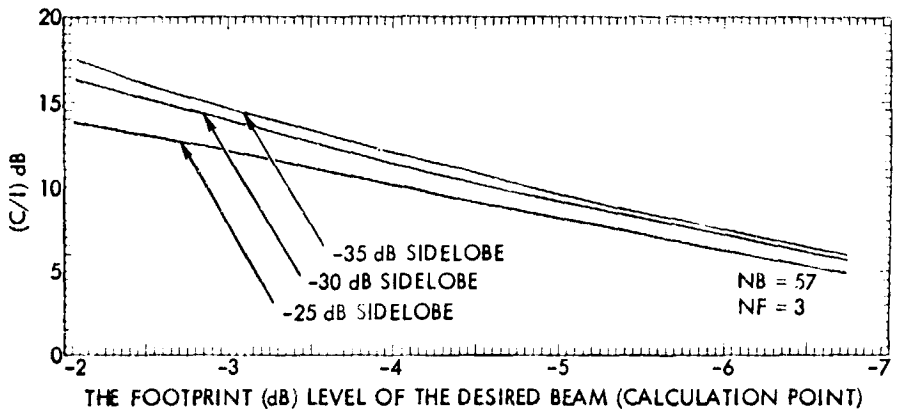

Figure 62. (C/I) Performance Calculated at Different Footprint (dB) Levels of the Desired Beam, for 3 Sidelobe Levels
Offset-Reflector Diameter = 100λ, F/D_p = 1.0, and
Type A Pattern
Beam Separation: 1 HPBW of the main beam

beams, frequencies, and sidelobe levels. Again, it could be seen that in all the cases the C/I values, as a function of the decreasing footprint level, are almost linearly decreasing.

5.3.7 Beam Spacing

Effects of the beam spacing variations on the C/I performance, for the offset-reflector antenna, were studied and the results are shown in Figure 63. The C/I performance improves as a function of increasing beam spacing.

5.3.8 Conclusion

The frequency reuse capacity of an offset-reflector multiple-beam antenna, with fixed number of beams and frequencies, has been shown to be primarily a function of sidelobe level (illumination taper) and beam spacing. However, as the number of frequencies increases, the frequency reuse factor becomes less sensitive to the sidelobe levels, but the C/I performance of the

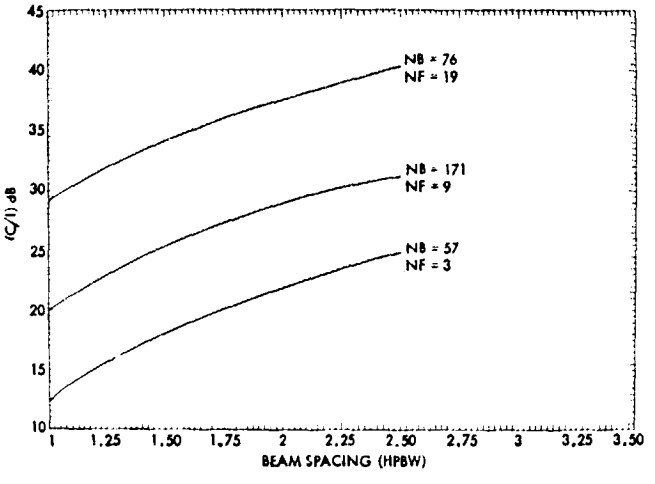

Figure 63. (C/I) Performance as a Function of Beam Spacing
Offset Reflector Diameter = 100λ, F/D_p = 1.0,
-10 dB Taper, and -25 Sidelobe Level
Calculation Point: -3 dB down from peak of the main beam

system improves. These are the same results as obtained for the axisymmetric reflector antenna. The other similar result is that the sidelobe levels have a more noticeable effect for larger number of beams when smaller number of frequencies are used.

It was shown that for a single linear polarization, when only the copolar patterns are considered, the C/I performance of the system was largely unaffected by the dimension of the offset-reflector (F/D_p). This could be due to the fact that the desired beam was assumed to be the beam generated at the focal point of the reflector and, therefore, does not incur any large scan losses for the smaller F/D_p. Also, the effects of the cross-polar components, which can be very serious in this case, are ignored.

The important fact discovered for the offset-parabolic reflector multiple-beam antenna is that the optimum crossover level is independent of the number of beams and frequencies.

In addition, the present results use a beam pattern model, which has been shown to approximate the envelope of calculated theoretical patterns very closely. Use of pattern models is expected to give an approximate worst case estimate of frequency reuse capacity because the model approximates the sidelobe peaks with an envelope function. Thus, the results show an upper bound on the number of frequencies or channels required to meet a specific C/I requirement.

SECTION 6
DISCUSSIONS AND DEVELOPMENTS FOR THE MULTIPLE-BEAM ANTENNA PROGRAM MODEL

The methods developed here can be used to analyze the interference rejection performance of uniform and non-uniform coverage systems, whether the antenna types are reflector antennas, lenses, or arrays. In this report the major effort has been to use space diversity to maximize the interbeam isolation and the frequency reuse capacity of the system. A second reuse of the same frequency band in each antenna beam may be achieved through the use of orthogonal polarization. The use of polarization diversity means to transmit two microwave carriers on the same frequency using either the two opposite "left-handed" or "right-handed" waves of circular polarization or two perpendicular linearly polarized waves. INTELSAT IV-A and V antennas take advantage of circular polarization. Use of dual polarization in multiple-beam antenna presents many more design problems than does a single polarization, because the antenna system and its design considerations are much more involved [3], [11]. But, since the combination of both space and polarization diversity is very attractive, one of the future tasks for development of the model program is to obtain the capacity of analyzing the interbeam isolation and frequency reuse when the combination of both diversities is used. Circular polarization is specially attractive for an offset-reflector when polarization diversity is used since an offset-parabolic reflector does not generate a cross-polarized signal when the feed has perfect circular polarization pattern [12]. Thus, for circularly polarized beams, good polarization isolation and axial ratio can be obtained by properly designing the feed elements and array configuration.

It was mentioned that the use of a sidelobe envelope function eliminates the effects of the sidelobe variations and the sidelobe nulls of the radiation patterns of the interfering beams in calculation of the interbeam isolation, and frequency reuse, and provides an approximate "worst case" estimate within the coverage area. Although, the sidelobe envelope functions were used in the model program, multiple-beam antennas have real sidelobe patterns and so, in some instances, the results could be much more optimistic at some areas within the coverage area. The usage of null-forming and null-steering, by adaptive feed arrays [13] in multiple-beam antennas, and use of real patterns in the model program comprises another one of the future tasks. The purpose of this task is to see how the interbeam isolation varies at different footprint levels within the various coverage areas, the pattern contours, and how we can obtain the maximization of interbeam isolation at some designated subareas within the various coverage areas.

In addition, the specific tasks for the future developments of the beam pattern model includes:

(1) Addition of the beam-maximum deviation factors;

(2) Consideration of the non-symmetry of the sidelobe patterns;

(3) Consideration of the effects of the off-axis location of the desired beam on C/I performance.

In conclusion, it must be remembered that the results presented here demonstrate the use of the method in the analysis of a few specific cases, and that more cases must be analyzed in order to obtain a full understanding of frequency reuse capacity of multiple-beam antennas. In the future, antenna patterns of some of the existing multiple-beam antennas will be obtained and comparisons of measured and theoretical patterns will be made. This will provide the necessary assessment of model adequacy and accuracy.

REFERENCES

1. CCIR Report 810 (1978), "Broadcasting-Satellite Service: Sound and Television; Reference Patterns and Technology for Transmitting and Receiving Antenna," CCIR XIVth Plenary Assembly, Vol. XI, pp. 271-285, Geneva, Switzerland.
2. A. W. Rudge, et al., "Study of the Performance and Limitations of Multiple-Beam Antennas," E.R.A. LTD. (RF Technology Center, England), p. 51, Rep. ESA Con. 2277/74 HP, Sept. 1975.
3. W. G. Scott, H. S. Luh, and E. W. Matthews, "Design Tradeoffs for Multi-beam Antennas in Communication Satellites," IEEE Communication Society Magazine, pp. 9-15, March 1977.
4. W. L. Pritchard, "Satellite Communication - An Overview of the Problems and Programs," Proc. IEEE, Vol. 65, p. 297, March 1977.
5. W. C. Jakes, Microwave Mobile Communications, New York: Wiley-Interscience, 1974, p. 562.
6. Lo Lundquist and M. Peritsky, "Co-Channel Interference Rejection in a Mobile Space Diversity System," IEEE Trans. Veh. Technol., Vol. VT-20, pp. 68-75, Aug. 1971.
7. A. W. Rudge, "Multiple-Beam Antennas: Offset-Reflectors with Offset Feeds," IEEE Trans. Antennas Propag., Vol. AP-23, pp. 317-322, May 1975.
8. Y. Rahmat-Samii, "Offset-Parabolic Reflector Program," IOM 3365-80-012, Feb. 28, 1980 (JPL internal document).
9. R. Mittra, Y. Rahmat-Samii, V. Galindo-Israel, and R. Norman, "An Efficient Technique for the Computation of Vector Secondary Patterns of Offset Paraboloid Reflectors," IEEE Trans. Antennas Propag., Vol. AP-27, pp. 294-304, May 1979.

10. Abramowitz and Stegun, Handbook of Mathematical Functions, Dover Pub., 1965, p. 364.

11. J. W. Duncan, S. J. Hamada, and P. G. Ingerson, "Dual Polarization Multiple-Beam Antenna for Frequency Reuse Satellite," AIAA/CASI 6th Communication Satellite Systems Conference, Montreal, Canada, April 1976, AIAA Paper No. 76-248.

12. T. S. Chu and R. H. Turrin, "Depolarization Properties of Offset-Reflector Antennas," IEEE Trans. Antennas Propag., Vol. AP-21, pp. 339-345, May 1973.

13. J. T. Mayhan and L. J. Ricardi, "Physical Limitations on Interference Reduction by Antenna Pattern Shaping," IEEE Trans. Antennas Propag., Vol. AP-23, pp. 639-646, Sept. 1975.